Spectrum Efficient Peak-to-Average Power Ratio Reduction for OFDM Systems

Md. Sakir Hossain

Student ID: 14DM053

Major: Science and Engineering

Course: Mathematics, Electronics and Informatics

Graduate School of Science and Engineering

Saitama University, JAPAN

Supervisor: Professor Tetsuya Shimamura

A thesis submitted in partial fulfillment of the requirements for the Degree of

Doctor of Philosophy

March 2018

Abstract

Wireless communications have witnessed an unprecedented growth in last two decades. This enables the explosive growth of multimedia communications in last decade, which demands high data rate. Since the spectrum is a limited resource, it is imperative to use it in the most efficient way to meet the demand. Orthogonal frequency division multiplexing (OFDM), the most spectrum efficient waveform to date, is regarded as the best tool to meet the data rate demand. Meeting the rate demand, OFDM, however, introduces new problems, such as low energy efficiency, adjacent channel interference (ACI) and in-band noise, because of its high peak-to-average power ratio (PAPR). The high PAPR reduces the power efficiency of a high power amplifier (HPA), thereby causing power wastage; this reduces battery life of portable devices. Furthermore, this escalates operating expenditure of the networks. The ACI badly affect quality of service of the network by degrading bit error rate (BER). The high PAPR problem is so serious issue that OFDM could not be included in the uplink of fourth generation cellular networks considering longer battery requirement of cell phones. In addition, since most of the candidate waveforms for the forthcoming fifth generation (5G) wireless systems are based on the OFDM and energy efficiency is an important requirement of the 5G, it is necessary to make OFDM as an energy efficient system by reducing the high PAPR.

This thesis deals with the high PAPR issue. In contrast to the most of the traditional PAPR reduction techniques where spectrum efficiency of OFDM is partly compromised to attain the reduced PAPR by reserving a portion of the available bandwidth for either reducing

PAPR or transmitting side information (SI), the aim of the thesis is to reduce PAPR maintaining 100% spectrum efficiency of an OFDM system. In this endeavor, we propose four different transmitter and receiver designs which attain significantly reduced PAPR without affecting the spectrum efficiency.

We propose a novel PAPR reduction scheme by utilizing pilot subcarriers in addition to their conventional use for channel estimation. We iteratively change the positions (which implies frequencies) of the pilot subcarriers among the data subcarriers to check which positions of the pilots produce the lowest PAPR. Instead of sending SI about the positions of the pilots, we design the receiver in such a way that it can detect the pilots blindly utilizing their comparatively higher power and equidistant properties. This scheme can attain up to 2.5 dB PAPR reduction without sacrificing spectrum efficiency. Furthermore, the amount of power saving attained by it is also analyzed.

Next, we improve the performance of an existing null subcarrier assisted PAPR reduction technique which suffers from extremely high computational complexity and BER. We propose a new transmitter by changing switching strategy between the data and null subcarriers incorporating a new feature of the switched null subcarriers: any two neighboring null subcarriers must be equidistant. Utilizing the equidistant and zero energy property of the null subcarriers, we propose a very efficient receiver design that can attain more than 5 dB signal-to-noise ratio (SNR) gain and 98% reduction of the computational complexity.

The third proposed scheme modifies an existing PAPR reduction technique based on orthogonal pilot sequence (OPS). The OPS scheme suffers from very limited PAPR reduction capability. Instead of just changing pilot symbols' phases according to a set of orthogonal sequences as is done in the OPS scheme, we propose to use the pilot

symbols' phases as the phase factors and multiply different groups of the data subcarriers by their respective phase factors produced from the corresponding pilot symbols' phases. This scheme can attain about three-times more PAPR reduction compared to the original OPS technique and requires 90% less computations compared to the existing modified OPS scheme.

Finally, we propose to improve dummy sequence insertion (DSI) and tone reservation techniques of PAPR reduction. These two techniques had been suffering from extremely low spectrum efficiency since their inception because of their requirement of the reservation of a certain number of subcarriers for the PAPR reduction. To overcome the shortcoming, we propose the notion of subcarrier group modulation which makes some data subcarriers free for the PAPR reduction by sending their corresponding data by some other means without any additional spectrum. This eliminates the rate loss caused by the PAPR reduction in the DSI scheme. In addition to the PAPR reduction application, it can be included for increasing spectrum efficiency of any unmodified OFDM system as well.

Keywords

Wireless communications, mobile, cellular communications, multicarrier communications, OFDM, PAPR, channel, energy efficiency, spectrum efficiency, CCDF, BER, dummy sequence insertion, tone reservation, null subcarrier, pilot subcarrier, power saving, orthogonal pilot sequence, walsh-hadamard sequence, Zadoff-Chu sequence, maximum likelihood detection, in-band noise, out-of-band distortion, adjacent channel interference, 4G, 5G, Wi-Fi, WLAN, WiMAX, consumer electronics.

To My Family

Acknowledgements

All praise belong to **Allah**, *The Almighty*, who has provided me with the opportunity and capability to complete the thesis.

Over the last three years of my doctoral study at Saitama University, a number of people have given me support and encouragement in many different ways. The first person that comes in that list is my supervisor Prof. Tetsuya Shimamura to whom I am deeply indebted. I am grateful to him for giving me the opportunity to work on wireless communications. Whenever I met him in some difficult times, he filled me up with a lot of optimism and I started working again with full of hope and confidence. Without his guidance and encouragement, it would not have been possible for me to complete the work.

I would also like to express my gratitude to Dr. Yosuke Sugiura for his comments on my research. I wish to thank all members of our laboratory to keep a friendly working environment which I really enjoyed. Special thanks to Japanese government for providing me the financial support of all kinds to pursue the doctoral study.

I would like to thank Dr. Sabbir Ahmed, University of Windsor, for his encouragement, constructive suggestions and comments on my research idea. I wish to thank Dr. Faisal Tariq, Queen Mary University of London, who supported me in all the ways he could have to help me overcome the difficulties of the doctoral research.

I would like to express my heart-felt gratitude to my wife, Rokshana Yesmin, for her unlimited support and encouragement. She took all responsibilities of caring our baby, Wardah Jinan, and running our family smooth throughout my doctoral study. I wish to thank my parents and siblings for their endless sacrifice for me throughout my life. There are many other people to whom I am deeply grateful.

Contents

List of Figures

List of Tables

Chapter 1

Introduction

Currently, mankind is witnessing the fastest rate of social, economic and cultural change in its history. Rapid flow of information across the world plays the key role behind such changes. Ubiquitous communication systems, wireless communications in particular, make such information flow possible. Mobile communications bring the communication facilities to the door of people of all classes in every corner of the earth. In 2014, the world-wide number of mobile phone subscribers hit 7 billions as is seen in Fig. 1.1. Almost 96% population of the world is under the umbrella of mobile networks. To make it more accessible, it is imperative to reduce prices of services. Since the price of the mobile Internet is more than 50% less compared to the fixed-broadband systems [5], wireless communication will dominate in future. It's other advantages include easy mobility and ubiquitousness. Wireless communications, however, poses a number of challenges such as efficient spectrum reuse, channel effects mitigation, designing of portable low-power devices, and so on. To ensure more data rate with the limited spectrum, the use of wireless local area network (WLAN) and small cell networks will increase dramatically in future. While WLAN uses unlicensed band of frequency, the small cell uses the frequency band used for cellular communications. The small cell networks enable us to attain several fold increase of throughput. In addition, both networks can effectively mitigate channel effects because of the short distance transmission. Furthermore, the short distance transmission requires less transmission power, thereby prolonging battery life. Most of the currently used WLAN and cellular standards are based on orthogonal frequency division multiplexing (OFDM), a bandwidth efficient modulation technique.

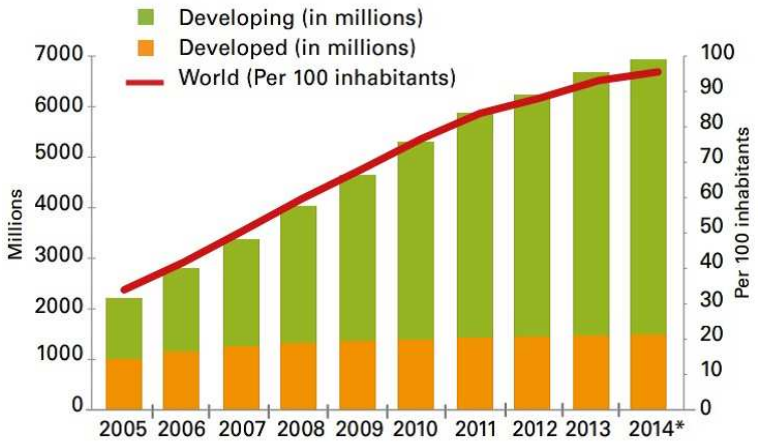

Figure 1.1: Cellular mobile subscriptions per year [1]

OFDM is a multicarrier communication system. It splits the available bandwidth into a number of orthogonal subbands, widely known as subcarriers, thereby transforming a wideband system into a narrowband one. While the wideband transmission suffers heavily from frequency selective fading, OFDM is free from such problem because of its narrowband transmission. OFDM signal is only affected by flat fading which can easily be mitigated using a one-tap equalizer; this results in a low complex receiver. Bandwidth efficiency is another merit of OFDM. By utilizing the orthogonality property of OFDM subcarriers, different subcarriers can overlap each other which results in more subcarriers from the same spectrum compared to the frequency domain multiplexing (FDM). Furthermore, it has resilience of multipath fading. In addition, the independent subcarriers of OFDM make it possible to use adaptive transmission depending on the data rate requirements and channel characteristics.

Inspired by the advantages of OFDM over conventional modulation techniques, it has been incorporated into a number of wireless system standards. It is first included in digital audio broadcasting (DAB) and digital video broadcasting (DVB) standards. In addition, the latest four WLAN (also known as Wi-Fi) standards, such as IEEE 802.11a, IEEE 802.11g, IEEE 802.11n and IEEE 802.11ac, use OFDM as their physical layer air interface. Furthermore, OFDM is used in cellular communication. Third generation (3G) standard IEEE 802.16 (widely known as worldwide interoperability for microwave access (WiMAX)) uses OFDM as

its air interface. OFDM is used in the downlink transmission of the recently deployed fourth generation (4G) cellular standard, named 3rd generation partnership project (3GPP) long term evoultion (LTE). It is used in a number of wired standards as well.

It is well-known that every coin has its two sides. Similarly, despite the many advantages of OFDM, it has few limitations as well. For example, it is sensitive to inter carrier interference (ICI) because of carrier frequency offset caused by the Doppler spreading and/or carrier frequency mismatch between the transmitter and receiver oscillators. However, the most serious problem of OFDM systems is the high peak-to-average power ratio (PAPR) of its waveform. It is due to the coherent addition of the available subcarriers. The high PAPR causes system performance degradation in different ways. For example, it degrades power efficiency of a high power amplifier (HPA) because the efficiency is inversely proportional to the PAPR of its input signal [6]; this causes energy efficiency loss of the OFDM system. The energy efficiency degradation is due to the back-off (BO) required to keep the operating point of the amplifier in the linear region. As a result, high PAPR results in the wastage of power. For portable devices, this reduces battery life, which restricts the application of OFDM to such devices. Another adverse effect is the adjacent channel interference (ACI). This is caused by the increased out-of-band energy leakage resulted from the high PAPR. In addition, if the PAPR is not reduced, the non-linearity of the HPA distorts the OFDM signal which results in a reduction of orthogonality among subcarriers. This causes bit error rate (BER) degradation at the receiver. Because of the high PAPR, it requires to use a digital to analog converter (DAC) having a large range, which is very difficult and expensive to design.

1.1 Problem Statement

The adverse effects of the high PAPR can be partly overcome by using a HPA having large linear region and DAC with large range. However, both are extremely difficult and expensive to build. This also increases network's capital expenditure (CAPEX). Alternative solution is to use HPA with a large BO. This, however, escalates operating expenditure (OPEX) due to huge power wastage.

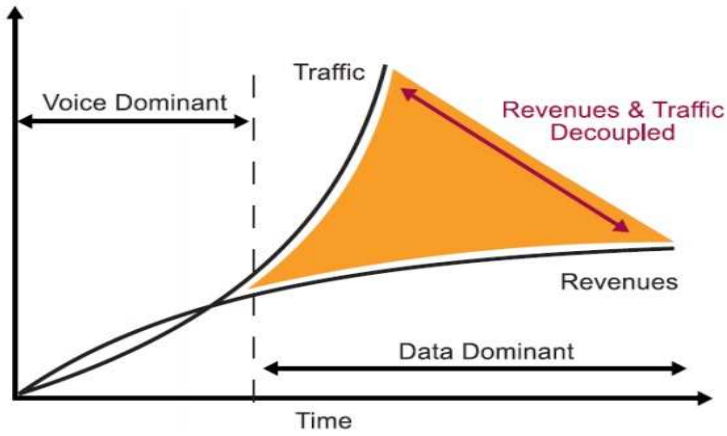

Figure 1.2: Growing gap between cellular network operator's revenue and data traffic [2]

From Fig. 1.2, it is seen that with the passage of time, the mobile network's revenue remains almost unchanged while the data traffic increases sharply. To support the increased traffic, the net profit goes down. One way to maintain the profit is to reduce OPEX. Since the HPA consumes about 65% energy of the whole network [7], [8], it is possible to cut down a significant portion of OPEX by increasing the efficiency of the HPA; and this can be done by reducing PAPR.

There has been a plethora of solutions proposed to mitigate this problem in last two decades. A detail survey on the PAPR reduction techniques can be found in [9, 10, 11]. Many of the proposals attain significant PAPR reductions. However, the problem which most of the existing schemes suffers from is spectrum efficiency degradation. The degradation occurs in one of different ways. For example, a group of techniques perform some kind of pre-processing of the frequency domain (FD) signal to reduce PAPR in such a way that the receiver needs some information, usually called as side information (SI), from the transmitter to recover the original FD signal; this requires to send the information to the receiver in each transmission, which needs to reserve a certain number of subcarriers for this purpose. On the other hand, there are another group of PAPR reduction schemes which explicitly reserve some subcarriers for PAPR reduction. Both groups ultimately reduces the number of subcarriers for data transmission, thereby reducing throughput. In short, most of the schemes achieve energy efficiency sacrificing spectrum efficiency of OFDM system. Pertinently, the spectrum

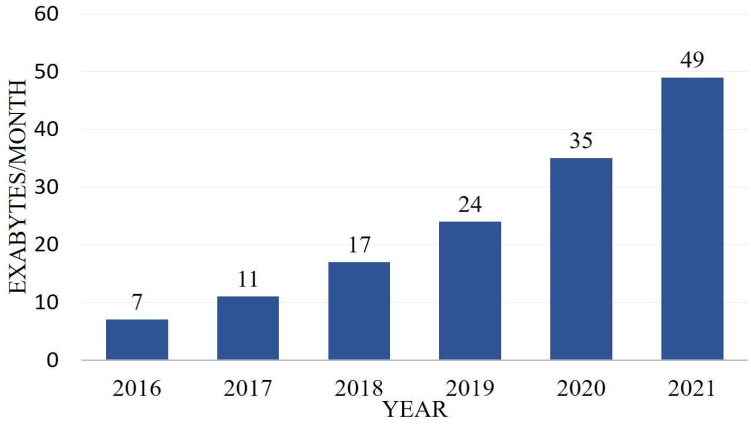

Figure 1.3: Prediction of monthly mobile data traffic by 2021 [3]

efficiency is one of the most important merits of OFDM. According to Fig. 1.3, the mobile data traffic will increase seven fold by 2021. To support such huge traffic, it is imperative to use the spectrum in the most efficient way. Thus, the spectrum efficiency should not be sacrificed to attain the energy efficiency. For this reason, the aim of the thesis is to propose new PAPR reduction schemes to attain as much energy efficiency as possible while maintaining 100% spectrum efficiency of the unmodified OFDM systems. In addition, orthogonality of the subcarriers will be preserved.

1.2 Contributions

The contribution that this research made to the field of wireless communication and signal processing is summarized as follows:

- A detail analysis of the principles and applications of OFDM is presented. In addition, a thorough critical analysis of the traditional PAPR reduction schemes is provided.

- A novel PAPR reduction scheme based on pilot subcarriers repositioning is proposed. It can achieve a significant PAPR reduction preserving the bandwidth efficiency. This scheme does not distort orthogonality of the

subcarriers and causes no BER degradation. BER performance in the presence of HPA is evaluated. Furthermore, the power savings due to the PAPR reduction is thoroughly analyzed.

- Null subcarrier switching based new PAPR reduction scheme is proposed. To improve BER performance, a novel switched null subcarriers detection technique is presented. Through simulation, it is found that the proposed OFDM system can reduce PAPR considerably with up to 5 dB signal-to-noise ratio (SNR) gain. It shades 98% computational complexity of the traditional schemes. All these achievements are attained preserving bandwidth efficiency.

- Changing pilot symbols' phases iteratively according to orthogonal pilot sequences (OPSs) and using the pilot values as phase factors, a PAPR reduction scheme is proposed that improves PAPR reduction performance significantly. It does not require to compromise the spectrum efficiency in the endeavor. The proposed scheme reduces computational complexity by about 90% compared to the traditional schemes.

- Finally the concept of subcarrier group modulation (SGM) is presented. It can simply be integrated to OFDM system to improve bandwidth efficiency. In addition, it can be used for PAPR reduction as well. Performance evaluation of the integration of the SGM to the dummy sequence insertion (DSI) scheme in a bid to reduce PAPR is explained; the DSI with SGM scheme attains 100% spectrum efficiency.

1.3 Publications Arising From The Research

- Journals
  - Md. Sakir Hossain and Tetsuya Shimamura, PAPR reduction for OFDM systems using pilot derived phase factors, *IEICE Communication Express (Accepted).*
  - Md. Sakir Hossain and Tetsuya Shimamura, Spectrum Efficient DSI-Based OFDM PAPR Reduction by Subcarrier Group Modulation, *IEEE Transactions on Broadcasting (Accepted).*

- Md. Sakir Hossain and Tetsuya Shimamura, Enhanced OFDM performance with pilot-aided reduced peak-to-average power ratio, *RISP Journal of Signal Processing*, vol. 21, no. 1, pp. 1 - 13, Jan. 2017.
- Md. Sakir Hossain and Tetsuya Shimamura, Low-complexity null subcarrier-assisted OFDM PAPR reduction with improved BER, *IEEE Communication Letters*, vol. 20, no. 11, pp. 2249 - 2252, Aug. 2016.

- Conference
  - Md. Sakir Hossain and Tetsuya Shimamura, PAPR reduction of OFDM through pilot shifting, in *Proc. 26th IEEE Symposium on Personal, Indoor, and Mobile Radio Communications (PIMRC)*, Hong Kong, Aug-Sept. 2015, pp. 402 - 407.

1.4 Thesis Outline

In the introduction of the thesis, some requirements of the next generation wireless systems and how can OFDM fulfill those requirements have been described. Afterwards, the research problem has been formulated.

The rest of the thesis is organized as follows:

- Chapter 2 thoroughly analyze the theory, principles and techniques of OFDM systems. It also discusses different fading issues of wireless channels. Furthermore, the inter symbol interference (ISI) and the underlying technique of reducing it is described in detail.
- Chapter 3 starts explaining the PAPR issue of OFDM. Then, it provides a short survey of the PAPR reduction schemes. Since the proposed PAPR reduction schemes in this thesis belong to distortionless category of PAPR reduction schemes, the existing distortionless PAPR reduction schemes are reviewed in detail.
- Chapter 4 introduces pilot subcarrier repositioning based PAPR reduction scheme. It provides an in-depth explanation of a pilot subcarrier detection schemes as well. In addition, the performance of the scheme is evaluated.

- Chapter 5 continues the problem-oriented literature review, which is followed by the description of the proposed null subcarrier assisted PAPR reduction technique. It also discusses the proposed switched null subcarrier detection scheme and performance evaluation.
- Chapter 6 provides a short review of an OPS based PAPR reduction scheme. Afterwards, it discusses an improved OPS scheme and its performance evaluation.
- Chapter 7 discusses the traditional DSI scheme. Then, the proposed DSI with SGM scheme is explained, which is followed by the performance evaluation through simulation.
- Finally, chapter 8 summarises the conclusions, and the possible suggestions of future work are noted at the end.

Chapter 2

Principles of OFDM

This chapter gives an overview of OFDM. First of all, wireless channels' characteristics are explained in Section 2.1. Section 2.2 provides a description of the evolution of OFDM. Then, the concept of multi-carrier communication is explained in Section 2.3. Section 2.4 gives a short comparison of OFDM with respect to other multiplexing schemes, which is followed the Section 2.5 where OFDM basics is explained, with details of the orthogonality, signal generation, system architecture, advantages and limitations.

2.1 Overview of Wireless Channels

Wireless systems are more complicated compared to the wired ones. The reason is that the effects of the wired media on the signal, transmitted through it, remains unchanged over time and space, while the impairments experienced by a signal over a wireless channel varies with time and space depending on the surrounding environment. The randomness of the wireless channels makes the communication very complicated and poses a number of challenges before system designers: signal fading, ISI and so on. A signal in wireless channel is affected in two ways: large-scale path loss, and small-scale fading, also known as fading.

2.1.1 Path Loss

The path loss is the loss of signal strength because of the signal propagation over a large distance from the transmitter. It is computed by averaging local signal

strength measurements over a measurement track of 5λ to 40λ, where λ is the wavelength of the signal; thus for a cellular system operating in the frequency range from 1 GHz to 2 GHz, the measurements are carried out over a movement of 1 m to 10 m [12]. The signal strength fall due to the large-scale path loss occurs much more slowly.

2.1.2 Small-Scale Fading

As the name implies, the small scale fading is the change of signal strength for the transmitter and/or receiver movements by a fraction of a wavelength. It is much more faster and causes signal strength fall of 30 to 40 dB. In addition to the signal strength degradation, it causes changes of frequency and phases as well. The fading is very complicated to predict because of its dependence on the propagation environment, the velocity of the transmitter and receiver, the movements of the surrounding objects, the signal spectrum and so on. The phenomena such as reflection, diffraction and scattering of the signal with respect to the surrounding objects produce multiple versions of the transmitted signal; each version may differ from others in terms of time of arrival, phase, amplitudes and frequency. Since the received signal is a result of a vectorially addition of all versions of the signal, the resulting signal's characteristics change dramatically depending on whether the different versions are getting added constructively or destructively. An important characteristics of multipath environment is the *time delay spread* which is defined as the time difference between the first received component and the last received component having amplitude greater than a threshold [13].

Fading Channel Statistics

The level of fading, a signal experiences, significantly depends on the surrounding objects. The objects in the signal propagation paths determine how many versions of the signal will be created. In macro-cellular systems, all versions of the signal are due to non-line of sight (NLOS) paths. However, it is more likely that one of the paths of the multipath propagation in micro-cellular system is line of sight (LOS) [14]. If all paths of a propagation are NLOS, the corresponding fading is called *Rayleigh fading* because such fading can be modelled using Rayleigh

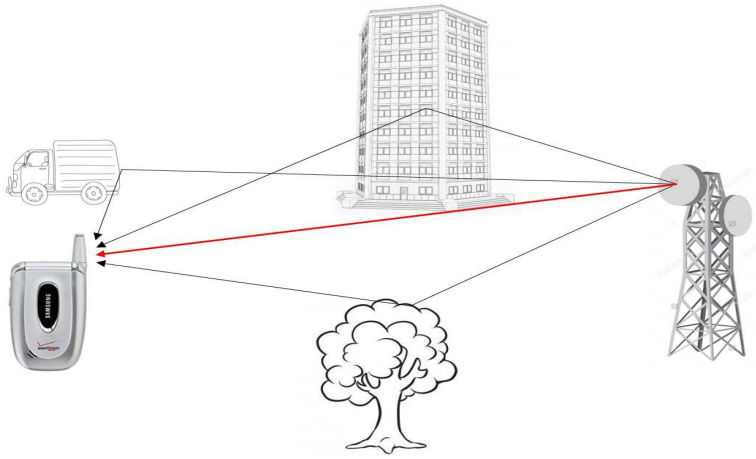

Figure 2.1: Illustration of multipath propagation

distribution. On the other hand, Rician distribution is used to model a received signal if there is a direct path from the transmitting antenna to the receiving one, and such fading is called *Rician fading*. The Rician fading propagation is shown in Fig. 2.1. However, if the red-colored line did not exist, the fading would be Rayleigh fading. The Rayleigh fading causes more signal distortion compared to the Rician fading.

Classification of Fading

Fading is also classified based on the nature of the transmitted signal with respect to the channel characteristics. In this regard, the bandwidth of the signal plays a vital role. Wireless channels are characterised by two important parameters: *coherence bandwidth* and *coherence time*.

Coherence bandwidth can be defined as the range of frequency over which all frequency components are equally affected by the channel. In other words, the channel passes all frequencies within the bandwidth with equal gain and linear phase [12]. Sometimes, it is defined as the range of frequency for which the autocorrelation function of the channel frequency response reduces by 3 dB [15]. It is equal to the reciprocal of the delay spread [16]. If the signal bandwidth is far less than the coherence bandwidth, the channel passes all frequency components with equal gain, and the corresponding fading is called *flat fading*. Narrowband

signals experience such type of fading, and the corresponding channel is called narrowband channel. On other hand, if the signal bandwidth is greater than the coherence bandwidth, different frequencies of the signal get affected differently; that is, the gain and phase of different frequency components become different. This type of fading is called *frequency selective fading*. It introduces much more signal distortion than the flat fading. In addition, it is more challenging to mitigate the effects of the frequency selective fading. Wideband signals encounter this type of fading. In such fading, multipath delay spread of the impulse response is greater than the symbol period (which is the reciprocal of the signal bandwidth). Under this condition, the received signal has multiple versions, each with a different attenuation and delay. As a result, the received signal is distorted.

Coherence time, on the other hand, represents the time varying nature of the channel. It is defined as the time duration over which the channel impulse response remains unchanged. If two signals are sent over the channel within the coherence time, both signals will be affected by the channel similarly because the impulse responses of the channel at these two different times will have strong correlation. As the time between the two channel impulse responses increases, the correlation decreases. The coherence time is the time duration over which the correlation between the corresponding impulse responses decreases by 3 dB. If the baseband symbol period is greater than the coherence time, the channel will change during the signal transmission which results in signal distortion. This type of fading is called *fast fading*. It is also known as time selective fading. However, if the coherence time is greater than the symbol period, the channel impulse response remains unchanged during the whole symbol period, and such fading is referred to as *slow fading*. The slow fading causes less signal distortion compared to the fast fading, and it is much easier to mitigate the effects of this fading compared to that of the fast fading.

Intersymbol Interference

Assuming that a wireless channel has a delay spread of T_m, the received symbol duration corresponding to a transmitted symbol of duration T will increases to $T + T_m$. If $T \gg T_m$, the multiple versions of the symbol are received very close in time to each other, and it appears as if the symbols are placed almost on

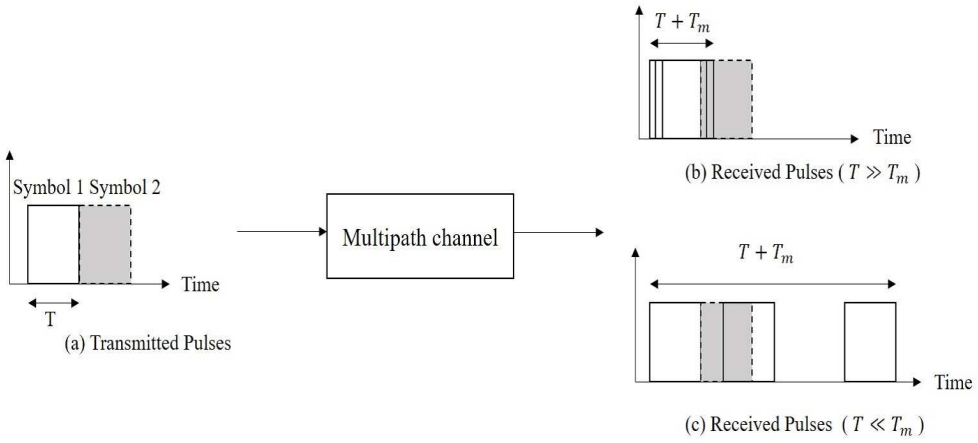

Figure 2.2: Illustration of how does ISI occur

top of one another [13]. It is illustrated in Fig. 2.2(b). Under this scenario, delays of different versions of the symbol received through different paths can be assumed equal. As a result, the energy of one symbol does not significantly spill over another symbol, and thus there is a little or no interference between subsequent symbols. However, if $T_m \gg T$, the multipath components reach the receiver over a long time, and before the arrival of the last multipath component with a significant amplitude, the next symbol arrives which results in smearing of the new symbol with the multipath component of the previous symbols, as is shown in Fig. 2.2(c). In other words, if a symbol of $T + T_m$ duration is repeated at a interval of T, there will be overlapping of symbols. This phenomena is called *intersymbol interference* (ISI). This occurs due to time dispersion caused by the frequency selective fading. Increased delay spread causes more ISI, which results in more BER. Simplest modulation schemes such as binary phase shift keying (BPSK) can tolerate a delay spread equal to 10-20% of the symbol period. Higher order modulations are more sensitive to ISI, thus the delay spread must be several percent of the symbol period [17].

2.2 History of OFDM

OFDM is one of those techniques which take long time to gain popularity and consumer-oriented applications. As a special form of FDM, its evolution started in the early era of telegraph. For better utilization of telegraph channel, time

division multiplexing (TDM), the earliest multiplexing scheme, was introduced by Baudot in 1870s [18]. The burst speed, however, became limited by the ISI because there was no good channel equalizer at the time. To overcome the ISI effect, several alternative multiplexing schemes were proposed. FDM, proposed by Alfred Graham Bell in 1870s [19], was a result of such attempts. However, its first application in analog telephony was done by George Squirer in 1910 [20]. With the inception of digital telephony, the FDM's frequency band per active call was replaced hybrid FDM/TDM. However, the wider bandwidth of the TDM systems suffered a lot by the frequency selective fading. For this reason, engineers turned back to the FDM systems providing more emphasis on simple equalization than the bandwidth efficiency. However, scientists did not forget the bandwidth inefficiency issue of FDM systems and continued research to overcome it.

A breakthrough came in 1966 when Robert W. Chang introduced the notion of orthogonality to FDM systems, thereby giving birth of the orthogonal FDM (OFDM) [21]. He achieved a corresponding patent in 1970 [22]. Chang used filters, one for each subcarrier, to produce band-limited orthogonal signals in the transmitter and a adaptive correlation receiver to separate the overlapping subcarriers. The orthogonality is obtained by imposing a condition that the subcarrier spacing must be $\frac{b}{2}$ for the signaling rate of b in each subcarrier. A performance analysis of the orthogonal multiplexing was performed by Burton R. Saltzberg, where it was found that a serious crosstalk might occur unless precise phasing of demodulation carriers and sampling time were maintained. In addition, it was proposed to use half cosine roll-offs instead of the full cosine roll-offs, used by Chang, to get better results in the presence of delay and amplitude distortions [23]. Furthermore, a staggered OFDM-offset quadrature amplitude modulation (OFDM-OQAM) was proposed by him to combat ISI and ICI. In 1968, Chang and Gibby followed up the performance evaluation in the presence of carrier phase offset, sampling timing error and phase distortion in the filters [24]. In 1971, discrete Fourier transform (DFT) based OFDM was proposed, which eliminates the need of the subcarrier oscillators and coherent demodulators [25]. In addition, such DFT-based OFDM could be completely realizable digitally. The notion of cyclic prefix, copying a certain portion from the last of the OFDM symbol to its prefix, was introduced in 1980 to mitigate the multipath effects [26].

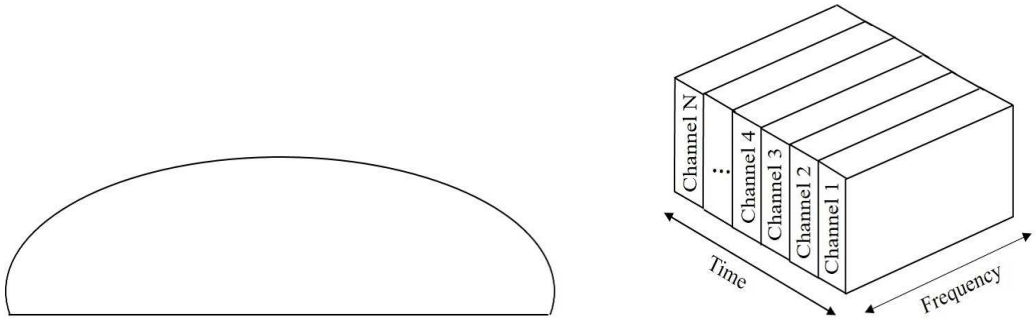

(a) Spectrum allocated to each signal source

(a) Spectrum allocation time slots

Figure 2.3: Principles of TDM

In 1981, the computational complexity further reduced when Hirosaki proposed to use $\frac{N}{2}$-point DFT instead of N point DFT under the condition that the ratio of the lowest subcarrier frequency and the subcarrier spacing must be 0.5 [27]. The idea of pilot subcarrier was proposed by Cimini in 1985 to perform proper channel estimation [28]. The advantages of using OFDM in cellular mobile systems were also explored by Cimini. Four years later, in 1989 the flexibility of OFDM is utilized to improve its performance using adaptive transmission [29]. The first large-scale consumer-oriented implementation of OFDM is carried out in early 1990s in asymmetric digital subscriber line (ADSL), about two decades after Chang had proposed the idea of OFDM [30].

2.3 Multiplexing Techniques

The necessity of the birth of OFDM can be better understood if it is described with respect to other multiplexing schemes. Let's start with the TDM. It is the earliest multiplexing scheme, as is discussed in the previous section. In this systems, the whole available bandwidth, B, is shared in time-slot basis; each time the whole bandwidth is allocated to a particular signal source, and it is allocated to a different signal source in the next time-slot. In this way, it is allocated to different signal sources in round-robin fashion. The mechanism is illustrated in Fig. 2.3. It is very easy to implement. The computational complexity involved with this technique is negligible. However, the downside of the technique is its high sensitivity to frequency selective fading. In TDM, the signal bandwidth is

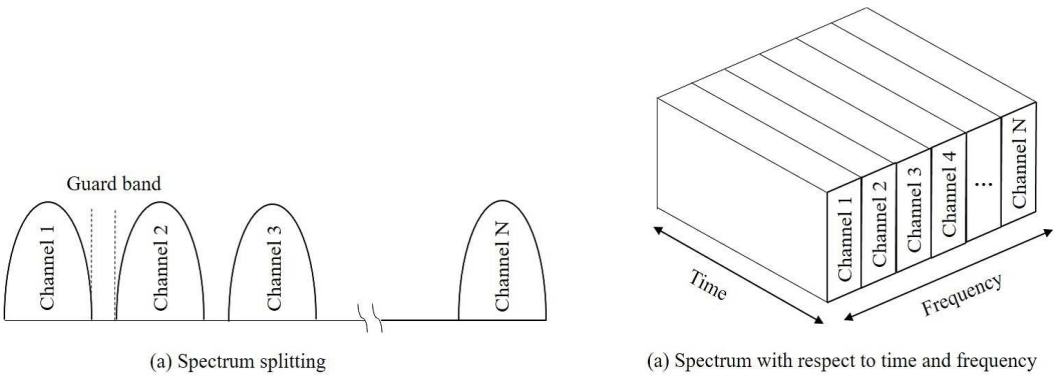

Figure 2.4: Principles of FDM

very large, hence $B > B_c$. As a result, the signal undergoes frequency selective fading which results in ISI. In multipath environment which is quite common in cellular mobile communication, the ISI effects become so serious that a very efficient equalization technique is required for proper data recovery at the receiver.

To combat the ISI effects, FDM is used. In FDM, the available bandwidth is split into a number of narrow subbands, and each subband is allocated to each signal source. In this way, all signal sources can transmit data simultaneously over their respective subbands. Since each source is using only a fraction of the available bandwidth, the data transmission is carried out relatively slowly. Because of the narrow subbands, the subband bandwidth is less than the coherence bandwidth. For this reason, each subband experiences flat fading. In this way, the ISI effect is largely mitigated. However, this technique requires to provide a large guard band between two neighboring subbands to keep ACI in a tolerable label, with a larger guard band results in better ACI mitigation. For this reason, the amount of bandwidth available for data transmission reduces significantly, which eventually makes the FDM a spectrum inefficient multiplexing technique. At the receiver, each subband is processed separately; a separate frequency tunable filter is used for each subband similar to the transmitter. Such a large number of filters make the FDM a computationally complex technique.

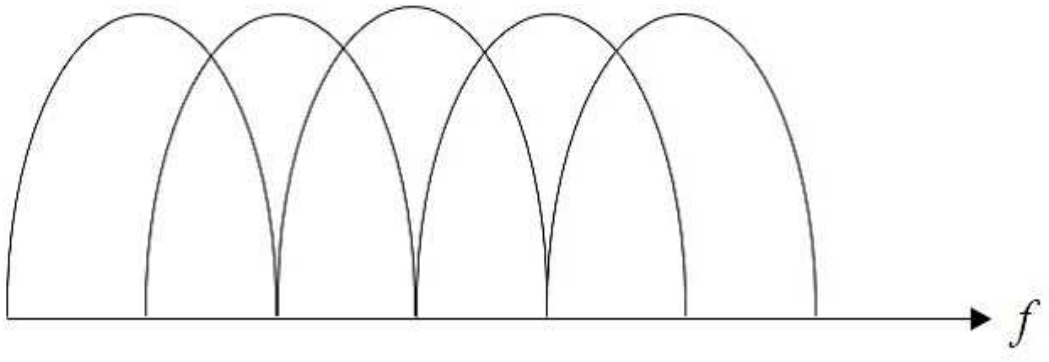

Figure 2.5: Conceptual spectrum of OFDM

To overcome the bandwidth efficiency limitation of FDM, OFDM is used. As the name says, orthogonal FDM (OFDM) is a special case of FDM. OFDM also splits the bandwidth into a number of subbands, which are commonly known as subcarriers in multi-carrier communication related literature. But such splitting is carried out with a special condition: orthogonality. That is, the subcarriers are generated in such a way that each subcarrier is orthogonal compared to the rest of the subcarriers. The orthogonality makes the subcarriers independent of one another, and enables the subcarriers to overlap. This eliminates the need for keeping the guard bands like FDM and allows more compact subcarrier arrangement. As a result, more subcarriers can be created from the same available bandwidth compared to the FDM technique. Fig. 2.5 illustrates the spectrum compactness of OFDM. While the narrow subcarriers provide resilience of frequency selective fading, the orthogonality ensures spectrum efficiency. Multi-carrier code division multiple access (MC-CDMA) is another example of MCM.

2.4 Principles of multi-carrier communications

In single carrier modulation (SCM), data is transmitted serially using a single carrier with data rate R and bandwidth B. The symbol period is given by $T_{ss} = \frac{1}{B}$. Because of the large bandwidth, $B_c < B$. From time-domain (TD) perspective, $T_{ss} < T_m$ where T_m is the delay spread. For this reason, the signal undergoes frequency selective fading. As a result, the signal gets distorted because of the ISI effect. One way to overcome the signal distortion is to use equalization. However,

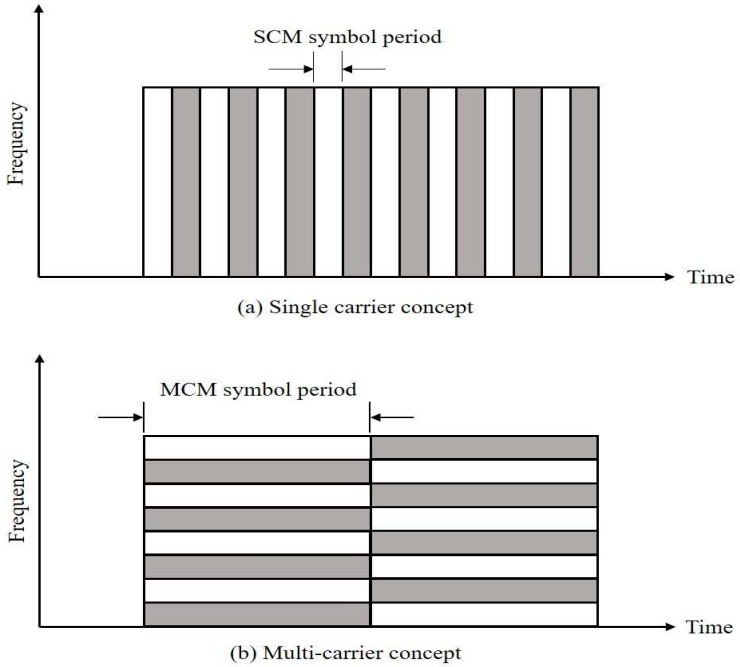

Figure 2.6: Difference between SCM and MCM

the equalization process puts excessive burden of computational overhead over the system.

To mitigate the frequency selective fading effects, multi-carrier modulation (MCM) techniques are used. In MCM, the available bandwidth B is equally divided into N subcarriers with subcarrier spacing, $\Delta_f = \frac{B}{N}$. The concept of the MCM with respect to the SCM is depicted in Fig. 2.6. Since the symbol period of a signal is reciprocal of its bandwidth, the symbol period of the MCM signal becomes N-times of the symbol period of the SCM signal. Hence, the MCM symbol period, $T_{sm} = \frac{1}{\Delta_f}$, can be rewritten as $T_{sm} = \frac{N}{B}$. So $T_{sm} = NT_{ss}$. That is, the MCM symbol period is N times longer than that of the SCM. This makes T_{sm} far larger than T_m. As a result, the frequency selective fading can not occur. From the FD perspective, each subcarrier is separately treated by the channel because all subcarriers are independent. Since Δ_f is N-times narrower compared to the SCM bandwidth, $\Delta_f \ll B_c$. For this reason, each subcarrier experiences flat fading only.

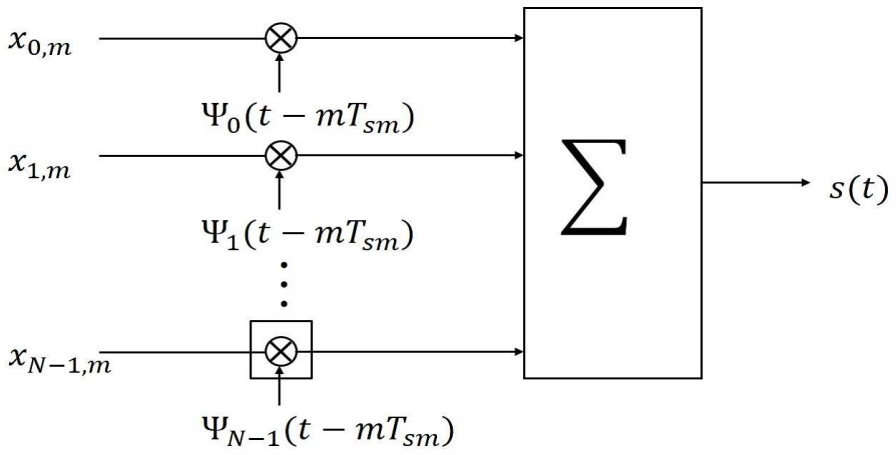

Figure 2.7: Conceptual architecture of MCM

The most general form of the MCM technique is shown in Fig. 2.7 A generalized multicarrier signal can be expressed as a summation of N modulated subcarriers as follows [15]:

$$s(t) = \sum_{m=-\infty}^{m=\infty} \left(\sum_{k=0}^{N-1} x_{k,m} \Psi_k \left(t - mT_{sm} \right) \right), \tag{2.1}$$

where $x_{k,m}$ is the data symbol which modulates k^{th} subcarrier in the m^{th} signaling interval, and Ψ_k is the waveform of the k^{th} subcarrier. From Eq. 2.1, it is clear that every subcarrier carries a data symbol; hence, more subcarrier results in more data transmission, which eventually increases spectrum efficiency. Furthermore, the increased number of subcarriers decreases subcarrier spacing, which causes symbol period increase. As a result, the symbol period can be far greater than the delay spread, which helps to overcome multipath fading. In a nutshell, the more the subcarrier, the more the throughput. Now, a natural question arises: Can we make an extremely large number of subcarriers irrespective of the available bandwidth? or is there an upper limit of the number of subcarriers for an efficient communication? The latter is true. This reason is as follows. If we make an extremely large number of subcarriers from a given bandwidth, the reciprocal of the subcarrier spacing will be excessively longer in time. The time will be so long so that it will become longer than the channel coherence time, which causes fast fading to affect each subcarrier and distort the signal. For this reason, there is an upper limit of the number of subcarriers for a given bandwidth depending on

the channel characteristics, and is given by [15]:

$$\frac{B}{B_c} \ll N \ll RT_c \tag{2.2}$$

The MCM symbol period is bounded by the maximum Doppler frequency, $f_{D_{max}}$, and the delay spread in the following way [31]:

$$4T_m \leq T \leq \frac{3}{100 f_{D_{max}}} \tag{2.3}$$

We can bound the subcarrier spacing as follows:

$$\frac{3}{100} f_{D_{max}} \leq \Delta_f \leq \frac{B_c}{4} \tag{2.4}$$

2.5 OFDM Basics

OFDM is a multi-carrier modulation technique. The general idea is to split the available bandwidth into a number of narrow subcarriers, with a condition that all subcarriers are orthogonal to each other. The notion of the orthogonality is the heart of OFDM. Different properties, architecture and advantages of OFDM will be explained in this Section.

2.5.1 Orthogonality

One of the prominent merit of OFDM is its high bandwidth efficiency. The efficient utilization of the spectrum is achieved by means of mutual orthogonality of the subcarriers. A set of subcarriers are orthogonal to each other if they are equispaced and the subcarrier spacing is reciprocal of the symbol period. In other words, if we split a bandwidth maintaining the subcarrier spacing of Δ_f between any two neighboring subcarriers and $\Delta_f = \frac{1}{T_{sm}} = \frac{1}{NT_{ss}} = \frac{N}{B}$, the subcarrier will be orthogonal over a duration of T_{sm} [32]. If the baseband frequency of each subcarrier is chosen to be an integer multiple of Δ_f, that is, $k\Delta_f$, for $k = 0, 1, 2, \ldots, N-1$, all subcarriers will have an integer number of cycles per unit time [17]. As a consequence, every subcarrier will be orthogonal with respect to others within the symbol period, and each subcarrier can be considered as a sinusoid. Thus the orthogonal subcarriers of an unmodulated real OFDM signal is given by [17]

$$\psi_k = \begin{cases} \cos(2\pi k \Delta_f t) & \text{for } 0 \leq t \leq T_{sm}, \\ 0 & \text{otherwise.} \end{cases} \tag{2.5}$$

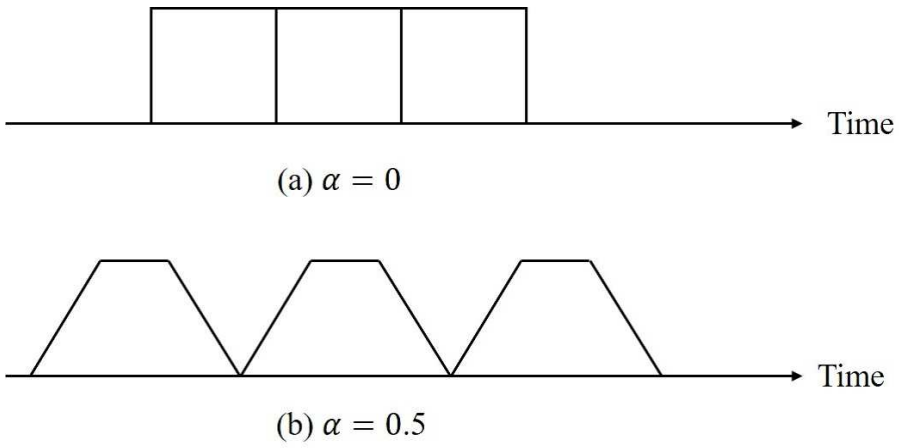

Figure 2.8: Time-limited orthogonal pulses

If two subcarriers $\psi_k(t)$ and $\psi_l(t)$ are orthogonal subcarriers, the following relation will hold:

$$\begin{aligned}\frac{1}{T_{sm}}\int_0^{T_{sm}} \psi_k(t)\psi_l^*(t)dt &= \frac{1}{T_{sm}}\int_0^{T_{sm}} e^{j2\pi k\Delta_f t}e^{-j2\pi l\Delta_f t}dt \\ &= \frac{1}{T_{sm}}\int_0^{T_{sm}} e^{j2\pi (k-l)\Delta_f t}dt \\ &= \delta[k-l],\end{aligned} \tag{2.6}$$

where * represents complex conjugate and $\delta[.]$ is a delta function defined by

$$\delta[k-l] = \begin{cases} 1 & \text{for } k = l, \\ 0 & \text{otherwise.} \end{cases}$$

The orthogonality can also be explained in case of pulses. Two pulses can be called orthogonal if they do not overlap either in frequency or time-domain [33]. To look into this statement, let's consider a transmit pulse with the property

$$\int_{-\infty}^{+\infty} g^*(t)g(t-kT)dt = \delta[k], \tag{2.7}$$

where T is a certain pulse period and $g(t-kT)$ is the time-shifted (k-times shifted by the duration T) version of the pulse $g(t)$. If this condition is satisfied, the corresponding pulses are orthogonal with respect to each other. If the pulse is transmitted at kT time, the output of the detector for the pulse transmitted at time iT will always be zero unless $i = k$. For this reason, the pulses

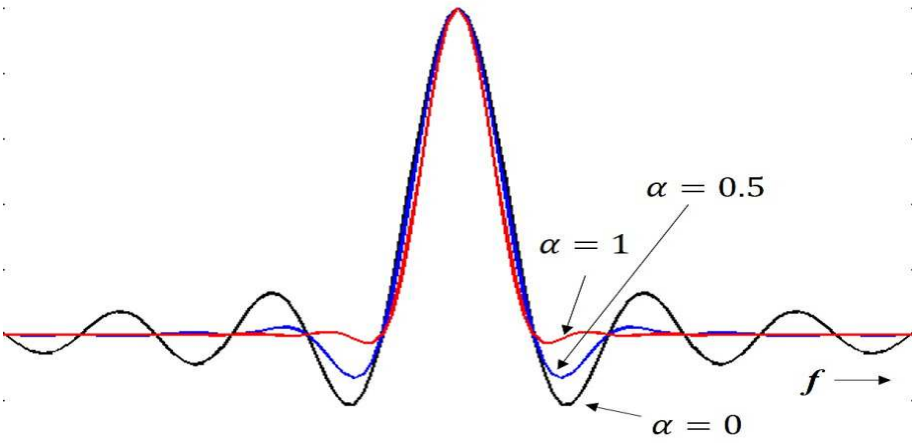

Figure 2.9: Spectrum of a time-limited pulse with different roll-off factors

will not interfere with each others. Fig. 2.8 shows the time-limited pulses that are orthogonal because each of the pulses are time-shifted version of the base pulse. Since the pulses in Fig. 2.8(a) with raised-cosine roll-off factor $\alpha = 0$ are strictly time-limited, their FD versions will stretch infinite; for this reason, such strictly limited pulses are not practically realizable. To limit the spectrum in the FD, $\alpha > 0$ is maintained; for example, $\alpha = 0.5$ shown in Fig. 2.8 is used. Fig. 2.9 shows the spectrum of the orthogonal time-limited pulses for different roll-off factors. The spectrum follows *sinc* function. Pertinently, one base pulse and its periodically time-shifted versions are orthogonal. Since TD and FD are mathematically equivalent, we can state the same condition of orthogonality in the FD.

2.5.2 OFDM Architecture

OFDM signal generation

OFDM signal is formed by a summation of different data symbols multiplied by a respective orthogonal subcarrier. First of all, a bit stream of R bits per second (bps) are divided into a number of group, with each group consists of $log_2(M) \times N$ bits for OFDM systems of N subcarriers and M is the constellation size of the used bandpass modulation. Then, the bits of each group are converted to a set of N complex number following a mapper such as (phase shift keying (PSK), quadrature amplitude modulation (QAM) and so on). Afterwards, input

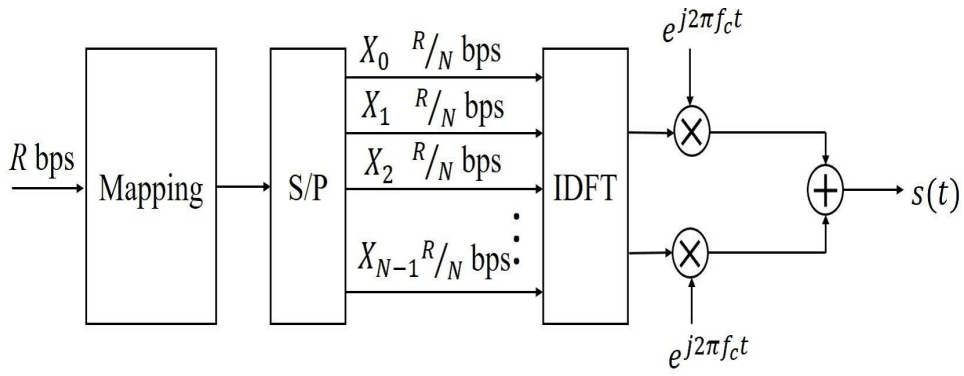

Figure 2.10: OFDM signal generation

data stream of R bps is converted to parallel N streams, with the rate of each parallel stream is $\frac{R}{N}$ bps. Each of the complex numbers are used to modulate a particular orthogonal subcarrier, which is accomplished by multiplying each complex number by a distinct subcarrier. Finally, an OFDM signal is formed by adding all the modulated subcarriers.

Suppose that B is the total bandwidth. B is then equally divided maintaining interval (widely known as subcarrier spacing) Δ_f to generate N subcarriers, with Δ_f and N must be chosen following the conditions in Eq. 2.4 and Eq. 2.2, respectively. Assuming that f_c is the lowest subcarrier frequency, all of the subcarriers' frequencies can be represented as $f_c + k\Delta_f$, where k is an integer ranging from 0 to $N-1$. Suppose that X_k, for k as defined above, is the k^{th} complex number out of the N complex numbers found after the mapping of a particular group of bits. Following Eq. 2.5, OFDM signal can be written as

$$\begin{aligned} s(t) &= \Re\left[\sum_{k=0}^{N-1} X_k \psi_k\right] \\ &= \Re\left[\sum_{k=0}^{N-1} X_k e^{j2\pi(f_c+k\Delta_f)t}\right] \\ &= \Re\left[e^{j2\pi f_c t}\sum_{k=0}^{N-1} X_k e^{j2\pi k\Delta_f t}\right] \\ &= \Re\left[e^{j2\pi f_c t} x(t)\right], \end{aligned} \tag{2.8}$$

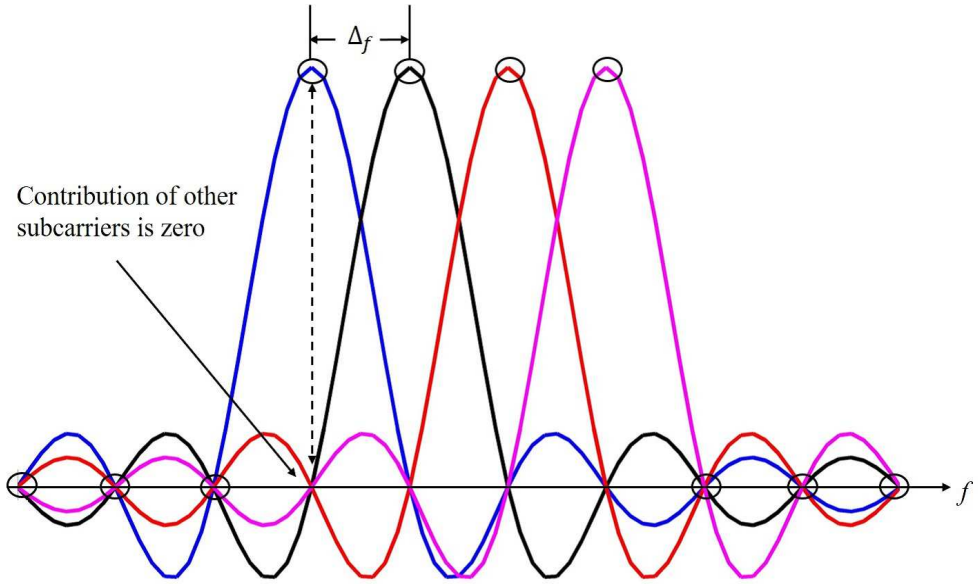

Figure 2.11: OFDM spectrum

where $x(t) = \sum_{k=0}^{N-1} X_k e^{j2\pi k\Delta_f t}$. Now, we sample $x(t)$ with the sampling interval of $\frac{T_{sm}}{N}$. Putting $t = \frac{nT_{sm}}{N}$ and $\Delta_f = \frac{1}{T_{sm}}$ in $x(t)$, we get the samples

$$\begin{aligned} x_n &= x(\frac{nT_{sm}}{N}) \\ &= \sum_{k=0}^{N-1} X_k e^{j2\pi k \frac{1}{T_{sm}} \frac{nT_{sm}}{N}} \\ &= \sum_{k=0}^{N-1} X_k e^{\frac{j2\pi kn}{N}} \\ &= IDFT(X_k), \end{aligned} \tag{2.9}$$

where n is an integer ranging from 0 to $N-1$ and $IDFT$ stands for inverse discrete Fourier transform. It is clear from the above equation that the OFDM signal can be generated using the IDFT operation. Similary, DFT can be used to demodulate the signal. Combining Eq. 2.9 and 2.9, we can conclude that the transmitted signal is the up-converted (following Eq. 2.9) OFDM signal which is generated by the IDFT operation. OFDM signal generation using IDFT is shown in Fig. 2.10. Mapped symbols are undergone a serial-to-parallel (S/P) conversion, followed by IDFT. The baseband OFDM signal is then multiplied by the lowest subcarrier frequency. The IDFT based OFDM signal generation

simplifies the implementation of OFDM system because we no longer require to use filters to generate the subcarriers in the transmitter and separate them at the receiver. Furthermore, the computational complexity can be greatly reduced using computational complexity efficient fast Fourier transform (FFT) and inverse FFT (IFFT). In addition, such systems can be implemented using digital signal processing (DSP) systems, which makes the implementation very simple.

OFDM spectrum

We have already discussed the spectrum of each subcarrier of OFDM in Section 2.5.1. Subcarriers have *sinc*, $\left(sinc(x) = \frac{sinx}{x}\right)$, shape frequency response. For a time-limited raised-cosine pulse, the energy of the corresponding subcarrier's spectrum does not remain confined within the main-lobe; rather, the first five lobes, including the main-lobe, contains almost all energy. Fig. 2.11 shows the spectrum of an OFDM signal with four subcarriers. The spacing between the peaks of two neighboring subcarriers is Δ_f. Thus, the spacing of each subcarrier with respect to any other subcarrier is an integer multiple of Δ_f. Since all subcarriers which are equally time- or frequency-shifted version of a base subcarrier are orthogonal, the subcarriers of the spectrum in Fig. 2.11 are mutually orthogonal.

We can observe from the spectrum that the peak of one subcarrier coincides with the null of the rest of the subcarriers. Utilizing this property of the spectrum, the receiver can perfectly separates all subcarriers even after their overlapping. When an OFDM signal is demodulated using DFT, the spectrum is not continuous as shown in Fig. 2.11; rather, it consists of a set of samples (indicated by small circles). If the DFT is time-synchronized, the frequency samples of the DFT corresponds to the peaks of the subcarriers. Hence, the overlapping of the subcarriers does not cause any problem for the DFT to separate different subcarriers.

OFDM System Model

The system model of an OFDM system is shown in Fig. 2.12. The incoming data are first converted to a set of complex numbers according to any bandpass modulation techniques such as PSK, QAM and so on. Then, the serial data

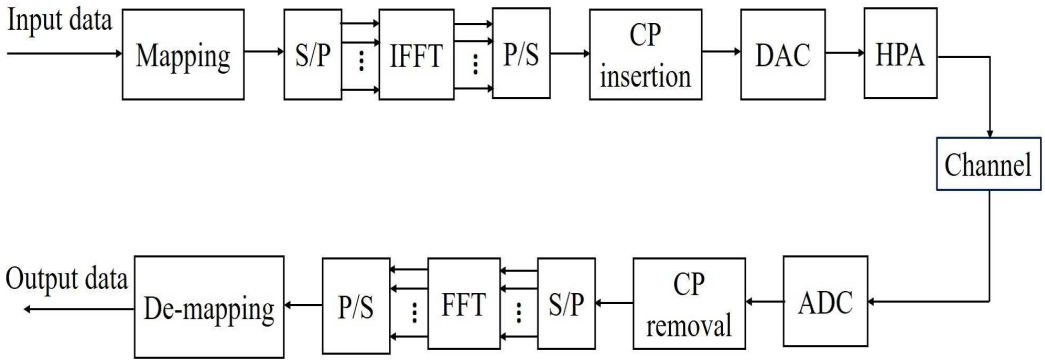

Figure 2.12: OFDM system model

symbols are converted to a parallel data stream with reduced bit rate using a S/P converter. IFFT operation is performed over the parallel data stream to convert the data symbols from FD to TD. Actually, IFFT brings orthogonality among the subcarriers. The IFFT block in the transmitter is sometimes referred to as OFDM modulator. The resulting TD samples stream is then converted back to the serial samples using a parallel-to-serial (P/S) converter. The output of the P/S converter is the baseband OFDM symbol of duration T_{sm}. In some literature, the TD samples set is also called OFDM block. Throughout the thesis, we will call all the TD samples collectively as a OFDM symbol. Then, a cyclic prefix (CP) is added to the serial TD samples , to the serial TD samples , where the CP is the set of a certain number of TD samples copied from the end part of the OFDM symbol and appended to the front end of the OFDM symbol. The purpose of using the CP is to increase the OFDM symbol period so that the effect of ISI can be kept in a tolerable limit. The CP will be discussed in detail later. The CP inserted TD samples are then undergone DAC to produce an analog OFDM signal before it is amplified by a HPA. Finally, the amplified analog OFDM signal is transmitted over a channel.

An OFDM receiver does almost reverse operation of the transmitter. First of all, the received analog signal is converted to digital TD samples by an analog-to-digital converter (ADC), which is followed by the removal of the CP. Then, the serial TD samples are converted to parallel samples before it is sent to the FFT block for OFDM demodulation. The demodulation involves utilizing the

orthogonality among the OFDM subcarriers. It is accomplished as follows:

$$\begin{aligned}\frac{1}{T_{sm}}\int_0^{T_{sm}} x_n e^{j2\pi l\Delta_f t}dt &= \frac{1}{T_{sm}}\int_0^{T_{sm}}\left(\sum_{k=0}^{N-1} X_k\psi_k(t)\right)\psi_l^*(t)dt \\ &= \sum_{k=0}^{N-1} X_k\left(\frac{1}{T_{sm}}\int_0^{T_{sm}}\psi_k(t)\psi_l^*(t)dt\right) \\ &= \sum_{k=0}^{N-1} X_k\delta[k-l] \\ &= X_k\end{aligned} \tag{2.10}$$

Finally, the demodulated parallel samples are converted to a serial sequence of samples before performing a de-mapping to get the original data.

2.5.3 OFDM Transmission over Time Varying Channels

Merits of OFDM modulation have been described in previous sections. In short, it is a highly spectrum efficient modulation, which is achieved by the overlapping of subcarriers and the orthogonality of different subcarriers makes such overlapping possible. The notion of adaptive transmission was illusive before the inception of OFDM. Exploiting the independence of the subcarriers, we can allocate different levels of energy to different subcarriers and vary bandpass modulation types from subcarriers to subcarriers. Such varying energy and/or modulation are used depending on the varying nature of the wireless channel. Because of the property, OFDM has emerged as one of the most robust modulation techniques against the time-varying channels. Furthermore, OFDM signal is not affected by frequency selective fading because of its narrow subcarriers, which simplifies its receiver design. Though the N-times increase in symbol period ($T_{sm} = NT_{ss}$) by the use of narrow subcarriers can greatly reduce the effects of frequency selective fading, its effects still remain in the form of multipath fading which is strong enough to distort the orthogonality among the subcarriers [34], and the loss of orthogonality will result in loss of the benefits of OFDM. Thus it is imperative to take measure to mitigate the effects of the multipath fading.

To eliminate the multipath effects, it is required to make the OFDM symbol period much longer compared to the delay spread. In this endeavor, OFDM

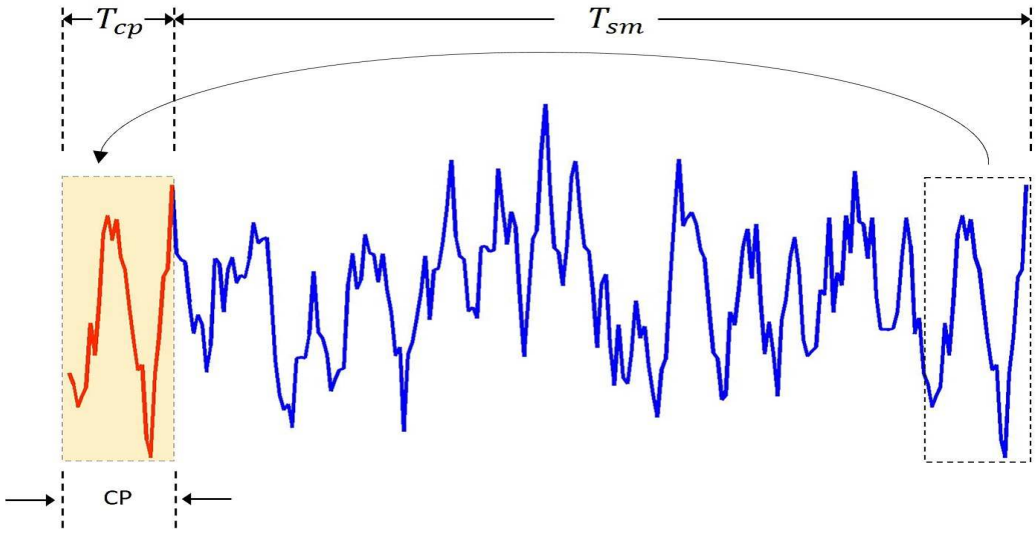

Figure 2.13: Cylic prefix insertion

symbol period is cyclically extended by coping a certain period of the OFDM signal from the end and appending it in front of the symbol. Thus, if the TD samples of the last T_{cp} period of an OFDM symbol of T_{sm} period is copied and appended to the front of OFDM symbol, the resulting extended OFDM symbol period will be $T_{ex} = T_{sm} + T_{cp}$. The procedure of the CP addition is shown in Fig. 2.13. The minimum length of the CP must be equal to the delay spread, that is, $T_{cp} = T_m$. If this condition is maintained, the effect of the multipath, ISI, will be confined within the CP duration of the symbol and the next OFDM symbol will remain unaffected. Fig. 2.14 shows how does CP eliminate the ISI. In the example, we consider a multipath scenario having only two paths for simplicity. Each of the paths provides its own version of the signal. Out of the extended period of the OFDM signal, T_{ex}, the useful period T_{sm} is considered for FFT processing. The FFT processing window starts after the end of CP of the first arrived multipath component. It is indicated in the example as t_s time. Thus, the FFT processing window starts at t_s and continue up to $t_s + T_{sm}$. For a delay spread of T_m, the second multipath component starts arriving at the receiver T_m second later. Thus, a part of the CP of this component falls in the FFT processing window. At time $t_s + T_{sm}$, when the processing window ends, the second component can not arrive completely; rather, a part of the signal, equal to the part of the CP fell inside the processing window, is yet to arrive

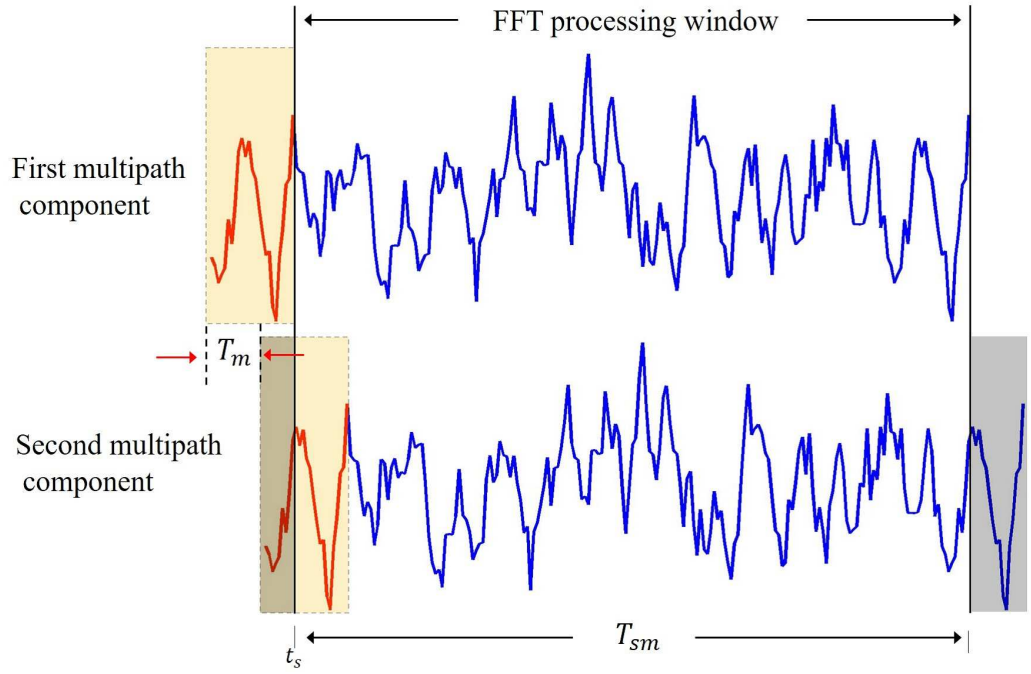

Figure 2.14: Cyclic prefix removal

and is discarded. The windows taken from the two multipath components are not processed separately; rather, they are processed after making one signal by adding them together. Although the sum of the two windows, we will call as aggregate signal, looks quite different from each of them, the original FD signal can be recovered from it because the FFT of the summation will consists of all the frequencies available in the windows. FFT outputs of the two windows and the aggregate signal will consist of the same set of frequencies [35]. Since the aggregate signal contains higher energy compared to the individual versions, the IFFT output generates better quality result. As long as $T_{cp} > T_m$, each multipath component consists of all information of the signal. This avoids the requirement to time synchronise with each multipath component before carrying out decoding. Another way to look into the CP is from the channel impulse response perspective. The received signal is a result of the convolution of the channel impulse response and the transmitted signal. Without CP, a linear convolution occurs between them. Thus, for a transmitted signal of length N and M channel taps, the length of the linear convolution output is $N+M-1$. Then if we repeat a received signal of length $N+M-1$ in a period of N, the end of each signal will overlap over the

start of the next signal. This causes ISI. To overcome such problem, CP is added. The CP converts the linear convolution into a circular one. The length of the output of the circular convolution of the two signals as mentioned before will be N, and the reception of the convolved signal of length N in every N interval does not cause overlapping, hence no ISI. It is pertinent to mention here a downside of adding the CP. Actually, the CP does not carry any information and is discarded at the receiver. Since more energy results in more OPEX, it is a limited-resource. For this reason, the use of CP reduces energy for data transmission, which reduces SNR by factor of $\frac{N}{N+N_{cp}}$, and eventually degrades BER performance [36, 37]. To maintain the BER, it is required to spend more for energy.

2.5.4 Spectrum Efficiency

The spectrum efficiency, S_{eff} of a OFDM system can be formulated in two conditions: with CP and without CP. We will figure out the spectrum efficiency in both cases.

The total number of bits transmitted in each symbol by an OFDM system with N subcarriers is given by:

$$N_b = N \times log_2(M) \tag{2.11}$$

where M is the modulation order. If the symbol period is T_{sm} under the without CP condition, the data rate is given by

$$\begin{aligned} R_{b,wocp} &= \frac{\text{Total number of bits}}{\text{Time duration}} \\ &= \frac{log_2(M)N}{T_{sm}} \\ &= \frac{log_2(M)N}{NT_{ss}} \\ &= \frac{log_2(M)N}{\frac{N}{B}} \\ &= B \times log_2(M), \end{aligned} \tag{2.12}$$

where B is the bandwidth. To get a clear idea about the bandwidth requirement of an OFDM signal, let's consider the spectrum of the OFDM system with four subcarriers (see Fig. 2.11). The aggregate bandwidth of the four subcarriers is

$4\Delta_f$. However, the actual bandwidth that the four subcarriers take is $5\Delta_f$. We can generalize that the aggregate and actual required bandwidths for an OFDM systems with N subcarriers are $B = N\Delta_f$ and $B_a = (N+1)\Delta_f$, respectively. Then we can define the spectrum efficiency of an OFDM system without CP as

$$\begin{aligned} S_{eff,wocp} &= \frac{R_{b,wocp}}{B_a} \\ &= \frac{B}{B_a} log_2(M) \\ &= \frac{N\Delta_f}{(N+1)\Delta_f} log_2(M) \\ &= \frac{N}{N+1} log_2(M). \end{aligned} \tag{2.13}$$

In practical systems, since $N \gg 1$, we can assume that $B \approx B_a$. Under this assumption, the spectrum efficiency becomes

$$S_{eff,wocp} = log_2(M). \tag{2.14}$$

To figure out the spectrum efficiency in the presence of CP of length L_{cp}, let's first find the data rate under this condition:

$$\begin{aligned} R_b &= \frac{log_2(M)N}{T_{ex}} \\ &= \frac{log_2(M)N}{T_{sm} + T_{cp}} \\ &= \frac{log_2(M)N}{NT_{ss} + L_{cp}T_{ss}} \\ &= \frac{log_2(M)N}{T_{ss}(N + L_{cp})} \\ &= \frac{log_2(M)N}{\frac{N+L_cp}{B}} \\ &= \frac{log_2(M)BN}{N + L_{cp}}. \end{aligned} \tag{2.15}$$

Then, the spectrum efficiency in the presence of CP is given by (considering large N),

$$\begin{aligned} S_{eff} &= \frac{\frac{log_2(M)BN}{N+L_{cp}}}{B} \\ &= \frac{1}{B} \times \frac{log_2(M)BN}{N+L_{cp}} \\ &= \frac{N}{N+L_{cp}} log_2(M). \end{aligned} \tag{2.16}$$

It is evident that the use of CP reduces the spectrum efficiency.

2.5.5 Impacts of Null Subcarriers on SNR

In some standards of OFDM, such as IEEE 802.11 a/g/n and IEEE 802.16e, some of the available subcarriers are kept unused by not giving any energy to the subcarriers. Such subcarriers are used for spectral shaping of OFDM symbol, and called null subcarriers or virtual subcarriers. The impact of null subcarriers on SNR will be investigated here. Let's start with the definition of energy per bit, E_b, given by

$$E_b = P_s T_b. \tag{2.17}$$

If R_b is the bit rate, $T_b = \frac{1}{R_b}$. Eq. 2.17 can be written as

$$E_b = \frac{P_s}{R_b}. \tag{2.18}$$

The spectrum efficiency for signal bandwidth, B_s, is defined by

$$S_{eff} = \frac{\texttt{Data rate}}{\texttt{Bandwidth}} = \frac{R_b}{B_s}$$

$$\therefore R_b = S_{eff} B_s \tag{2.19}$$

Putting the value of R_b from Eq. 2.19 to Eq. 2.18, we get

$$\begin{aligned} E_b &= \frac{P_s}{S_{eff} B_s} \\ \therefore P_s &= E_b S_{eff} B_s \end{aligned} \tag{2.20}$$

The noise power spectral density for noise power, P_n, and for noise bandwidth, B_n, is defined as

$$\begin{aligned} N_o &= \frac{P_n}{B_n} \\ \therefore P_n &= N_o B_n \end{aligned} \tag{2.21}$$

we can define SNR as a ratio of signal power to noise power, i.e.,

$$SNR = \frac{P_s}{P_n}$$

From Eq. 2.20 and Eq. 2.21, we can write

$$SNR = \frac{E_b S_{eff} B_s}{N_o B_n} \tag{2.22}$$

If the noise and signal have equal amount of bandwidth, $B_n = B_s$, we get

$$SNR = \frac{E_b S_{eff}}{N_o} \tag{2.23}$$

In decibel (dB), we can write the above equation,

$$SNR = \left(\frac{E_b}{N_o}\right) + 10log_{10}\left(S_{eff}\right) \tag{2.24}$$

Alternative derivation of Eq. 2.24 can be found in [38, 39, 40]. The spectrum efficiency of two-dimensional M-ary modulations (such as MPSK or MQAM) is $log_2(M)$ [39, 40]. Thus, Eq. 2.24 can be written as

$$SNR = \left(\frac{E_b}{N_o}\right)_{dB} + 10log_{10}\left(log_2(M)\right) \tag{2.25}$$

According to [38], SNR is actually E_s/N_o (energy per symbol over noise power spectral density). For this reason, [38] calls the SNR as SNR per symbol while E_b/N_o as SNR per bit. Since the SNR is all about a symbol, the modultion order, M, is needed to know how many bits each symbol consists of.

We will now find the SNR for OFDM system. Let us consider an OFDM system of N subcarriers and all subcarriers carry data. Suppose that the subcarrier spacing is Δ_f, where $\Delta_f = \frac{B}{N}$, where B is the bandwidth. The spectrum efficiency of the OFDM system is given by [36]

$$S_{eff} = \frac{Nlog_2(M)}{N + L_{cp}} \tag{2.26}$$

In practice, CP length, L_{cp}, of an OFDM system is far less than N. Furthermore, the CP is not used in non-fading channel. Thus, we can assume that $L_{cp} = 0$ [41]. Hence, the spectrum efficiency becomes, $S_{eff} = log_2(M)$ which is indentical to that of the 2-D M-ary modulations. Thus, we can say that Eq. 2.25 is valid for an OFDM system which uses all of its subcarriers for data transmission.

Some standards of OFDM (such as WLAN and WiMAX) use null subcarriers. If N_n out of N subcarriers are null subcarriers, the number of used subcarriers $N_{used} = N - N_n$. The signal bandwidth is $B_s = N_{used}\Delta_f$. However, the noise will be available in all subcarriers, so $B_n = N\Delta_f$. Putting the values of signal and noise bandwidth in Eq. 2.22, we get

$$\begin{aligned} SNR &= \frac{E_b S_{eff} N_{used} \Delta_f}{N_o N \Delta_f} \\ &= \frac{E_b}{N_o} \times \frac{S_{eff} N_{used}}{N} \end{aligned} \tag{2.27}$$

Putting $S_{eff} = log_2(M)$, the above equation can be written in dB as

$$SNR = \left(\frac{E_b}{N_o}\right)_{dB} + 10log_{10}\left(log_2(M)\frac{N_{used}}{N}\right) \tag{2.28}$$

To convert $\frac{E_b}{N_o}$ to SNR, Eq. 2.25 is widely used [38, 39, 40, 42]. However, Eq. 2.28 is valid only for OFDM. We can conclude from the above equation that SNR increases compared to the $\frac{E_b}{N_o}$ for higher order modulation and decreases for increased number of null subcarriers.

We will now look into the relationship between $\frac{E_b}{N_o}$ and SNR when null subcarriers are used. Suppose that BPSK modulation is used as the bandpass modulation. For BPSK, $M = 2$. Then, Eq. 2.28 becomes

$$SNR = \left(\frac{E_b}{N_o}\right)_{dB} + 10log_{10}\left(\frac{N_{used}}{N}\right) \tag{2.29}$$

For OFDM systems where all subcarriers are used, $N_{used} = N$; then $SNR = \left(\frac{E_b}{N_o}\right)$. However, in WLAN, $N_{used} = 52$, $N = 64$ and 12 subcarriers are used as null subcarriers. Hence we can write

$$10log_{10}\left(\frac{N_{used}}{N}\right) = -0.91018 \tag{2.30}$$

Eq. 2.29 becomes

$$SNR = \left(\frac{E_b}{N_o}\right)_{dB} - 0.9018 \tag{2.31}$$

Thus, for the WLAN standard with BPSK modualtion, the SNR will be 0.9018 dB less than the corresponding $\left(\frac{E_b}{No}\right)_{dB}$. For this reason, the white noise generated by the AWGN channel for $\left(\frac{E_b}{No}\right)_{dB} = 7$ dB will be equivalent to the noise generated by the AWGN channel for SNR=6.1 dB. For this reason, the extent of BER found for $\left(\frac{E_b}{No}\right)_{dB} = 7$ will be equal to the BER found for SNR=6.1 dB.

2.5.6 Limitations of OFDM

In the previous section, we have discussed about many advantages of OFDM. Despite the advantages, there are some limitations which are unique to the OFDM systems. The limitations will be explained here.

Symbol Time Offset

For proper demodulation of the received OFDM signal by FFT, we need to have a FFT processing window that contains all samples of the OFDM symbol. Determining the correct FFT window largely depends on the detection of the starting times of all multipath components. Any erroneous detection of any component can severely degrade the system performance. The effects are investigated in [43, 44]. The exact detection of the symbol starting point provides a perfect demodulation. The timing errors are classified into two groups: (i) positive errors which occurs if the FFT window consists of a part of the next symbol, and (ii) negative errors which is the capture of a part of the previous symbol. A perfect detection of the starting point results in a perfect demodulation. However, if the start time is detected too early compared to the actual time and the delay spread of the previous symbol is not yet over, the ISI effect will destroy the orthogonality among subcarriers, and ICI occurs. If the delay spread of the previous symbol is over, it will cause no ISI effect but will cause phase rotation that can be corrected using a one-tap FD equalizer. On the other hand, if the starting point is detected a little bit later so that the end of the current symbol occurs during the CP period of the next symbol, the FFT processing window will consist of a major part of the current symbol and a small part of the next symbol, both ISI

and ICI occur. Among the four scenarios, the fourth one is the most challenging to compensate. One way to reduce the possibility of the timing error is to use a large CP. Another way is to use pilot subcarriers with known phases and amplitudes [45]. Estimating the amplitude attenuation and phase rotation, it might be possible to correctly detect the start time.

Carrier Frequency Offset

A baseband OFDM signal is up-converted to passband by a carrier modulator at the transmitter. Receiver needs to perform a corresponding down-conversion to recover the original baseband OFDM signal. This requires to generate the same frequency signal in both sides. Unfortunately, it is quite a difficult (if not impossible) task to generate exactly the same frequency signal using two oscillators. The frequency mismatch greater than 2% causes a severe difference between the two versions of the baseband signals [44]. It degrades the performance of OFDM systems in two ways. Firstly, the spectrums of two neighboring subcarriers can not maintain the equispaced property (Δ_f); as a result, the samples can not be taken at the peak of each subcarrier, which results in the reduction of amplitude of the samples. Secondly, due to the loss of the equispaced property, the orthogonality among the subcarriers is lost by some degree. As a result, ICI occurs. Effect of the carrier frequency offset on BER over AWGN channel is evaluated in [43]. Another reason behind the frequency offset can be Doppler effect. The Doppler effect may change the frequency of a signal after it is transmitted. In this case, the receiver oscillator produces the original transmission frequency. However, since the signal frequency has got changed on the way, a mismatch between the received signal frequency and the oscillator frequency occurs, which results in ICI and amplitude reduction. It has been found that compared to a single carrier modulation, OFDM is much more sensitive to the frequency offset [46].

Non-linearity

OFDM signal can be considered as a summation of N modulated sine waves. When the sine waves get added in phase at a particular instant, the summation at the point becomes much higher than the values at other points. As a result, the ratio of peak power and average power of the resulting signal becomes very

high. To amplify this signal of a large dynamic range, it is required to have an amplifier with a large linear region. However, such an amplifier has very low power efficiency. For this reason, using such amplifier results in an increase of OPEX. To reduce the OPEX, network operators usually prefer to use nonlinear amplifier. Such amplifier works as a linear device for a certain range of input signal amplitude. If the input signal exceeds the range, it operates in nonlinear operating region. In this region, the amplified signal undergoes intermodulation distortion if the input signal consists of multiple frequencies. Since OFDM signal has a very high amplitude range, such signal often forces amplifier to operate in the nonlinear region, thereby experiencing intermodulation distortion. The impact of nonlinearity on the OFDM signal will be investigated next.

The relationship between the input and output of a nonlinear device can be expressed using Taylor's series as follow [47]:

$$y = \sum_{i=0}^{O_d} a_i x^i \tag{2.32}$$

where O_d is the order of the non-linearity, a_i is the coefficient of the i^{th} product and x is the input signal. Usually the non-linearity up to third order is significant in most nonlinear devices; thus, putting $O_d = 3$, we get

$$y = a_0 + a_1 x + a_2 x^2 + a_3 x^3 \tag{2.33}$$

The first term, a_0, is dc voltage which can be neglected without loss of generality[47]. Then Eq. 2.32 can be written as

$$y = a_1 x + a_2 x^2 + a_3 x^3 \tag{2.34}$$

An OFDM signal is a summation of different sinusoids. For the sake of simplicity, let's consider an OFDM system of two subcarriers. Then, $x = v_1 sin(\omega_1 t) + v_2 sin(\omega_2 t)$, where v_1 and v_2 are the amplitude of the first and second sinusoid, respectively, while ω_1 and ω_2 are the frequencies of the first and second sinusoid, respectively. The first term of the right hand side of Eq. 2.34 is given by

$$a_1 x = a_1 \{v_1 Sin(\omega_1 t) + v_2 Sin(\omega_2 t)\} \tag{2.35}$$

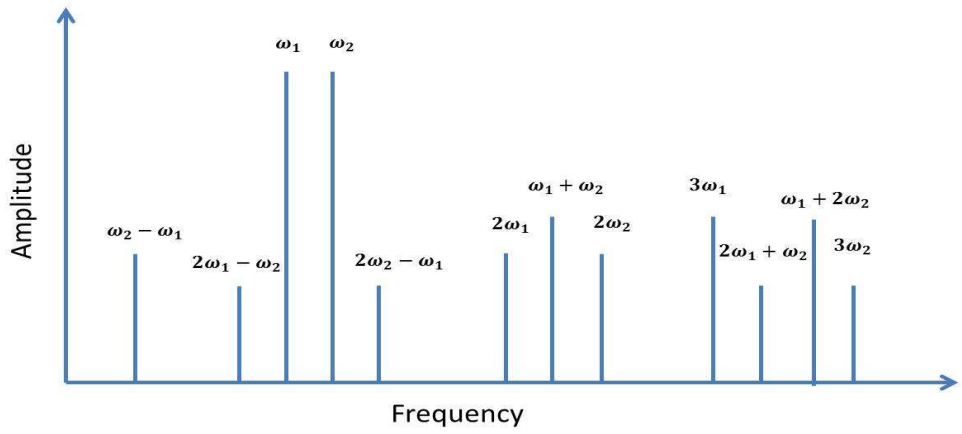

Figure 2.15: Distribution of harmonics and intermodulation products for a third order non-linear amplifier

which is the input signal amplified by a factor of a_1. The second term, which is usually called as the second order intermodulation product or IP2, of the right side of Eq. 2.34 can be written after some manipulations:

$$a_2x^2 = a_2\{\frac{1}{2}(v_1^2 + v_2^2) - \frac{v_1^2}{2}cos(2\omega_1 t) - \frac{v_2^2}{2}cos(2\omega_2 t) + v_1v_2(cos(\omega_1 - \omega_2)t - cos(\omega_1 + \omega_2)t)\} \tag{2.36}$$

This term consists of harmonics and mixed frequencies of ω_1 and ω_2. While $2\omega_1$ and $2\omega_2$ are harmonics, $\omega_1 - \omega_2$ and $\omega_1 + \omega_2$ are mixed frequencies. All these components cause OOB interference. Next, the third term of right hand side of Eq. 2.34 will be figured out. It can be written after few manipulations as follow:

$$\begin{aligned} a_3x^3 = \left(\frac{v_1^3}{2} + \frac{3}{2}v_1v_2^2 - \frac{v_1^2}{4}\right)sin(\omega_1 t) + \left(\frac{v_2^3}{2} + \frac{3}{2}v_1^2v_2 - \frac{v_2^3}{4}\right)sin(\omega_2 t) - \frac{v_1^3}{4}sin(3\omega_1 t) \\ -\frac{v_2^3}{4}sin(3\omega_2 t) - \frac{3}{4}v_1^2v_2sin(2\omega_1 + \omega_2)t - \frac{3}{4}v_1v_2^2sin(2\omega_2 + \omega_1)t \\ -\frac{3}{4}v_1^2v_2sin(2\omega_1 - \omega_2)t - \frac{3}{4}v_1v_2^2sin(2\omega_2 - \omega_1)t \end{aligned} \tag{2.37}$$

In the third term, harmonics are $3\omega_1$ and $3\omega_2$, and the mixed frequencies are $2\omega_1 + \omega_2$, $2\omega_2 + \omega_1$, $2\omega_1 - \omega_2$ and $2\omega_2 - \omega_1$. The distribution of the harmonics

and intermodulation products are shown in Fig. 2.15. Thus, the harmonics of the sum of all the three terms, that is y, are $2\omega_1$, $2\omega_2$, $3\omega_1$,and $3\omega_2$. The intermodulation products are $\omega_1 - \omega_2$, $\omega_1 + \omega_2$, $2\omega_1 + \omega_2$, $2\omega_2 + \omega_1$, $2\omega_1 - \omega_2$ and $2\omega_2 - \omega_1$. The harmonics are out-of-band frequencies and are well separted from the desired frequencies ω_1 and ω_2. These harmonics cause interference to the adjacent frequency bands. On the other hand, the intermodulation products produce in-band as well as out-of-band frequencies. The energy in the in-band frequency causes in-band noise which is very difficult to remove. The in-band noise and adjacent channel interference can be avoided by providing backoff in the power amplifier. However, such backoff reduces power efficiency of the amplifier, which results in the escalation of OPEX and reduction of battery life. Thus, providing backoff is not a desirable solution of the problem from the views of both network operators and users.

Chapter 3

Traditional PAPR Reduction Techniques

In this chapter, the insight of the high PAPR of OFDM system will be described thoroughly. It will be followed by a short survey of the existing PAPR reduction techniques. Then, we will figure out further research scope.

3.1 PAPR

OFDM signal is formed by adding N subcarriers each of which is modulated by a bandpass digital signal such as PSK or QAM modulated signal. If the OFDM signal is generated using IFFT, we can replace each subcarrier by a sine wave with frequency satisfying the orthogonality condition and by multiplying the output of the IFFT by the carrier frequency. In this case, the OFDM signal is formed by adding N sine waves. During the addition, it is highly probable that the waves get added coherently at a certain instant within the symbol period T_{sm}. For an OFDM system with N subcarriers, the peak of the complete coherent addition causes the peak of the resultant signal equal to N. Fortunately, the possibility of the complete coherent addition is negligible; rather, most of the sinusoids may get added coherently and the amount of coherency may differ from time to time. Although there are very few points within the symbol interval where the partial coherent addition occurs, one of the points results in the peak power in the resultant OFDM signal. Such peak power is much more higher than the power of the signal at the rest of the period of the symbol. Although the average

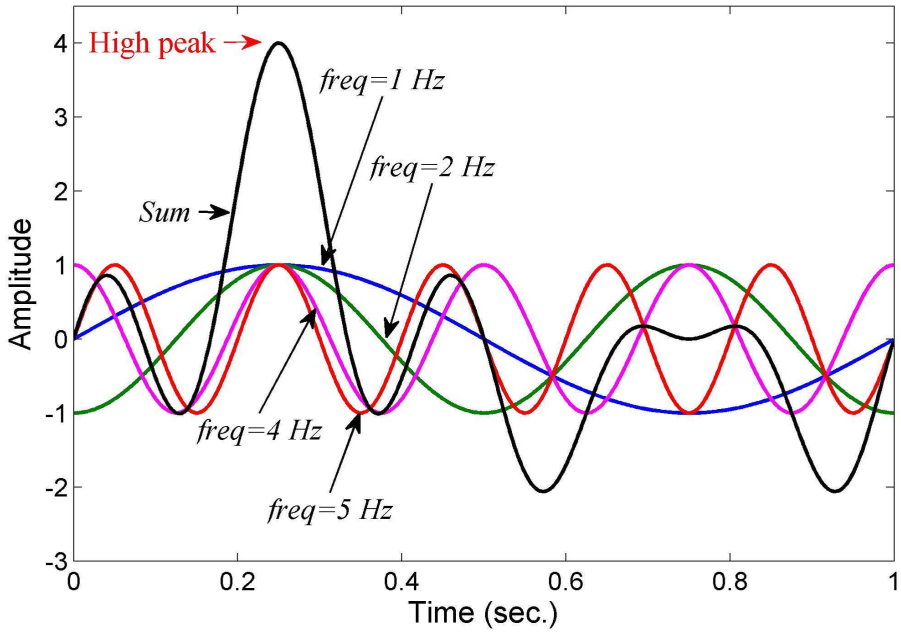

Figure 3.1: High peak of OFDM due to the summation of sinusoids

power of the summation remains unchanged irrespective of the frequencies of the individual sine waves, the high peak power results in a high ratio of the peak-to-average power of the signal. An example of how does high peak occur is shown in Fig. 3.1 for four sinusoids which satisfy the orthogonality condition. Although the maximum amplitude of each sinusoid is 1, the peak amplitude of the sum signal is four times higher because of the coherent addition of all sinusoids at time 0.25 second. Another observation is that such high peak occurs very rare within the signal. The average power of each sinusoid and the sum signal are 0.5 and 2, respectively. While the peak power of each sinusoid is 1, it is 16 for the sum signal. Thus, PAPR of the sum signal is 8, which is 4-times higher compared to that of the individual sinusoid.

When the sum signal is applied as an input to a HPA, the high peak at time 0.25 will drive the HPA to its non-linear region, which will cause signal distortion and sprectral spreading [48]. These result in BER degradation and ACI, respectively. Furthermore, if one decides to use a DAC with range 0-2, it will not be able to accommodate the signal value at time 0.25 second; Thus, it will be required

to use a large-range DAC, which is very expensive. The high PAPR affects the efficiency of the HPA as well. The input signal of a HPA should be such that the resulting output signal does not enter the non-linear region. If it enters, a signal clipping will occur. To avoid such clipping, the input to the HPA is adjusted by providing input back-off (IBO) which is directly related to the PAPR of the input signal and the HPA efficiency, with a large PAPR requires more IBO which in turn reduces the efficiency. Although a class A HPA can have a maximum of 50% efficiency [49], the large PAPR reduces it in the following manner [50]

$$\eta = \frac{0.5}{PAPR}. \tag{3.1}$$

If we consider Fig. 3.1, the sum signal reduces HPA efficiency to only 6.25% from 25% which could be achieved for the individual sinusoid. The efficiency reduction will result in more power wastage, hence more OPEX.

If N is large enough, according to the central limit theorem, an OFDM signal x_n, defined in Eq. 2.9, follows a complex Gaussian process [51]. In other words, both real and imaginary parts of the samples x_n are Gaussian distributed. Its amplitude has Rayleigh distribution with zero mean and variance which is N-times the variance of one complex sine wave. However, the power of an OFDM signal follows exponential distribution. PAPR of an OFDM system of N subcarriers is defined mathematically as:

$$PAPR = \frac{max(|x_n|^2)}{E\left\{|x_n|^2\right\}}, \tag{3.2}$$

where $|x_n|^2$ is the power of the n^{th} sample and $E\left\{|x_n|^2\right\}$ is the expected value of $|x_n|^2$, where n is an integer satisfying $0 \leq n \leq N-1$. If samples are taken at the Nyquest rate (that is, N samples), the computed peak may not coincide with that of the corresponding continuous-time waveform [52]. To improve the accuracy of determining the peak value, NL samples are taken, where L is an integer called as oversampling factor. The oversampling factor having a value of at least 4 can provide a good approximation of the continuous-time waveform [53]. When the oversampling is carried out, Eq.2.9 becomes

$$x_n = \frac{1}{NL} \sum_{k=0}^{NL-1} X_k e^{j2\pi kn/(NL)}. \tag{3.3}$$

A detail explanation about the relationship of the PAPR of a continuous and discrete OFDM signals is provided in [52, 54]. The PAPR discussed up to now is the PAPR of a baseband OFDM signal. To figure out a relation of the baseband PAPR with the passband PAPR, let's recall Eq. 2.8

$$\begin{aligned} s(t) &= \Re\left[x(t)e^{j2\pi f_c t}\right] \\ &= \Re\left[x(t)\right] cos(2\pi f_c t) + j\Im\left[x(t)\right] sin(2\pi f_c t) \\ &= x_I(t)cos(2\pi f_c t) + x_Q(t)sin(2\pi f_c t). \end{aligned} \tag{3.4}$$

Since $f_c \gg N\Delta_f$, we can say from Eq. 3.4 that the peak of the passband signal equals to that of the baseband signal [55], i.e.,

$$max(|x(t)|) \approx max(|s(t)|). \tag{3.5}$$

For a bandpass modulation such as QAM,

$$E\left(|x_I(t)|^2\right) = E\left(|x_Q(t)|^2\right) = \frac{E\left(|x(t)|^2\right)}{2}. \tag{3.6}$$

From Eq. 3.4, the average power can be written as

$$E\left(|s(t)^2|\right) = \frac{E\left(|x_I(t)|^2\right)}{2} + \frac{E\left(|x_Q(t)|^2\right)}{2} = \frac{E\left(|x(t)|^2\right)}{2}. \tag{3.7}$$

Combining Eq. 3.5 and Eq. 3.7, we can define the PAPR for the passband signal, which is given by

$$\begin{aligned} PAPR_{PB} &= \frac{max\left(\left(|s(t)|^2\right)\right)}{\frac{E\left(|x(t)|^2\right)}{2}} \\ &= \frac{2max\left(\left(|x(t)|^2\right)\right)}{E\left(|x(t)|^2\right)} \\ &= 2PAPR. \end{aligned} \tag{3.8}$$

Thus, the PAPR of a passband OFDM signal is twice (3 dB higher) of the PAPR of the corresponding baseband OFDM signal. Throughout the thesis, PAPR will refer to the baseband PAPR.

In last two decades, a lot of proposals to solve the high PAPR problem is presented, which will be discussed in next section. However, not all techniques are suitable for all conditions. Each of them has its strength and weakness. There are several performance criteria against which a PAPR reduction scheme is evaluated. Each of the criteria is explained next.

A. Complementary cumulative distribution function: The complementary cumulative distribution function (CCDF) is used to measure the capability of a PAPR reduction technique in reducing the PAPR. It gives the probability of an OFDM signal's envelope exceeding a certain PAPR value within the OFDM symbol period [11]. Mathematically, it is defined by

$$CCDF[PAPR(s(t))] = P_r(PAPR(s(t)) > PAPR_o), \tag{3.9}$$

where $PAPR_o$ is the threshold PAPR. The CCDF indicates the probability of the OFDM signal $s(t)$ having PAPR greater than the threshold PAPR, $PAPR_o$. Since the power distribution of an OFDM signal follows exponential distribution, the cumulative distribution for peak power per OFDM signal can be expressed as

$$CDF(PAPR_o) = 1 - e^{-PAPR_o}. \tag{3.10}$$

If the ratio of each sample power to the average power of an OFDM signal is lower than the threshold $PAPR_o$, we can say that the OFDM signal's PAPR is below the threshold. If sampling is carried out following the Nyquest criteria, the samples are mutually independent. Under this condition, it can be written as [56, 57]:

$$CDF(PAPR < PAPR_o) = \left(1 - e^{-PAPR_o}\right)^N. \tag{3.11}$$

The above equation is valid as long as the samples are mutually independent. When oversampling is performed, the condition is no longer valid. In this case, the distribution of an oversampled OFDM signal with N subcarriers is represented by the distribution of a Nyquest sampled OFDM signal with αN subcarriers [56]. Thus, for the oversampling, Eq. 3.11 becomes

$$CDF(PAPR < PAPR_o) = \left(1 - e^{-PAPR_o}\right)^{\alpha N}, \tag{3.12}$$

where $\alpha = 2.8$ [56]. It also reveals that PAPR increases with the increase of the number of subcarriers used in an OFDM system. However, α has been estimated to 4 in other references [53]. We can express the probability of an OFDM signal with PAPR greater than the threshold in the following way:

$$CCDF(PAPR > PAPR_o) = 1 - \left(1 - e^{-PAPR_o}\right)^{\alpha N}. \tag{3.13}$$

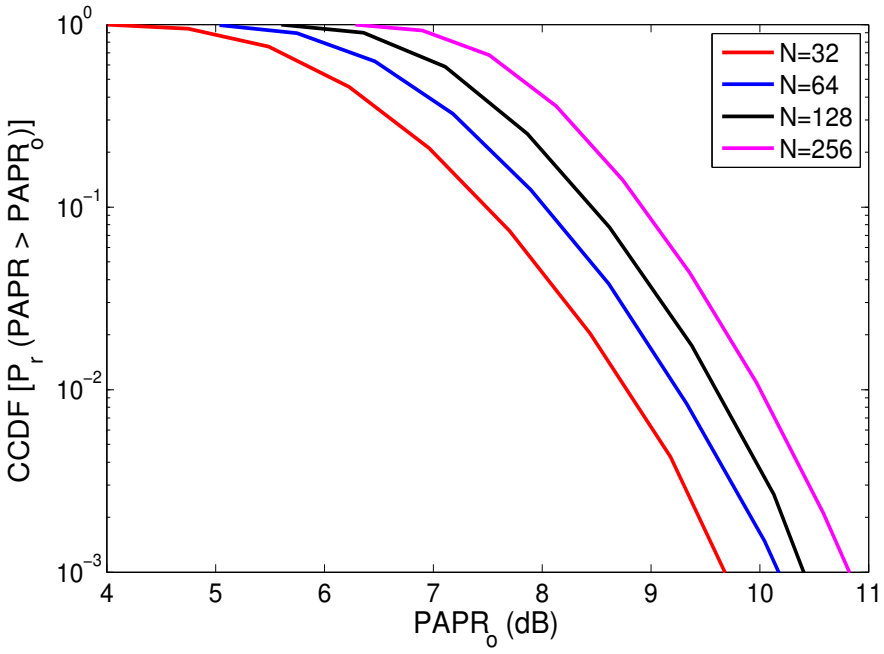

Figure 3.2: Impact of the number of subcarriers on CCDF

The main focus of a PAPR reduction technique is to reduce the CCDF. It is clear that the CCDF is affected by the number of subcarriers used in an OFDM system. The impact of the number of subcarriers on CCDF is investigated in Fig. 3.2 for oversampling factor $L = 2$. It reveals that twice the number of subcarriers increases CCDF by 15%. The impact of the oversampling factor on CCDF is shown in Fig. 3.3 for 128 subcarriers. The oversampling can approximate continuous-wave better, this results in higher CCDF. Two-times oversampling provides a significant increase in CCDF; However, more increase in the oversampling factor does not increase the CCDF considerably.

B. Bit error rate: While the CCDF measures the level of PAPR of a signal in terms of probability, BER indicates the effect of reducing PAPR on the data rate. Many schemes reduce PAPR by distorting signal structure. For proper BER, a perfect recovery of the original signal structure is required. Practically, many PAPR reduction schemes can not recover the original structure completely, thereby increasing BER. There are another group of PAPR reduction schemes which need to send SI to the receiver. If the SI is not received with 100% accuracy,

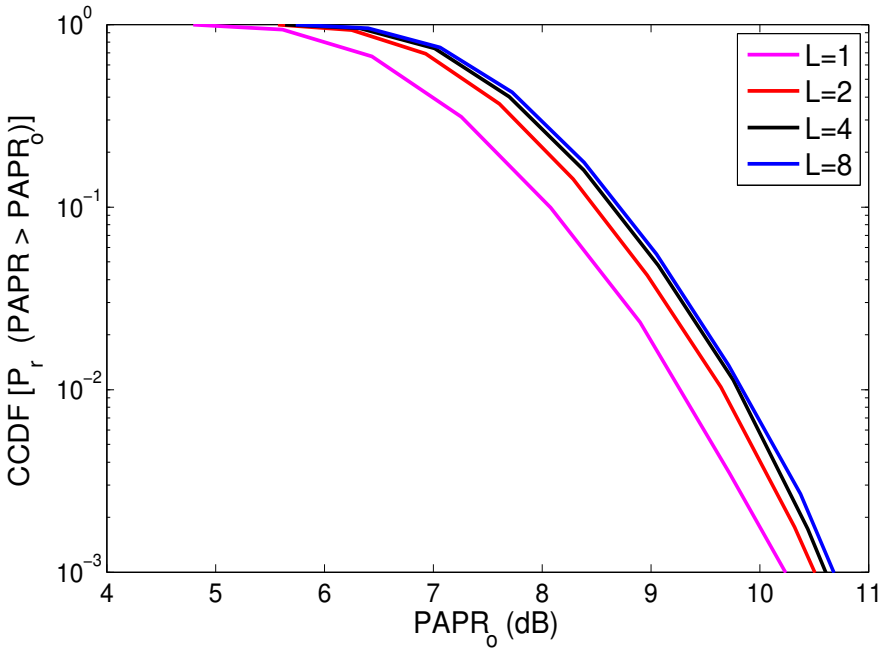

Figure 3.3: Impact of oversampling factor on CCDF

the reverse operation of the PAPR reduction method can not be carried out; this also incurs BER degradation.

C. Signal average power: Some PAPR reduction techniques increase average power of the signal to get the reduced PAPR. To support the increased power, the transmission cost goes up. Furthermore, if the linear region of the HPA is not stretched to accommodate the signal, the output enters the non-linear region which causes signal distortion. In addition, the HPA with a large linear region is very expensive. Moreover, such techniques are not suitable for energy-constrained devices such as any kind of portable devices.

D. Spectral spreading: High PAPR causes more clipping by the HPA used in the transmitter. There are some PAPR reduction techniques which perform a deliberate clipping to reduce the PAPR. Such clipping causes increased IB noise and out-of-band (OOB) distortion. While the IB noise increases BER, the latter one results in energy leakage of one symbol to its neighboring symbols

which escalates ACI. More clipping results in more ACI. If the PAPR is reduced avoiding the deliberate clipping, such non-linearity effects can be reduced.

E. Computational complexity: The computational complexity involved in a technique is very important in system performance because higher computational complexity reduces the speed of a system. To overcome such problem, it is required to use high speed hardware. Unfortunately, such hardware is very expensive. For this reason, it is highly desirable to reduce the PAPR with minimum rise of the computational overhead.

F. Throughput loss: There are many PAPR reduction schemes which require to send SI to the receiver to perform a reverse operation of the PAPR reduction technique, used in the transmitter, for proper data recovery. This requires to reserve a part of the available bandwidth for the SI transmission. Thus, the bandwidth for data transmission reduces, which decreases throughput of the system. There are some other techniques which sends some non-information bearing bits for the PAPR reduction. This also reduces the amount of information bits, hence the throughput. If N_s out of N subcarriers are used for PAPR reduction or SI transmission, the spectrum efficiency loss is given by (using Eq. 2.16)

$$\begin{aligned} S_{eff,loss} &= \frac{log_2(M)N}{N+L_{cp}} - \frac{log_2(M)(N-N_s)}{L+L_{cp}} \\ &= \frac{N_s}{N+L_{cp}} log_2(M). \end{aligned}$$

3.2 Conventional PAPR Reduction Techniques

The high PAPR issue is a long-standing problem of OFDM. Since mid-90s, there has been a plethora of research work to find an efficient solution of the problem. In this section, we will present a short survey of the PAPR reduction techniques. A broad classification of the techniques is provided in Fig. 3.4. All techniques can be categorised into three different broad groups: signal distortion, multiple signaling and coding. Each of the group with some examples with be described next.

3.2.1 Signal distortion based PAPR reduction

There are some PAPR reduction techniques which work on TD samples of OFDM. Such techniques change energy distribution (by changing the total signal energy), produced by IFFT, among the TD samples to reduce the PAPR, thereby distorting the OFDM signal. For this reason, this group of PAPR reduction techniques are widely called as signal distortion PAPR reduction techniques. As shown in Fig. 3.4, there are four techniques in the group, each of which will be described next shortly.

Clipping and filtering

The simplest method to reduce the PAPR of an OFDM signal is to clip the amplitude of those samples which are higher than the threshold before the signal goes to the HPA. The clipping technique acts as a soft limiter whose output is given by [58]

$$\overline{x}_n = \begin{cases} x_n & \text{for } |x_n| \leq A_{th} \\ A_{th} e^{j\angle x_n} & \text{for } |x_n| > A_{th}, \end{cases} \tag{3.14}$$

where A_{th} is the threshold amplitude and $\angle(x_n)$ indicates the angle of the n^{th} sample. That is, if the sample amplitude is greater than the threshold, it replaces the sample amplitude by the threshold while keeping its angle unchanged. Since this technique shades some samples' energies, it generates IB noise and OOB interference [59]. While the IB noise can not be removed [60], hence causes BER degradation, the OOB interference can be reduced by filtering. However, the filtering process can cause peak regrowth so that the signal amplitude at some points exceeds the threshold [61]. To avoid the peak regrowth, several repeated clipping and filtering based techniques are proposed [62, 63]. However, such techniques suffer from extremely high computational complexity.

Peak Windowing

Peak windowing is performed by multiplying the OFDM signal by a weighting function, called window function, to reduce PAPR and decrease OOB distortion [4, 64, 65]. The multiplication is done in such a way that a valley of the window function gets multiplied with the peak of the OFDM signal and vice-versa. The window function should be narrowband and short in TD [56]. Examples of such

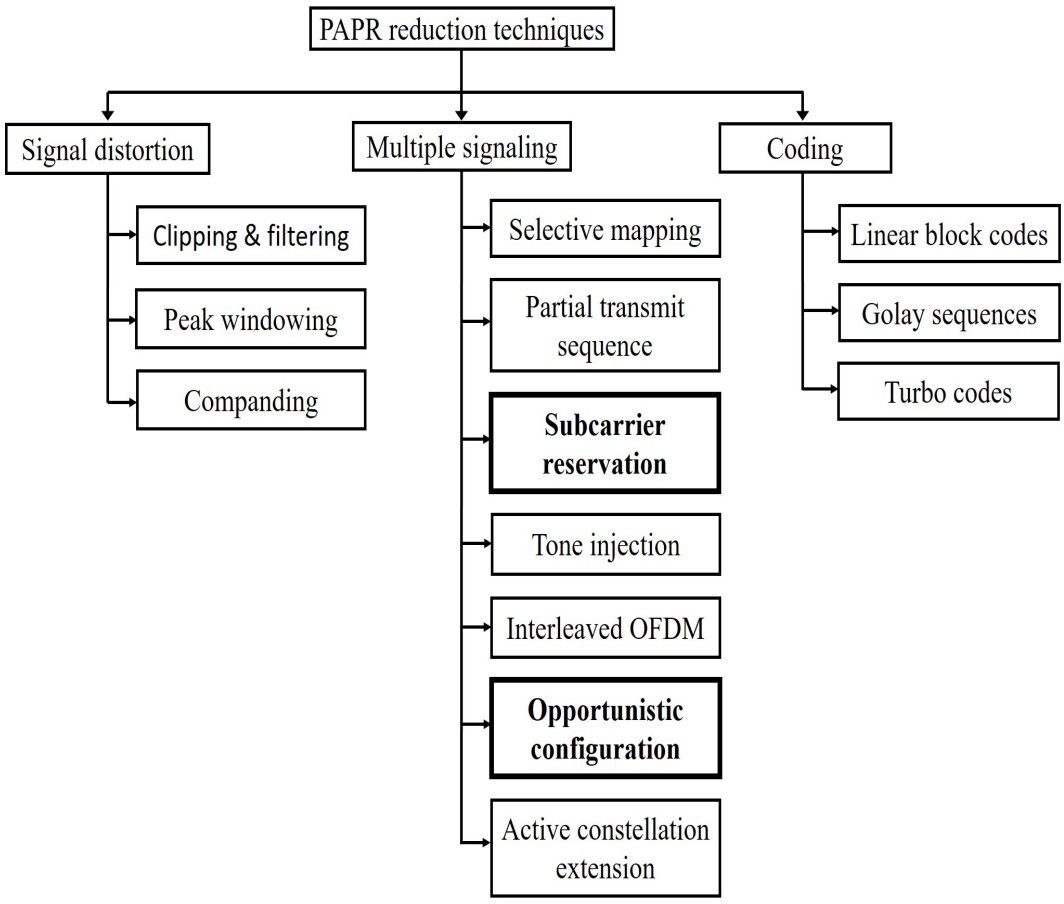

Figure 3.4: Classification of OFDM PAPR reduction techniques

windows include Hamming, cosine, Kaiser window and so on. A general block diagram of the window technique is shown in Fig. [4]. The windowing processing limits peaks in much smoother way compared to the clipping, thereby reducing distortion. However, the remaining OOB after the windowing operation is still much higher than that of the unmodified OFDM.

Companding

The companding is usually used in speech processing for restricting speech amplitude within a certain limit so that all samples of the signal can be represented by a pre-determined number of bits. There is a similarity between the speech and OFDM signals in the sense that high peak compared to the average power occurs infrequently in both signals. The high peak also a problem in OFDM

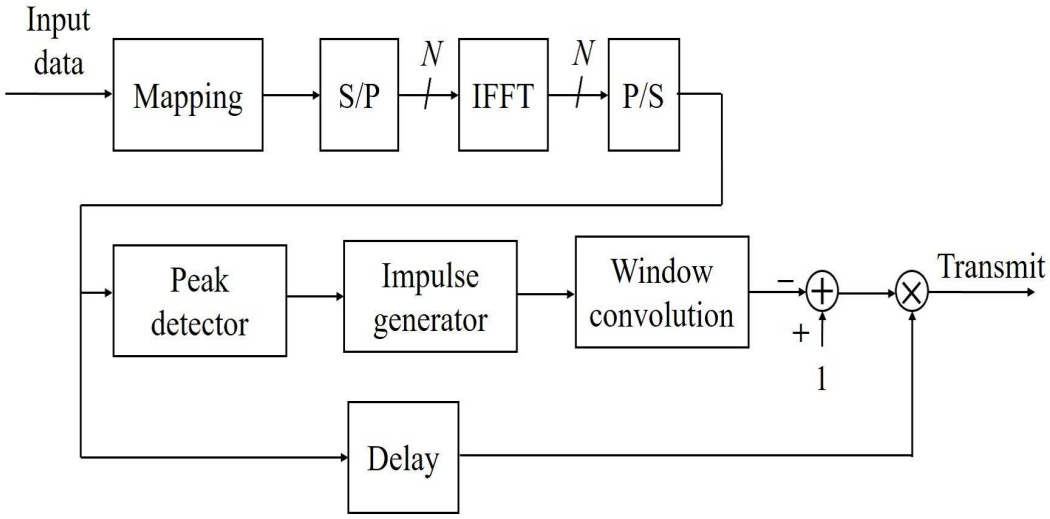

Figure 3.5: Block diagram of peak windowing technique [4]

just like in speech processing. For this reason, researchers have come up with an idea of utilizing the companding processing to reduce the peak of the OFDM signal [66, 67]. The companding based PAPR reduction techniques attain very good PAPR reduction. Their computational complexity is very less. Another interesting feature is that they do not require to send SI, hence no spectrum efficiency loss. Some examples of the companding for OFDM signal is described next.

One of the most investigated compandings for PAPR reduction is μ-law companding defined by [68, 69]

$$x_n^c = \frac{A_c \; sgn(x_n) \; log\left(1 + \mu \left|\frac{x_n}{A_c}\right|\right)}{ln(1+\mu)}, \tag{3.15}$$

where x_n^c is the companded version of the sample x_n, A_c is a normalized constant such that $0 \leq \left|\frac{x_n}{A_c}\right| \leq 1$, and $sgn(.)$ and μ are sign function and companding parameter, respectively. This companding increases the signal average power only while keeping the signal peak unchanged. Due to the increase of the average power, PAPR gets reduced. At the receiver, signal is decompanded to get the original signal according to [68]

$$\overline{x}_n = A_c \frac{e^{\frac{r_n \; log(1+\mu)}{A \; sgn(r_n)}} - 1}{\mu \; sgn(r_n)}, \tag{3.16}$$

where $\overline{x}_n$ is recovered x_n from the received sample r_n. Such companding technique suffers from BER. The signal expansion by the decompanding amplifies channel noise as well [70]. This further degrades the BER. Furthermore, the OOB escalates significantly compared to the unmodified OFDM.

To reduce the average power increase, found in the μ-law companding, a companding based on error function is proposed in [71] where the companded signal is given by

$$x_n^c = k_1 \; erf \; (k_2 x_n), \tag{3.17}$$

where the coefficients k_1 and k_2 depends on the OFDM signal statistics. In this companding, the high peaks are compressed and low sample values are expanded. It transforms the Gaussian distributed OFDM signal into a quasi-uniform distributed signal. Some techniques perform the companding by converting the Rayleigh distributed OFDM envelope into uniform distributed [72] and trapezium distributed signals [73]. There are many other work based on companding technique which can be found in [11]. However, all techniques suffer from BER increase, mean power escalation and OOB degradation in varying degrees.

3.2.2 Multiple Signalling

PAPR reduction techniques of this group produce multiple versions of the OFDM signal by modifying the FD signal. Then the OFDM signal having the lowest PAPR is transmitted. At the receiver, a reverse operation is performed on the received FD signal to recover the original FD signal. Since the techniques of this kind carry out all operations in the FD signal, they do not distort the OFDM signal. For this reason, there is no IB and OOB degradation unlike the clipping and companding techniques. Furthermore, it achieves OOB improvement in the presence of a HPA due to the PAPR reduction. However, most of the techniques of this group suffers from spectrum efficiency degradation.

Selective Mapping

The Selected mapping (SLM) is a very popular PAPR redcution technique because of its simplicity. In SLM, a number of OFDM signals are generated for

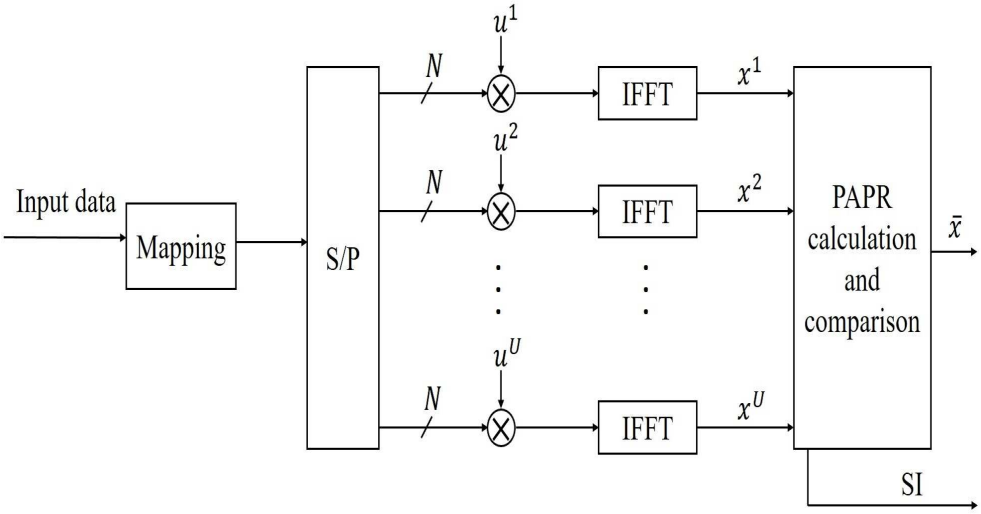

Figure 3.6: Block diagram of selective mapping technique

the same data sequence and the sequence having the lowest PAPR is transmitted [74, 75]. The incoming data is first converted to a sequence of N complex numbers using a mapping technique before it is converted to a parallel sequence with low data rate. The parallel stream is then multiplied (element-by-element) by U phase sequences (one sequence at a time) with each sequence is of length N, where U is an integer and N is the number of subcarriers. Each phase sequence can be defined as $u^i = e^{\sqrt{-1}\theta_{i,j}}$, where $1 \leq i \leq U$ and $1 \leq j \leq N$. These multiplications produce U versions of the original parallel stream, with each sequence contains the same information but with shifted phase. Then each of the sequences is undergone IFFT to produce a corresponding TD OFDM signal, x^i. These U TD signals have different PAPRs which are computed next. Then the TD signal that has the lowest PAPR is selected for transmission. The extent of the PAPR reduction depends on U and the phase sequence generation.

One important point is that the transmitted signal is the TD samples of a phase shifted version of original FD complex numbers. Which phase sequence out of the U candidate sequences has produced the transmitted signal is required at the receiver to recover the original FD complex numbers. For this reason, usually the value of i that gives the lowest PAPR TD samples is transmitted to the receiver as SI. To transmit the SI, SLM needs to send $log_2(U)$ bits. It requires

to reserve a portion of the available bandwidth to transmit the $log_2(U)$ bits. A perfect transmission is required for proper recovery of the FD signal. For this reason, a high rate coding and smaller constellation are required to use. This further increases the number of overhead bits. For example, if $U = 16$ and $\frac{1}{2}$-rate convolution code is used for sending the SI, the number of SI bits becomes 8. If BPSK modulation is used for the SI transmission, we need to reserve eight subcarriers for the SI transmission. The spectrum efficiency of OFDM is defined by Eq. 2.16

$$S_{eff} = \frac{log_2(M)N}{N + L_{cp}}, \tag{3.18}$$

where M is the constellation size. Thus, the SI transmission reduces the spectrum efficiency by 12.5% for the CP length of $\frac{N}{16}$.

The SLM technique has been modified to improve its performance in terms of PAPR reduction , computational complexity and SI-free transmission. In [76, 77], modified SLM techniques are proposed with new phase sequence generations which attain more PAPR reduction. Since the computational complexity of the SLM technique is a major bar in its practical implementation, a number of low-complex SLM techniques are proposed [78, 79]. In addition, there are some modified SLM techniques to remove the necessity to transmit SI [80, 81]. Although such techniques can effectively overcome the spectrum efficiency loss, they incurs excessive computational overhead.

Partial Transmit Sequence

The partial Transmit Sequence (PTS) technique divides the incoming data into a number of disjoint sub-blocks and produces a sequence of TD samples of length N for each sub-block using IDFT. Then each sequence of TD samples are multiplied by a phase factor so as to reduce PAPR of the resultant OFDM signal which is obtained by summing all TD sample sequences [82, 83]. Figure 3.7 shows the block diagram of the PTS technique. For greater detail, suppose that $X = [X_1\ X_2\ X_3 \ldots X_N]$ is a vector of N complex numbers representing the incoming data sequence. Then X is divided into U disjoint sub-blocks, X^i for $1 < i < U$, with each block consists of $\frac{N}{U}$ complex numbers. The blocks are generated in such a way that $X = \sum_{i=1}^{U} X^i$. Then, each of the sub-block is converted to a

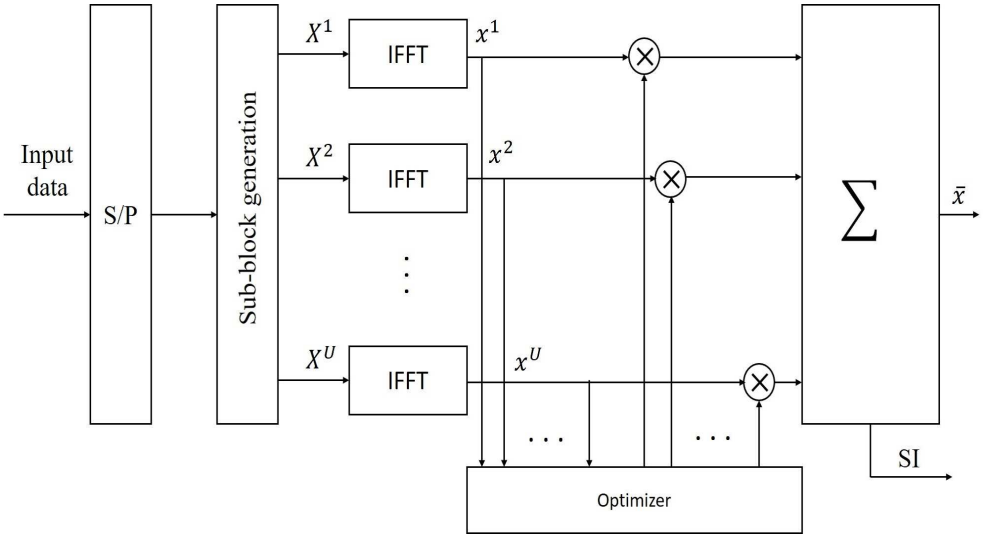

Figure 3.7: Block diagram of partial transmit sequence technique

sequence of TD samples by the IDFT operation. Each TD sample sequence is multiplied by a phase factor $b_i = e^{\sqrt{-1}\theta_i} = e^{\sqrt{-1}\,2\pi k/W}$ for k is an integer ranging from 0 to $W-1$ and W is the number of allowed phase factors, which is followed by an addition of all multiplied sequences. That is, $x = \sum_{i=1}^{U} b_i x^i$, where x^i is the TD version of the FD sub-block X^i. Then, PAPR of x is computed and stored. In the next iteration, a new phase sequence set b_i is generated in such a way that PAPR reduces. So, the objective is to find an optimum phase factor vector that will provide the desired PAPR. Setting $b_1 = 1$, the rest $U-1$ phase factors are searched exhaustively to achieve the lowest PAPR signal. The extent of the PAPR reduction and computational complexity depend on the phase factor vector. The receiver requires the phase factor vector to recover the original TD samples. For this reason, it also requres to send the phase factor vector to the receiver as SI. Similar to the SLM technique, PTS also suffers from spectrum efficiency degradation. The amount of the SI for this technique is $log_2 W^{U-1}$ bits [84]. For $U = 16$ and $W = 2$, the number of SI bits is 16. If a $\frac{1}{2}$-rate coding and BPSK modulation are used for the SI transmission, we need to transmit 32 bits which requires to reserve 32 subcarriers. For $N = 64$, this reduces 50% spectrum efficiency.

The PTS technique can effectively reduce PAPR. However, one problem with the PTS is its high computation complexity because of the exhaustive search for the optimum phase factor vector. The complexity increases exponentially with increase of the number of sub-blocks. To reduce the complexity, several algorithms for modifying the PTS technique are proposed [85, 86, 87]. Furthermore, PTS technique is also modified to improve its spectrum efficiency [88, 89]. However, a degradation of BER performance is experienced in the spectrally-efficient design.

Subcarrier reservation

As the name implies, this group of PAPR reduction techniques reserve a certain number of subcarriers for PAPR reduction and hence they carry no data, thereby reducing data rate. Two widely known techniques of this kind are tone reservation (TR) and dummy sequence insertion (DSI).

Tone reservation: It was initially proposed fo digital subcarrier line (DSL) where subcarriers are usually called as tones [55]. In OFDM perspective, it can be termed as subcarrier reservation. In TR technique, a total N subcarriers are divided into two disjoint groups: R and R^c, that is, if the k^{th} subcarrier $S_k \in R$, $S_k \notin R^c$, and $R < R^c$. Suppose that R consists of N_R subcarriers, then R^c consists of the rest $N - N_R$ subcarriers. Also suppose that C is a vector of length N whose N_R elements are non-zero, and X is another vector of length N whose $N - N_R$ elements are non-zero. In addition, if the k^{th} element of C, $C_k = 0$, $X_k \neq 0$. The non-zero entries of C and X correspond to the values assigned to the subcarriers of the R and R^c groups, respectively. Each non-zero entry of X consist of a complex number which represents a bandpass modulated data.

In TR, the R group of subcarriers are called peak reduction carriers (PRCs) which carry no data and are solely used for PAPR reduction. The TD version of C, c, is added to the TD version of X, x, to change the statistical properties of x in order to reduce PAPR of x. Then, the resulting OFDM signal can be written as

$$\overline{x} = x + c = IDFT(X + C). \tag{3.19}$$

If the sample x_k has large amplitude, the amplitude of the sample $\overline{x}_k$ can be reduced by setting the phase of c_k to opposite (near opposite) phase of x_k. To

do this, C should be modified in such a way that the phase of the x_k becomes opposite to that of the x_k. Thus, the objective is to find c that reduces the peak of x [11], that is,

$$\min_{c}||x+c||_{\infty} = \min_{C}||X+C||_{\infty}, \tag{3.20}$$

where $||.||_{\infty}$ indicates the infinity norm. The non-zero entries of C are determined using a convex optimization, which is a linear programming problem with complexity $O(RN^2)$ [90]. This makes the TR technique practically infeasible to implement. The extent of the PAPR reduction depends on N_R, locations of the subcarriers and the computational complexity of the optimization algorithm [11]. The locations of the PRCs are required to be known to the receiver to separate the data subcarriers. This requires to send the locations of the PRCs to the receiver. For applications such as WLAN, where $N = 64$ only, N_R will be a significant number which considerably reduces the number of data subcarriers, thereby reducing the spectrum efficiency. There are many modifications of the TR technique to either improve its PAPR reduction capability or to reduce computational complexity. For examples, an adaptive scaling based gradient-project technique is used in [91] to improve the PAPR reduction performance. A lot of modified TR techniques is proposed to reduce the extensively high computational complexity of this techniques [92, 93, 94].

Dummy sequence insertion: In dummy sequence insertion (DSI) technique, a certain number of subcarriers out of the available subcarriers are reserved for PAPR reduction and either a complementary or correlation sequence is assigned to these subcarriers [95, 96]. Then an OFDM symbol is formed combining the data subcarriers and the reserved subcarriers. To these reserved subcarriers, each time a new set of sequence is assigned and an OFDM symbol is generated. Thus, for U sequences, there are U OFDM symbols with U PAPRs. The symbol having the lowest PAPR is transmitted. It does not require to send any SI to the receiver. However, it is still a spectrally inefficient technique. This technique will be discussed in detail in Chapter 7.

Tone Injection

The tone injection (TI) technique creates a number of alternative constellation points for each constellation point of a particular modulation, and then each point

of the original constellation is shifted to its corresponding alternative points iteratively to check which alternative point provides the desired lowest PAPR. Then the TD signal corresponding to the FD complex numbers based on the newly created constellation is transmitted [90]. Substituting a point in the original constellation to another point in the extended constellation is equivalent to changing phase and frequency of the OFDM signal [84]. For this reason, this technique is called as tone injection. In Fig. 3.8, the constellation with the solid box shows the original constellation of 16-QAM and the dotted boxes show the extended constellations. Suppose that the upper-right point (red-colored) of the original constellation will be shifted. Its alternative points are determined in such a way that each of the alternative point remains in the same distance, D, in the real and imaginary axes. Following this condition, it has eight alternative points (green-colored) in the eight extended constellations, which are denoted by A_1, A_2, A_3 , , , A_8. Among the alternatives, the point with which the shifting provides largest PAPR reduction will be performed. The receiver must have a priori information about D. It performs modulo-D operation with the received modulated symbol to recover the original symbol, which is followed by the conventional remaining process.

The TI technique can effectively reduce PAPR and does not require any SI transmission. The extent of the PAPR reduction depends on D and how many points are shifted. The higher D results in more PAPR reduction. Although the computational complexity of the receiver is negligible, it is very high in the transmitter. Furthermore, the use of the alternative points increases symbol energy which in turn increases signal average power. One way to reduce the average power is to use closer constellation points. However, this degrades BER performance and PAPR reduction. Two less complex versions of the TI technique are proposed in [97, 98]. To reduce the average power increase, the use of hexagonal constellation is proposed in [99].

Interleaved OFDM

One simple way to reduce the PAPR is to use interleavers, where the interleaver is a device to produce a permutation of an input sequence. The idea is similar to the SLM technique. However, instead of using several phase sequences, several

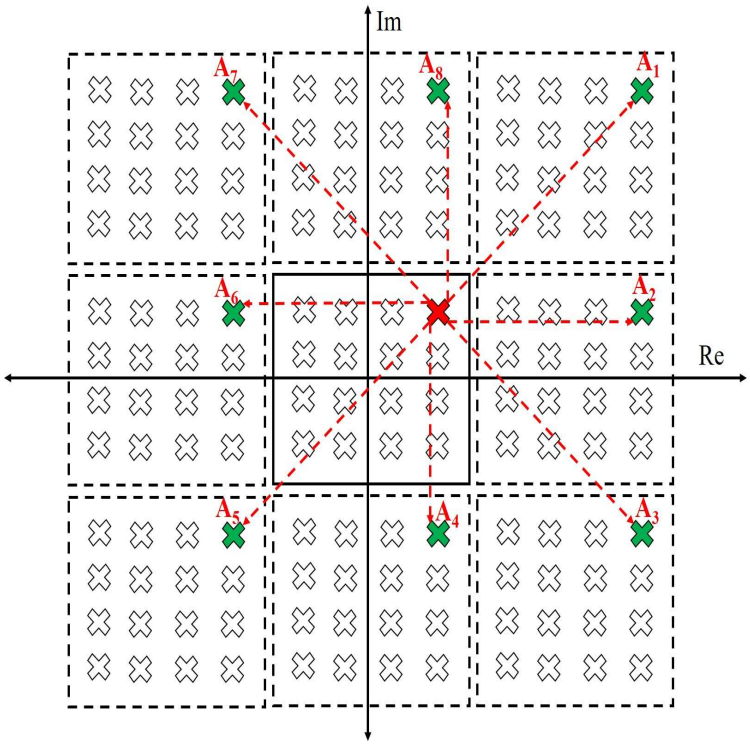

Figure 3.8: Principle of tone injection technique

interleavers are used. For a bandpass modulated FD symbol sequence, a number of interleavers are used to interleave the sequence [100, 101]. If there are U interleavers, the FD sequence is interleaved U times to produce U permutations. Each of the U permutation sequences is then converted to a TD sample sequence. Out of the U sequences, the sequence having the lowest PAPR is transmitted. Both transmitter and receiver must have all the interleavers. However, the reciever needs to know which interleaver provides the lowest PAPR to recover the original sequence. For this reason, this technique requires to send $log_2(U)$ bits as a SI.

Opportunistic Configuration

PAPR reduction techniques of this group are based on wireless standards. They utilize any possible opportunity that can be derived from the standards. For example, the wireless standard IEEE 802.11a consists of three types of subcarriers: data subcarriers, pilot subcarriers and null subcarriers. While other PAPR reduction techniques such as DSI and TR use the data subcarriers for the PAPR

reduction, the techniques of this group uses non-data bearing subcarriers such as pilot and null subcarriers. The conventional purpose of using the pilot subcarriers is to estimate channel impulse response for channel equalization. On the other hand, the null subcarriers are used for spectral shaping of an OFDM signal. However, there are some techniques that utilize these subcarriers for PAPR reduction in addition to their conventional purposes.

Beside the channel estimation, pilot subcarriers are used for sending side information in SLM technique [102, 103]. There are several work where the pilot subcarriers are used for reducing the PAPR. Similar to the data subcarriers, pilot subcarriers also play role behind the high PAPR. In [104], the phases of the pilot subcarriers are designed in such a way that their contributions become minimum in producing the high PAPR for all data sequence, thereby reducing the PAPR. It does not require to send any SI because the same set of phases of the pilot subcarriers are used in all transmissions. However, it can achieve very little PAPR reduction. Furthermore, the optimum phases of the pilot subcarriers are determined using an exhaustive search through simulation. For this reason, its computational complexity is very high. A TR technique is proposed in [105] using the pilot subcarriers instead of the data subcarriers, where pilot tones are directly used for PAPR reduction. By using the pilot subcarriers, it avoids to use any SI. However, the major problem with the technique is its excessively high BER, which practically makes it infeasible. The phases of the pilot subcarriers are iteratively changed to find the lowest PAPR providing phases in [106]. It requires to send the used phases of the pilot subcarriers to the receiver as pilots. To overcome the SI issue, the phases are changed iteratively according to a number of Walse-Hadamard (W-H) orthogonal pilot sequenes [107]. Using the orthogonality, it detects the phases of the pilot subcarriers at the receiver, hence does not require any SI transmission. However, this scheme can not attain much PAPR reduction due to the limited number of W-H sequences available for a specific number of pilot subcarriers. In [108], a sub-sampled zadoff-chu sequence was proposed in replace of the W-H sequence. Although it can achieve more PAPR reduction, it requires SI.

Recently, the use of null subcarriers for PAPR reduction has drawn significant attention. Few of the available null subcarriers are used for PAPR reduction, and it is found that the effect of such use on OOB radiation is negligible [109]. In [110], an iterative random switching of frequencies between a pre-selected null subcarriers and data subcarriers are proposed. Although it does not require to send any SI, its excessive computational complexity and high BER make its implementation impractical. To reduce the complexity, a number of modifications of the technique are proposed [111, 112, 113]. Even after such efforts, the computational complexity still remains very high. To overcome the problem, a null subcarrier shifting based approach is proposed in [114]. Overcoming the complexity issue, it creates a new problem: SI transmission.

Active Constellation Extension

The active constellation extension (ACE) is a constellation modification technique to reduce PAPR. Similar to the TI technique, it also shifts a certain number of constellation points. However, it does not require to send any SI. The technique of constellation extension is shown in Fig. 3.9. For 4-PSK, each constellation point can be shifted to any direction to its respective shaded region. However, only the outer constellation points of 16-QAM can change their positions. While each outer point located in the corner can shift similar to a 4-PSK point, the rest of the outer points can only move along the direction of the respective arrows. Because of the 12 outer points, the 16-QAM has greater degree of freedom compared to the 4-PSK. If a point is shifted to its new location, it must be ensured that Euclidean distance of the new location from any other constellation points is not less than the distance between any two conventional constellation points. This condition is necessary to maintain the desired BER. This technique is based on a convex optimization. Two algorithms for the optimization are projection onto convex set (POCS) method [115] and smart gradient project (SGP) [116]. The POCS is an optimal solution; however, its convergence speed is very slow. On the other hand, the latter one is sub-optimal with fast convergence speed. It is more suitable for large OFDM symbol and smaller constellation size.

The ACE technique can attain PAPR reduction well and does not require SI transmission. However, its computational complexity is significantly high. Signal

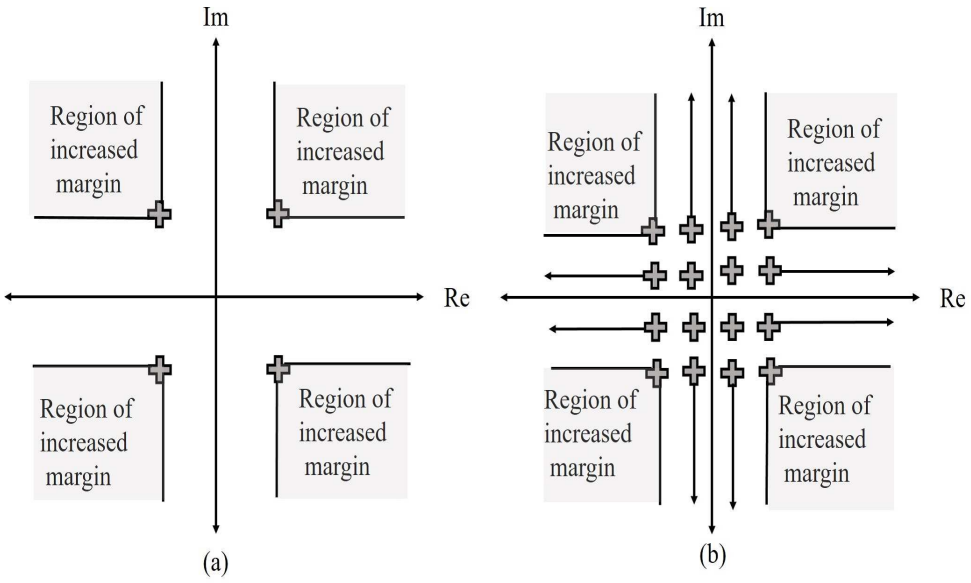

Figure 3.9: Constellation extension technique of ACE: (a) 4-PSK (b) 16-QAM

average power increases. Furthermore, if the minimum distance is maintained, it may cause peak regrowth and increase average power [10]. In addition, it also slows down the convergence speed. However, the use of reverse extension can reduce the peak regrowth by a certain amount at the price of increased BER [117] . The convergence speed can be improved using subcarrier grouping technique [118].

3.2.3 Coding

Coding techniques are usually used for error detection and correction in communication systems. Beside their usual functions, they are applied in reducing PAPR of OFDM systems as well. Basically, three types of coding techniques are used in this purpose: linear block codes, Golay complementary sequence and turbo code.

Linear block codes: The most basic idea of of using this code for the PAPR reduction is to convert every three information bits to a 4 bit codeword by adding a parity bit [119]. For the same three bits of data, it generates two alternative codewords, and the codeword having the lower peak envelope power is transmitted.

This technique transmits 25% redundant bits, thereby reducing 25% spectrum efficiency. In [120], a less complex coding based PAPR reduction technique is proposed, where data bits are divided into a number of sub-blocks and a parity bit is inserted to each block in such a way that the corresponding OFDM signal will have reduced PAPR. An alternative to this is to use two different coding techniques in the data sequence and they are used in each sub-block so as to reduce the PAPR [121]. Both techniques require to send SI to the receiver to inform it the locations of the parity bits and the coding technique used in a particular sub-block, respectively. To reduce PAPR, precoders are designed in [122, 123]. Although they can achieve a significant PAPR reduction, a degradation of BER performance is found.

Golay Sequences and Turbo Codes: Golay sequence is used as a codeword for the purpose of PAPR reduction [124, 125]. This can achieve a very good PAPR reduction. However, the amount of non-data bearing bits are so significant that the loss of the spectrum efficiency is considerably high [10]. In addition, the computational complexity involved with these technique is prohibitively high. Another approach of reducing PAPR is to use turbo encoder with different interleaver to generate different candidate sequences of the SLM technique [126]. It does not require to send any SI. However, the computational complexity is very high.

3.3 Scope of Work

There has been a plethora of work on the PAPR issue, as we have discussed in the previous section of the chapter. Although the computational complexity of the signal distortion techniques such as clipping and companding is very low, their signal distortion property highly escalates OOB radiation, IB noise and BER. For this reason, the merits of the PAPR can not be obtained completely. The multiple signaling techniques, on the other hand, free from such limitations because they do not distort the TD signal. However, most of the techniques of this group suffer from spectrum efficiency loss because of the requirement of SI. Similar to the multiple signaling techniques, the coding based PAPR reduction techniques also free from the problem involved with the distortion techniques. Although no

SI is required to be sent, still these techniques are spectrum inefficient due to the redundant bits of the coding techniques. Even this group cause far more spectrum efficiency loss compared to the multiple signaling techniques which require SI transmission.

From the discussion in the previous sections, it is clear that the techniques of the opportunistic configuration does not require SI transmission. They suffer from other problems such as low PAPR reduction, high computational complexity and BER degradation. Regarding the pilot subcarriers, we will present a novel PAPR reduction scheme that can effectively reduce PAPR with moderate computational complexity and excellent BER performance in Chapter 4. There is scope of work to improve some existing techniques as well. For example, the null subcarrier switching based technique [110] suffers from an extremely high complexity and BER degradation due to the inefficient null detection technique. We will look into the problem in Chapter 5. The downside of the pilot subcarrier based technique [107] is that it achieves very little PAPR reduction. We will investigate this limitation to find a better PAPR achieving technique in Chapter 6. Then we look into the low spectrum efficiency issue of the DSI scheme [95] in Chapter 7.

Chapter 4

Enhanced OFDM Performance with Pilot-Aided Reduced Peak-to-Average Power Ratio

In this chapter, we will present a novel PAPR reduction scheme. The proposed scheme uses pilot subcarriers to attain the reduced PAPR. Before discussing the scheme, a short description of the background of the proposed scheme will be provided.

4.1 Background

Wi-Fi is gaining an unprecedented popularity because of its easy access. There are several Wi-Fi standards such as IEEE 802.11a, IEEE 802.11g, IEEE 802.11n and IEEE 802.11ac, where the OFDM waveform is used. In all the standards, a total of 64 subcarriers are divided into three categories:

- Data subcarriers: Forty eight subcarriers are used for carrying data, hence they are called data subcarriers.
- Pilot subcarriers: The pilot subcarriers are used for channel estimation and synchronization. Four subcarriers are used as the pilot subcarriers in the Wi-Fi standards, hence they carry no data. These subcarriers are placed among the data subcarriers. In addition, they are provided with equal power for proper channel estimation [127].

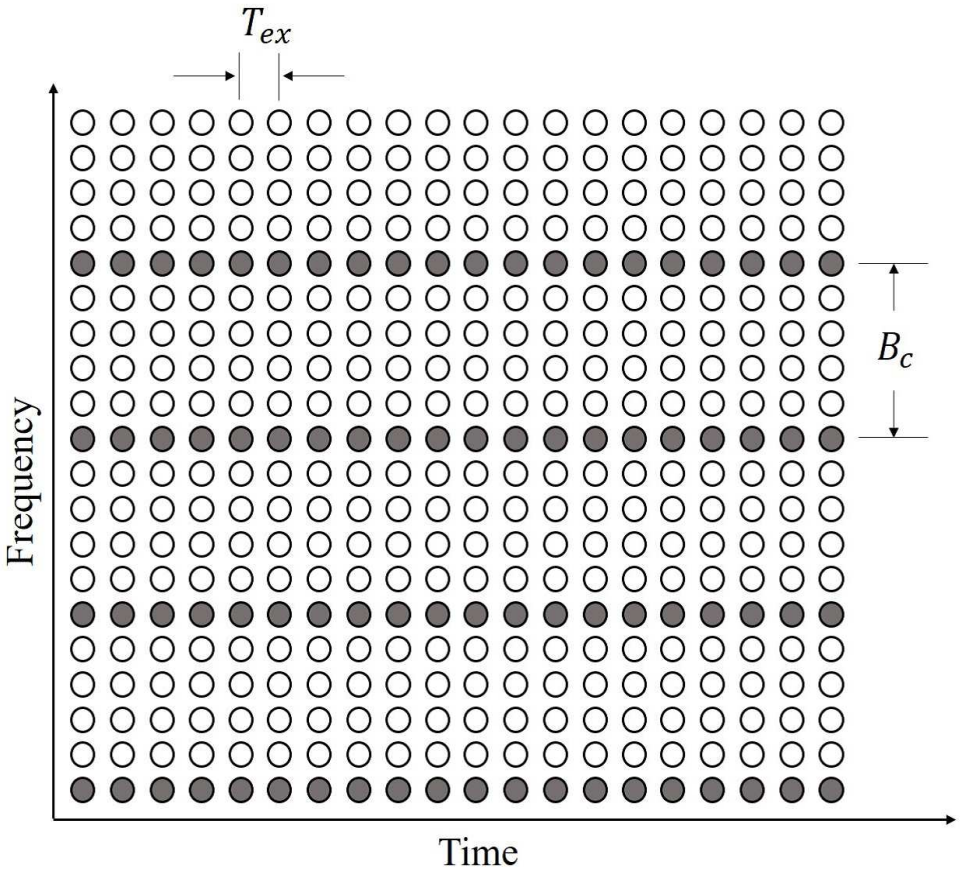

Figure 4.1: Comb-type pilot arrangement

- Null subcarriers: The null subcarriers are used for spectral shaping of an OFDM waveform. Twelve subcarriers are used as the null subcarriers. Instead of using computationally complex bandpass filtering, the null subcarriers are used to provide a rectangular shape to the OFDM symbol waveform [34]. This reduces OOB energy leakage of an OFDM signal to its neighboring symbols. The null subcarriers are allocated no energy and placed on both sides of the data and pilot subcarriers (together they are called as used subcarriers) with one of them is placed in the middle of the used subcarriers. Because of the no energy allocation, they are kept unused. This is why, they are also known as virtual carriers (VCs).

Finding the best arrangement of the data and pilot subcarriers is an open research topic. However, the WLAN standards use comb-type pilot arrangement

where the pilot subcarriers are placed among the data subcarriers maintaining equal distance between any two neighboring pilot subcarriers. WiMax standard (IEEE 802.16) also uses the comb-type subcarrier arrangement with 192, 8 and 56 subcarriers are used as the data, pilot and null subcarriers, respectively [128]. The comb-type pilot arrangement is shown in Fig. 4.1, where each column is an OFDM symbol, and the white and gray circles indicate the data and pilot subcarriers, respectively. The maximum separation between two pilot subcarriers should be less than or at most equal to the coherence bandwidth, B_c, of the channel. The conditions of an efficient pilot arrangement are that the pilots must be in equidistant and equipowered, where the equidistant means the separation between any two neighboring pilots must be constant, and the equipowered means all pilots must have the same power. Pertinently, the position of a pilot indicates the corresponding subcarrier's frequency. However, there is no restriction about the frequency of the pilot subcarriers, their power level and phase. The pilots can have any power level, but all of them must have the same power level.

The use of pilot subcarriers for PAPR reduction has been shortly described in Section 3.2.6. We saw that the pilot phase design technique for reducing PAPR can attain very low PAPR reduction [104]. In [129], the phases and amplitudes of clipped data symbols are sent to the receiver using pilot tones and null subcarriers, respectively. This approach significantly reduces OOB distortion compared to the conventional clipping. However, the extent of BER degradation in this technique is similar to the conventional clipping technique. Positions and phases of the pilot symbols are used for PAPR reduction in [130]. Pilot symbols' positions are *pseudorandomly* changed among the data symbols, and PAPR is computed for each arrangement of pilot and data symbols. The arrangement providing the lowest PAPR is transmitted. According to [127], the channel estimation performance is markedly degraded if the distance between any two neighboring pilot symbols is not constant and not all pilot symbols have the same level of power. In [130], the pilot symbols are made *equiprobable* among the data subcarriers allocating various levels of power to different pilot symbols. This equiprobability, however, does not ensure an equal space between any two neighboring pilot symbols. Therefore, the channel estimation performance of this technique is adversely affected. In addition, a very large power is assigned to the pilots, which increases

the mean power of the OFDM signal, thereby increasing OPEX [11]. Since the pilot symbols' locations are randomly changed, the large pilot power is the only clue [130] for pilot detection at the receiver. However, the pilot detection accuracy and BER of the proposed system have not been discussed. The BER will be unsatisfactory if the pilot detection is carried out using only a high pilot power. This technique is unfeasible in practice due to the breach of the equipowered and equidistant properties, the extremely low pilot detection accuracy and the high average signal power.

4.2 Contribution

Here, a new PAPR reduction technique is proposed utilizing pilot symbols in addition to their conventional roles in channel estimation and synchronization. To ensure the optimal channel estimation, all pilots are allocated equal power and a certain constant distance between any two neighboring pilots is maintained. We shift pilot symbols among the data symbols by one position at a time. In each a shift, the PAPR of the arrangement of the corresponding pilot and data symbols is computed. The arrangement providing the lowest PAPR is transmitted. The shifting of the pilot symbols among the data symbols avoids the necessity of the mathematical computation involved in [130]. Although the relative gap among the pilots is not changed, the positions of the pilots among the data symbols are varied over the OFDM symbols. This makes it necessary to know the pilot symbols' positions at the receiver. We propose a robust pilot detection algorithm exploiting the constant distance between the pilots and the larger power allocated to each pilot. The performance of the proposed system is investigated in terms of PAPR reduction capability, BER, power savings and throughput improvement. Although this detection algorithm increases the computational complexity of the receiver, it paves the way for a spectrum- and energy-efficient OFDM system.

4.3 Proposed Scheme

Our proposed PAPR reduction scheme causes changes in both the transmitter and receiver of the conventional OFDM system. On the transmitting side, it changes the pilot symbols' positions iteratively in a predetermined manner among

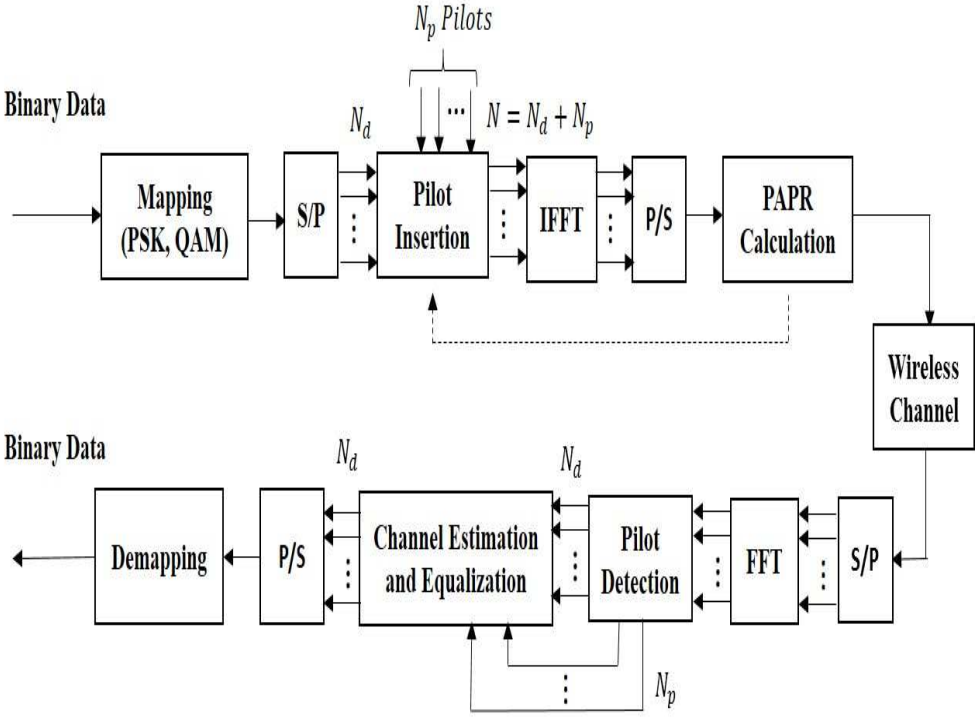

Figure 4.2: Block diagram of the proposed system

the frequency domain data symbols, which is followed by the computation of PAPR of the corresponding time-domain signal. The arrangement of the pilot and data symbols providing the lowest PAPR is transmitted. Since the pilots' locations are not fixed in different OFDM symbols and the transmitter does not send any SI to inform the receiver about the pilots' locations, the receiver must detect the pilot symbols' locations blindly. Therefore, we propose a blind pilot detection algorithm based on the equidistance, equipower and relatively large power properties of the pilot symbols. The proposed transmitter and receiver are described in the following subsections.

4.3.1 Transmitter Design

A block diagram of our proposed system is shown in Fig. 4.2. For simplicity, only the baseband modulation is considered. A mapped data vector of length N_d is sent to a pilot insertion block after performing a S/P conversion operation on it. The pilot insertion block takes a pilot symbol vector of length N_p in addition

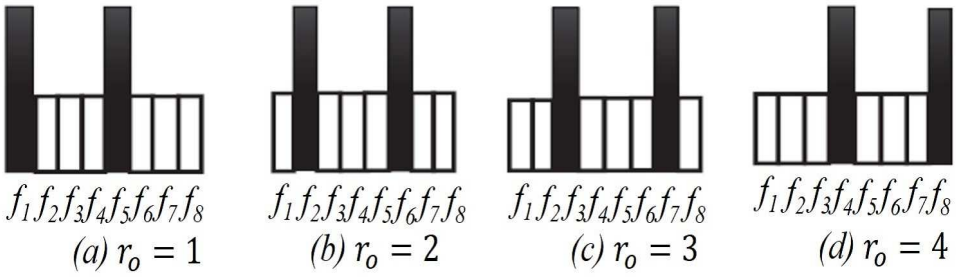

Figure 4.3: Iterative shifting of pilot symbols inside data symbol sequence

to the data vector and inserts these pilot symbols inside the sequence of data symbols to produce a vector of length $N = N_d + N_p$. The PAPR of this combined vector of length N is computed after carrying out an IFFT operation on it. This vector along with its PAPR is stored, and the control returns to the pilot insertion block (the dotted arrow in the transmitter indicates this iterative process), where the previously inserted pilots are shifted. The shifting procedure of the pilots is illustrated in Fig. 4.3. In the first step (see Fig. 4.3(a)), for a pilot symbol sequence of length N_p, the first pilot is inserted immediately before the first data symbol and the second pilot is inserted maintaining a predetermined distance from the first pilot. The third pilot is placed in the data sequence in such a way that the same predetermined distance is maintained from the second pilot. In this way, each pilot symbol maintains a constant distance from the immediate pilot symbols located on both its sides. For example, for $N = 8$ and $N_p = 2$, the predetermined constant distance between any two neighboring pilots is 4 and the indexes of the first and second pilots are 1 and 5, respectively (see Fig. 4.3(a)). For this arrangement, PAPR is computed after the IFFT operation. In the second step, each pilot symbol interchanges its location with the data symbol located immediately to the right of it, that is, while the data symbol immediately to the right occupies the location of the pilot symbol located to its left, the pilot symbol occupies the position of the data symbol. All pilot symbols are shifted in the same manner. As a result, it appears as if the pilot symbols are shifted by one position to the right among the data symbols. Figure 4.3(b) portrays this new scenario. Similarly to in the first step, the IFFT of this combination of pilot and data symbols is performed and the PAPR of the corresponding TD signal is computed. This process of shifting the pilots inside the data sequence, followed by a FD to

TD conversion and PAPR computation of the corresponding TD signal, continues as long as the index of the right most pilot symbol remains less than or equal to N. All arrangements of pilot and data symbols, with their corresponding PAPR, are stored, and the sequence having the lowest PAPR is selected for transmission. Unlike the conventional WLAN standards, where pilots' locations are known to both sides of the communication system, the pilots' locations are not known to the receiver and no SI is sent to the receiver to inform it which symbols are pilots; the receiver detects pilot symbols blindly.

In general, for a system with an OFDM symbol length of N and N_p pilots, the constant distance between any two neighboring pilots is given by

$$R = \frac{N}{N_p} \tag{4.1}$$

If the difference in indexes between any two neighboring pilots is R, the index of any pilot in the combined sequence, β_i, can be found for $1 \leq i \leq N_p$ by the following equation:

$$\beta_i = K_i R + r_o \tag{4.2}$$

where K_i is an integer taking any value from 0 to $N_p - 1$, and r_o is the index of the first pilot in the combined sequence, ranging from 1 to R.

4.3.2 Receiver design

The receiver of the conventional WiFi standard OFDM knows the pilot locations in the received TD symbols. The receiver of our proposed system, however, does not have any information about the pilot symbols' locations. Therefore, this blindness of the receiver regarding the pilot locations forces it to detect the pilot symbols from the received symbol sequence. The proposed receiver design is shown in the system model in Fig. 4.2. Our proposed pilot detection algorithm is based on the relatively high power of pilot symbols compared with that of data symbols, the constant distance between any two neighboring pilots and the equipower property of the pilot symbols. The received serial TD sample sequence, contaminated by thermal noise and the communication channel, is first converted to a parallel sequence before it is converted back to the FD symbol sequence. The pilot detection is carried out on the FD symbols.

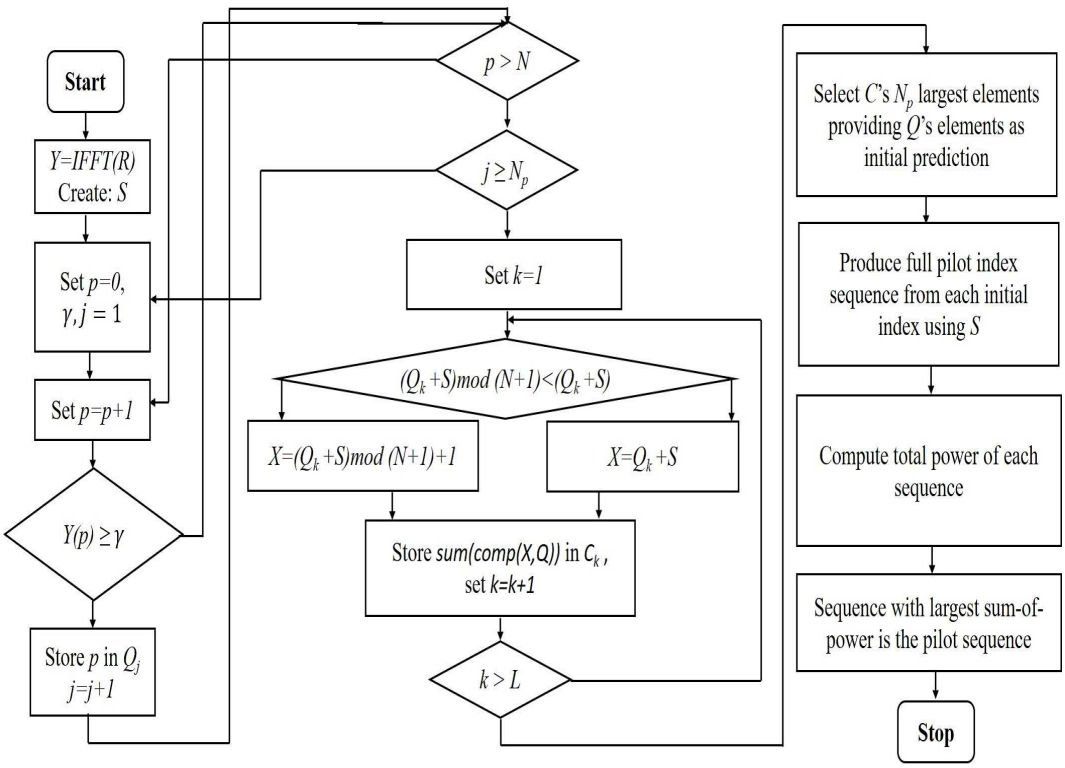

Figure 4.4: Flow chart of the pilot detection algorithm

The step-by-step procedure of the detection process is shown in Fig. 4.4. A set of FD symbols having amplitudes greater than a certain threshold are separated for further processing. The equidistant property of the pilot symbols is then utilized to find which of these separated symbols are pilot symbols. To show how this equidistant property is utilized, let us consider a vector $X_p = [x_{p1}\ x_{p2}\ x_{p3}\ x_{p4}\ \ldots]^{\mathrm{T}}$, where each element is an integer and maintains a certain constant distance, x_{q1} (that is, $x_{p2} - x_{p1} = x_{p3} - x_{p2} = x_{p4} - x_{p3} = \ldots = x_{q1}$), from its neighboring elements. Also let us consider another vector $X_q = [x_{q1}\ x_{q2}\ x_{q3}\ \ldots]^{\mathrm{T}}$, where the elements of X_q are integers satisfying $\frac{x_{q(1+\kappa)}}{x_{q1}} = \kappa + 1$ and $\kappa = [1,\ 2,\ 3,\ \ldots]$. We use the addition operation of modular arithmetic [131] to limit the sum of two positive integers to less than or equal to a specified integer number. For example, if we perform the modular addition of 10 to 15 using modulus 16, the sum will be 9. In our example, the modular addition of x_{p1} to the vector X_q can reproduce the rest of the members of the vector X_p. For example, assume that $X_p = [1\ 17\ 33\ 49]^{\mathrm{T}}$ and $X_q = [16\ 32\ 48]^{\mathrm{T}}$. If

we add $x_{p1} = 1$ to X_q using modular arithmetic with modulus 64, the result will be $[17\ 33\ 49]^{\mathrm{T}}$, the rest of the elements of X_p. However, if there is an element in X_p that does not satisfy this property (that is, the distance from its neighboring elements is x_{q1}), the modular addition of this element to X_q cannot reproduce any element of X_p. For example, let us consider $X_p = [1\ 3\ 17\ 33\ 49]^{\mathrm{T}}$. If $x_{p2} = 3$ is added to X_q using modular arithmetic, the result is $[19\ 35\ 51]^{\mathrm{T}}$. Since $x_{p2} = 3$ does not maintain the property mentioned above, it cannot reproduce any element of X_p. Since the pilot symbols are placed equdistantly among the data symbols, this property can easily lead to the detection of the indexes of the pilot symbols among the segregated indexes. To improve the performance of the pilot detection, the whole set of candidate pilot symbols' indexes is computed from each pilot symbol's index found in the previous step. Then the set of indexes having the highest power is finally selected as the set of indexes of the pilots.

Suppose that R_x is the received TD sample sequence. The corresponding FD sequence Y is obtained as

$$Y = FFT(R_x). \tag{4.3}$$

Each element of Y is associated with an index, where the index of an element is its position among all elements of Y; for example, the index of the fifth element of Y is 5. Suppose that the index vector is $A = [a_1\ a_2\ a_3\ \ldots\ a_N]^{\mathrm{T}} = [1\ 2\ 3\ \ldots\ N]^{\mathrm{T}}$. There is a one-to-one correspondence between the elements of A and those of Y, that is, the index of the n^{th} element of Y, y_n, is a_n, where n is an integer ranging from 1 to N. The next step is to segregate the elements of Y that exceed a certain threshold amplitude. If B is the vector of length N that contains the differences between the amplitude of each element of Y and the threshold amplitude, each element of B, b_i, is obtained in the following way:

$$b_i = |y_i| - \gamma\sqrt{P}, \tag{4.4}$$

where $|y_i|$ is the amplitude of the i^{th} element of Y, γ is the design parameter, which defines how many elements of Y are considered for further processing as candidate pilot symbols, ranging for $0 < \gamma < 1$, and P is the power assigned to the pilot symbols, which is known to the receiver. For all $b_i > 0$, the index of the

corresponding y_i, a_i, is segregated in the vector $Q = [q_1\ q_2\ q_3\ \ldots\ q_M]^T$ of length M such that $0 < M < N$, that is,

$$q_j = a_i \quad if \quad b_i > 0,$$

where $0 < j \leq M$. For a noise-free communication channel, the utilization of only the higher pilot power would be sufficient to detect pilots. In such a case, the vector Q would consist of the indexes of all the pilots. Since there are no noise-free channels in practice, Q consists of true pilot indexes and spurious pilot indexes due to the variation of the signal power over time caused by thermal noise. For this reason, a series of operations are carried out on these segregated indexes of the candidate pilot symbols exceeding the threshold amplitude to find the indexes of the true pilots. The cyclic distances of each pilot symbol from the other pilot symbols, which are known to the transmitter and receiver, are given by

$$S_i = T_i R, \tag{4.5}$$

where $T = [T1\ \ T2\ \ T3\ \ \ldots\ \ T_{N_p-1}]^{\mathrm{T}} = [1\ \ 2\ \ 3\ \ \ldots\ \ N_p - 1]^{\mathrm{T}}$ and $S = [S_1\ \ S_2\ \ S_3\ \ \ldots\ \ S_{N_p-1}]^{\mathrm{T}}$, which will be called the distance vector hereafter. We now utilize the equidistance property of the pilot symbols to find which of the indexes of Q are the indexes of the true pilot symbols. A new matrix, D, in which each row contains the result of the modular addition of each element of Q to the distance vector S, is created. Each element of D, D_{ij}, is given by

$$D_{ij} = \begin{cases} v_j mod(N+1) + 1 & \text{for } v_j mod(N+1) < v_j \\ v_j & \text{otherwise,} \end{cases} \tag{4.6}$$

where $i = 1, 2, 3,\ \ldots\ , M$, $j = 1, 2, 3,\ \ldots\ , N_p - 1$, $v_j = q_i + S_j$ and mod represents modulo operator. A count vector $C = [c_1\ c_2\ c_3\ \ldots\ c_M]^{\mathrm{T}}$ is defined in which each element, c_i, represents the number of elements of Q produced in matrix D by each element of Q, q_i. The desired pilot locations are determined from C. The index of each pilot symbol corresponds to an index from Q that provides one of the N_p largest elements of C. This results in a set of estimated pilot symbol's indexes, U, in which each element is defined as

$$u_i = q_j, \tag{4.7}$$

if c_j is among the N_p largest elements of C, where i is an integer and ranges from $0 < i \leq N_p$.

This pilot detection procedure can detect pilot symbols well. However, its performance degrades at a low SNR because Q cannot hold the indexes of most of the pilots and many segregated spurious indexes also satisfy the distance vector S at a low SNR. In this case, the number of elements reproduced by the spurious pilots outnumbers the number of elements produced by the true pilot indexes. As a result, the vector U consists of a small number of pilot symbols' indexes and the detection accuracy degrades significantly. To make our detection technique robust in low-SNR environments, the initially estimated pilot index vector U is processed further. Since both the transmitter and receiver know the distance vector S, the complete set of pilot indexes is created using S from each element of U. The indexes of the N_p pilot symbols are calculated from U as

$$Z_{ij} = \begin{cases} w_j mod(N+1)+1 & \text{for } w_j mod(N+1) < w_j \\ w_j & \text{otherwise,} \end{cases} \tag{4.8}$$

where $w_j = (u_i + nR)$, and n, i and j are integers all ranging from 1 to N_p. This gives N_p sets of candidate pilot indexes. For each set, the total power of the symbols having the corresponding indexes is computed. The set of indexes giving the highest total power is finally selected as the indexes of the desired pilot symbols. The power of each of the N_p sets is given by

$$\alpha_i = \sum_{j=1}^{N_p} |Z_{ij}|^2, \tag{4.9}$$

where α_i is the total power of the symbols of the i^{th} set of indexes and $i = 1, 2, 3, \ \ldots \ , N_p$. These detected pilots are then used in the usual manner for channel estimation and equalization. The equalized signal is demapped using the corresponding demodulator before P/S conversion. A decoded binary data stream is then obtained from the serial decimal symbols.

There is a further scope to improve the performance of the proposed pilot detection scheme depending on the application concerned. For a delay-tolerant system, we can improve the detection accuracy in an extremely low SNR case by incorporating further processing. The idea is to use a soft γ parameter instead of a hard γ. In the technique discussed above, we have used a specific value of γ (which we call a hard γ) for all SNR cases. Since the channel noise is completely random,

this hard γ may end up capturing no or a very small number of elements in Q, especially at an extremely low SNR. This will undoubtedly cause the erroneous detection of pilots, thereby deteriorating the BER performance. To prevent such a scenario, we can use a soft γ in the sense that if a specific γ results in fewer than N_p indexes in Q, the parameter γ will be decreased by a certain amount to make the number of elements contained in Q at least equal to N_p; the parameter γ is further decreased if this new value of γ does not result in N_p or more elements in Q. This process continues until Q has at least N_p elements or the allowable maximum number of iterations is reached.

4.3.3 Example of pilot detection

The pilot detection algorithm can be better understood by the following example. Suppose that $R = 16$, $N = 64$, $\beta = [1 \ 17 \ 33 \ 49]^{\mathrm{T}}$ and $S = [16 \ 32 \ 48]^{\mathrm{T}}$. Also suppose that the indexes of the symbols whose amplitudes exceed a certain threshold γ are $Q = [7\ 17\ 1\ 23\ 33\ 61\ 19]$. Then the matrix D is given by

$$D = \begin{bmatrix} 23 & 39 & 55 \\ 33 & 49 & 1 \\ 17 & 33 & 49 \\ 39 & 55 & 7 \\ 49 & 1 & 17 \\ 13 & 29 & 45 \\ 35 & 51 & 3 \end{bmatrix}$$

where the first row of D is the result of the modular addition of the first element of Q to S, the second row is the result of the same operation between the second element of Q and S, and so on. The second, third and fifth elements of Q maintain the distance vector S, hence the modular addition of each of these elements produces several elements of Q in a specific row (see rows 2, 3 and 5) of D. However, since the first and fourth elements of Q maintain the distance vector S with one element each, they each reproduce only one element of Q. The sixth and last elements of Q are not located at the distance defined by S, hence they cannot reproduce any other elements of Q. This outcome is exploited to find the indexes of the true pilot symbols. The first and second elements of Q reproduce one (23) and two (1 and 33) elements of Q in the first and second rows of D, respectively. For this reason, the first two elements of the count vector C are 1

and 2, respectively. Thus, C is $[1\ 2\ 2\ 1\ 2\ 0\ 0]^{\mathrm{T}}$. It can be seen that the second, third and fifth elements of Q reproduce the largest number of elements of Q; the first and fourth elements reproduce one element each. Out of these two elements, one is selected randomly to obtain the indexes of $N_p = 4$ elements. If the first element is selected, the vector U will be $U = [7\ 17\ 1\ 33]^{\mathrm{T}}$. In the next step, from each element of U, a complete vector of pilot indexes is generated using Eq. 4.8 and the resulting matrix Z becomes

$$Z = \begin{bmatrix} 7 & 23 & 39 & 55 \\ 17 & 33 & 49 & 1 \\ 1 & 17 & 33 & 49 \\ 49 & 1 & 17 & 33 \end{bmatrix}$$

In the final step, the sum of the powers of the symbols having indexes defined by each row of Z is computed and the row providing the largest sum of powers is considered to comprise the indexes of the true pilot symbols.

4.3.4 Features of the proposed system

The advantages of the proposed PAPR reduction technique compared with other related techniques are noted below. (1) It does not send any SI to the receiver, unlike in [74] or reserve any portion of the bandwidth for PAPR reduction, unlike in [95], hence the whole bandwidth can be used for data transmission, making it a spectrally efficient scheme. (2) It does not cause spectral regrowth, which is usually found in clipping and companding. (3) Since it involves pre-IDFT processing for PAPR reduction, it does not affect the orthogonality of the time-domain signal. (4) It does not require an exhaustive search for the optimum phases of pilots, unlike in [104], or pilots' phases and locations, unlike in ven07, or suitable subcarriers for exchanging with null subcarriers, unlike in wong11. (5) Unlike companding, our proposed system does not affect the average signal power significantly. All these advantages, however, are accompanied by increased computational complexity in the detection of pilot symbols at the receiver. Nevertheless, the advantages of the proposed technique undoubtedly outweigh the demerit of an increased computational overhead.

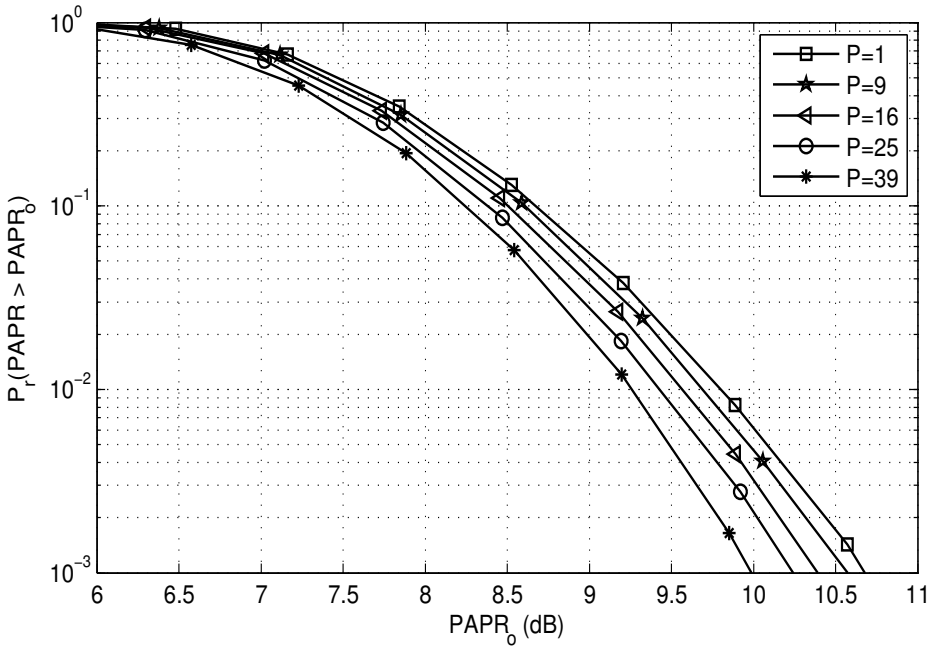

Figure 4.5: Effects of pilot power on PAPR

4.4 System Evaluation

The performance of the proposed system is investigated from different viewpoints, such as PAPR reduction capability, BER, power saving due to the PAPR reduction. During the simulation, a baseband system is considered. Since a passband system has twice the PAPR of a baseband system, the PAPR reduction performance observed in the baseband system will follow a similar trend in the passband system. The bandpass modulations used throughout this paper for the pilot symbols and data symbols are BPSK and Quadrature Phase Shift Keying (QPSK), respectively, unless otherwise stated. To measure PAPR more precisely, the oversampling factor $L = 4$ is used. Every simulation result in this paper is obtained by sending 1×10^5 OFDM symbols.

Usually a larger power is allocated to the pilot symbols than to the data symbols. While the use of an extremely large pilot power increases the average signal power, the use of a low pilot power makes channel estimation difficult. Therefore, determination of a suitable pilot power is crucial. The effects of the pilot power

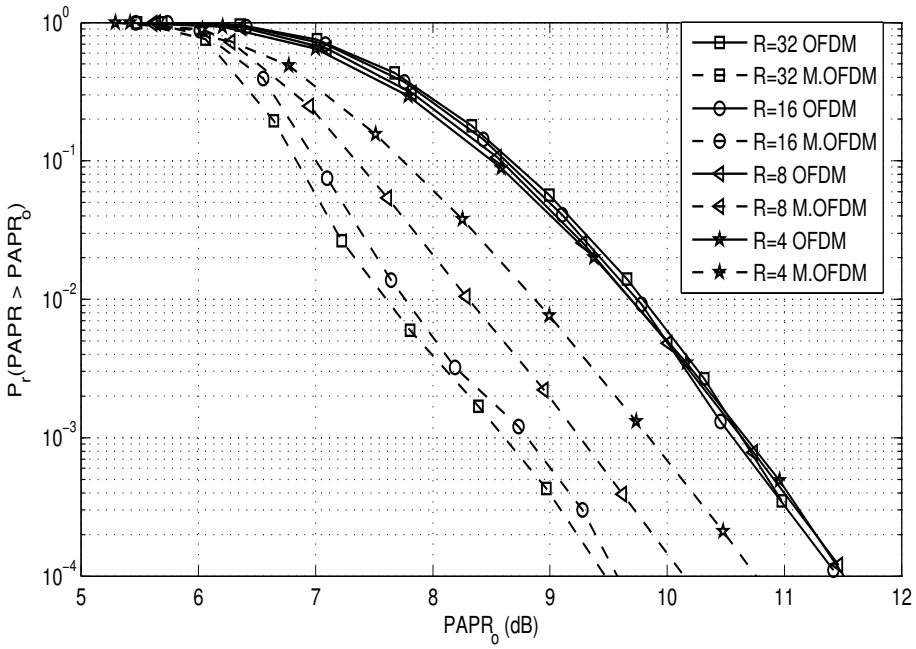

Figure 4.6: CCDF comparison between the proposed and conventional OFDM for various numbers of pilots

on PAPR, caused by an increase in the average power, are investigated and are shown in Fig. 4.5 for a conventional OFDM system with $N = 128$ and $N_p = 4$ in the form of a CCDF. It is evident that PAPR decreases owing to the increased average power caused by the higher pilot power. The pilot power $P = 39$ used in [130] itself decreases PAPR by roughly 1 dB at a CCDF level of 10^{-3}. This indicates a significant increase in the average signal power. A pilot power of $P = 9$, however, does not increase the average power significantly, which is revealed by the insignificant reduction of PAPR. Since a higher pilot power is required to facilitate effective pilot detection at the receiver, $P = 9$ will be used throughout this paper, unless otherwise stated.

4.4.1 PAPR reduction

Figure 4.6 shows the PAPR reduction capability of the proposed system, where solid lines are used for the PAPR of the conventional OFDM and dashed lines are used for the proposed modified OFDM (M.OFDM). The total number of

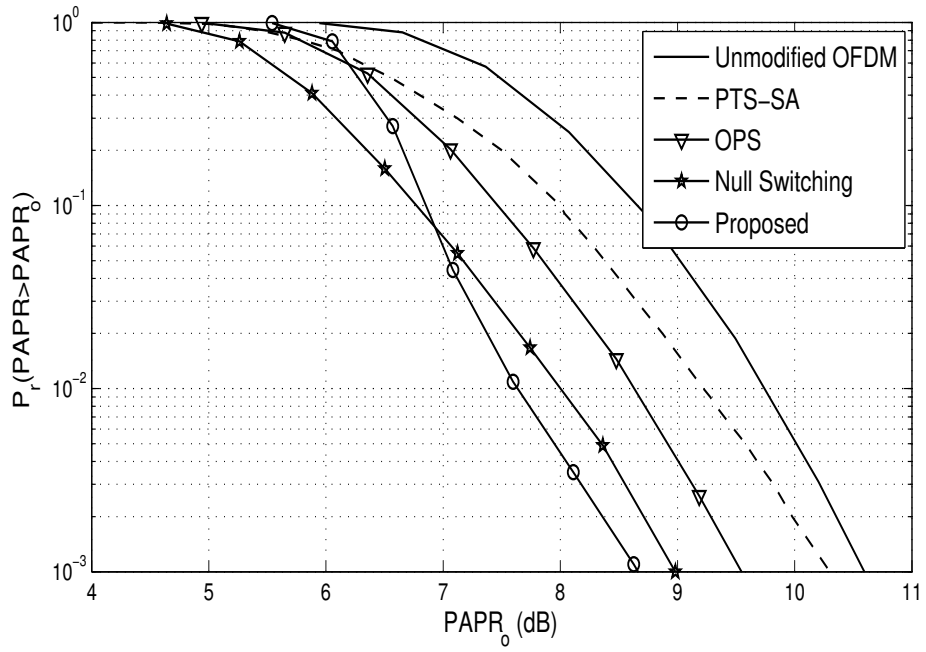

Figure 4.7: CCDF comparison between the proposed and conventional PAPR reduction schemes

subcarriers is 128 and the ratio of the numbers of data and pilot subcarriers, R, is varied. The simulation result reveals that R has no noticeable effect on the PAPR of the conventional OFDM system. This property, however, is not found for the proposed system. A negative correlation is found between R and PAPR for the proposed system, where a higher PAPR reduction can be achieved for a smaller number of pilot symbols. This is due to the fact that a smaller number of pilots provides a larger search space for a signal with a smaller PAPR, thereby making the probability of achieving a lower PAPR higher. For $R = 32$, the PAPR of the proposed system is 2.2 dB smaller than that of the conventional system at a CCDF level of 10^{-2}. A slight deterioration of PAPR of roughly 0.2 dB for the proposed system is observed at CCDF levels of 10^{-3} and 10^{-4}. A noticeable difference in the PAPR of the proposed system is observed for different R. The PAPR reduction capability is degraded by 5%, 33% and 65% for data-to-pilot subcarrier ratios of 16, 8 and 4, respectively, from the PAPR reduction capability of 2 dB obtained using $R = 32$ at a CCDF level of 10^{-4}. The loss of the PAPR reduction capability can, however, be considered as beneficial because it allows

Table 4.1: Pilot detection rate (%) over AWGN channel

N	R	SNR (dB)			
		0 dB	3 dB	6 dB	9 dB
64	16	95.16	99.99	100	100
	8	95.48	98.57	99.97	100
128	16	98.51	99.68	100	100
	8	89.11	93.52	99.77	100
256	16	95.73	98.13	99.99	100
	8	83.59	85.1	98.13	100

complexity of the system to be reduced by 87.5% by reducing the required number of IFFT operations from 32 to 4. While up to 1128 and 71 IFFT operations are required to reduce PAPR by 0.5 dB at a CCDF level of 10^{-3} by the methods proposed [110] and [112], respectively, our proposed method can reduce PAPR by 0.75 dB using only four IFFT operations. This also makes the proposed system suitable for delay-sensitive devices.

A comparison of the PAPR reduction capability of the proposed scheme with three existing schemes is given in Fig. 4.7. The compared existing schemes are PTS based on simulated annealing (PTS-SA) [132], an OPS scheme [107] and a null subcarrier-switching-based scheme[112]. For PTS-SA, the values of the simulation parameters are as follows: number of iterations=28, initial annealing temperature=100, attenuation factor=0.98, final annealing temperature=0.00001. In [112], two null subcarriers are used for PAPR reduction. As is shown, the proposed scheme outperforms the existing schemes. At a CCDF level of 10^{-3}, the proposed scheme reduces PAPR by 87%, 44% and 17% compared with PTS-SA, OPS and the null-switching-based scheme, respectively. However, at a CCDF level of 10^{-1}, the performance of the proposed scheme is slightly worse that of the null-switching-based scheme. This slight degradation, however, reduces the transmitter complexity by 77% because the required numbers of IFFT operations are 71 and 16 for the scheme in [112] and the proposed scheme, respectively.

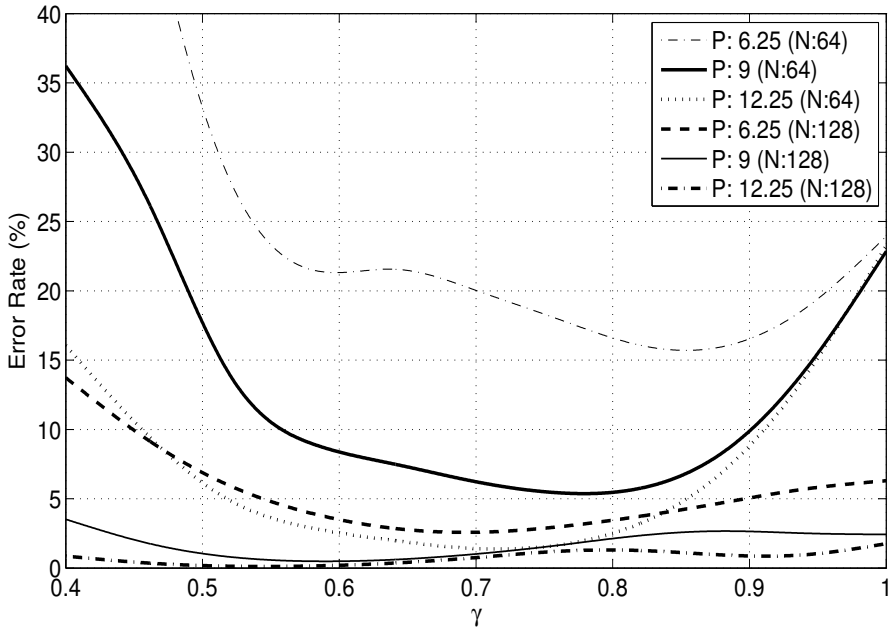

Figure 4.8: Dependence of error rate in detection of pilot symbols on γ and pilot power

4.4.2 BER improvement

The robustness of the proposed PAPR reduction system strongly depends on effective detection of the pilot symbols at the receiver because erroneous pilot detection can increase BER degradation. In addition to the pilot symbols' power and the number of pilots used, the detection performance also depends on the parameter γ defined in Eq. 4.9. The computational complexity of the receiver also depends on γ.

Determining a suitable value of γ is imperative for efficient performance. Figure 4.8 shows the effect of γ on the percentage error rate for various pilot powers and total numbers of subcarriers at 0 dB SNR over an additive white Gaussian noise (AWGN) channel. The error rate is smaller for $N = 128$ than that for $N = 64$. Figure 4.8 also reveals that a higher pilot power ensures better detection accuracy. The error rate is minimum for γ values between 0.6 to 0.85. A soft γ with an initial value of 0.66 is used in the rest of this paper. For a specific γ, the pilot detection accuracy is also affected by the SNR. Table 4.1 shows

the pilot detection accuracy of the proposed system for various SNRs over an AWGN channel. In most cases, the detection accuracy is more than 95%. For $R = 16$, the accuracy is roughly 95% at 0 dB SNR, 99% at 3 dB SNR and almost 100% for SNR values of greater than or equal to 6 dB. The detection accuracy, however, degrades significantly for $R = 8$ at an SNR of less than 6 dB except when $N = 64$. The highest detection accuracy is found at $N = 128$ and $R = 16$, where the detection accuracy is more than 98% for any SNR. The pilot detection accuracy, however, degrades significantly over a known flat fading channel as is revealed in Table 4.2. Similarly to the cases of an AWGN channel, $R = 16$ provides far better accuracy than $R = 8$ over the fading channel (with the exception of $N = 256$, at which $R = 16$ provides far better detection accuracy than $R = 8$ over the AWGN channel). The accuracies for $R = 16$ and $R = 8$ are very similar over the flat fading channel. While the detection accuracy over the AWGN channel at 0 dB SNR is around 95%, it decreases to roughly 85% over the fading channel, a degradation of 10% in the detection rate. Over the fading channel, a detection rate of around 95% is observed at 5 dB SNR, which is 5 dB higher than that over the AWGN channel. The detection accuracies over the fading channel are around 98% and 99% at SNRs of 10 dB and 20 dB, respectively. It becomes very close to 100% for SNRs of 20 dB or more. According to Tables 4.1 and 4.2, the data-to-pilot subcarrier ratio, R, plays a noteworthy role in determining the detection accuracy. For this reason, the number of pilots that optimizes the detection accuracy for a particular total number of subcarriers is investigated as shown in Fig. 4.9. The use of a larger number of pilots is detrimental to the detection accuracy. While the lowest detection accuracy is observed when the

Table 4.2: Pilot detection rate (%) over fading channel

N	R	SNR (dB)						
		0	5	10	15	20	25	30
64	16	75.1	91.1	97.1	99.1	99.7	99.9	100
	8	87.5	95.6	98.5	99.6	99.8	100	100
128	16	88.6	95.9	98.7	99.6	99.9	100	100
	8	84.8	94.9	98.3	99.5	99.8	99.9	100
256	16	88.7	96.0	98.7	99.6	99.7	100	100
	8	87.4	94.8	98.2	99.4	99.8	99.9	100

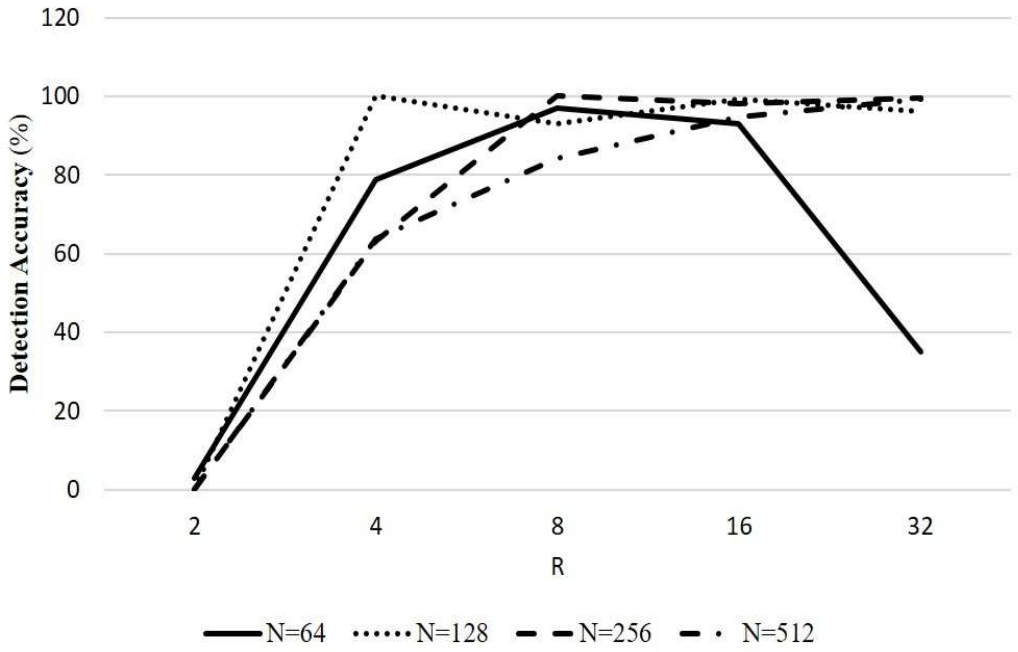

Figure 4.9: Determination of optimum number of pilot symbols for different values of N

number of pilots is half the number of data subcarriers ($R = 2$), $R = 16$ results in the highest average accuracy. The optimum numbers of pilot symbols for $N = 64$, $N = 128$, $N = 256$ and $N = 512$ are 8, 4, 8 and 32, respectively.

The BER of the proposed system is investigated while considering the non-linearity effects of the HPA. We employ Rapp's model [133] of a solid-state power amplifier (SSPA) to simulate the HPA. Since the amplitude modulation (AM)/phase modulation (PM) conversion effect of an SSPA is negligible [134], only the AM/AM conversion of the SSPA will be considered in this paper. Rapp's HPA model for the AM/AM conversion is simulated using the relation [134]

$$g(x) = \frac{|x|}{(1 + |x|^{2\tau})^{\frac{1}{2\tau}}}, \tag{4.10}$$

where $|x|$ is the amplitude of the scaled version of the input signal and τ represents the smoothness of the transition from a linear region to a saturation region. A typical value of τ is 1 [135], which is used throughout this paper. For a specific input saturation power $P_{i,sat}$ and IBO, the average power of the input to the

SSPA is scaled to set its operating point at a required position using the following formula:

$$P_{i,avg} = \frac{P_{i,sat}}{IBO}. \tag{4.11}$$

Figure 4.10 shows the BER of the proposed system over both the AWGN and Rayleigh flat fading channels. For BER investigation, $P = 16$ and BPSK is used as the modulation scheme for the data sequence. The IBOs mentioned in Fig. 4.10 are in dB and $P_{i,sat} = 3$ dB. The improvement of the BER due to the reduction of PAPR at the transmitter by the proposed system is revealed in Fig. 4.10. It also shows the effect of the IBO on the BER. The lower the IBO, higher the BER because of the increased clipping by the HPA. The BER performance of the proposed system, however, improves with decreasing IBO. While the SNR of the conventional OFDM system required to obtain a BER of 2×10^{-2} is 15 dB with 0 dB IBO over the AWGN channel, the proposed system can achieve the same BER with a 13 dB SNR, resulting in an SNR improvement of 2 dB. A similar SNR gain is observed over the fading channel to achieve the same BER. For IBO = 3 dB, SNR gains of 3 dB and 2.5 dB are found at BER of 5×10^{-3} over the AWGN and fading channels, respectively. With further increasing IBO, the SNR improvement decreases significantly over the fading channel, but less significantly over the AWGN channel. A slight degradation in the BER of the proposed system at a very low SNR (< 2 dB) is observed due to the increased erroneous detection of the pilot symbols.

4.4.3 Power Saving

Reducing the PAPR in OFDM improves the energy efficiency of a network. The power saving reduces OPEX. A linear amplifier has very low efficiency in converting the input dc power to the output ac power. PAPR reduction techniques save power by improving the efficiency of the HPA by making it possible for it to be operated close to its saturation region. The efficiency of an HPA, η, is given by

$$\eta = \frac{P_{o,avg}}{P_{dc}}, \tag{4.12}$$

where $P_{o,avg}$ is the average output power and P_{dc} is the input dc power. A larger η allows a greater output power from the same input dc power. For a

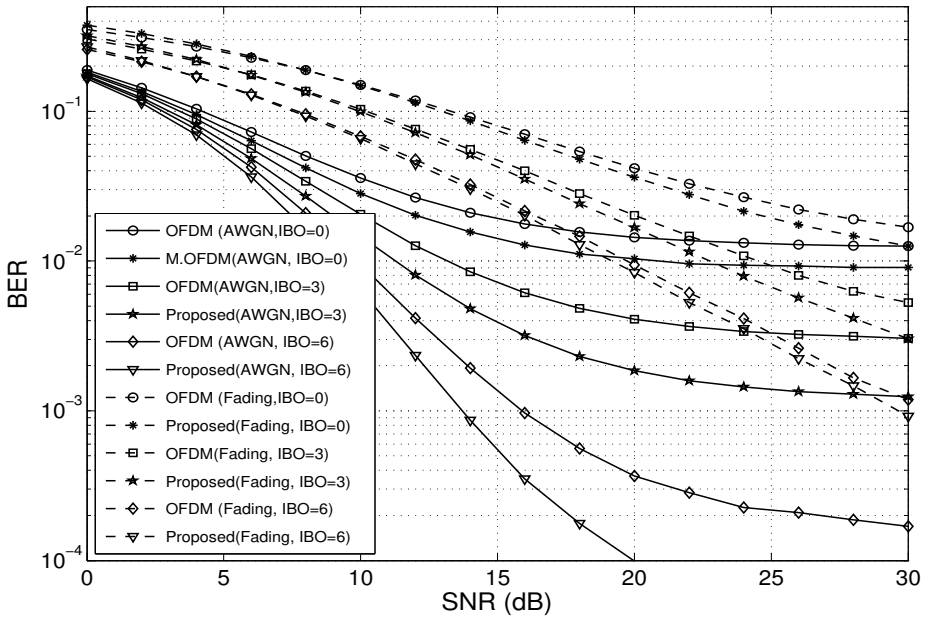

Figure 4.10: BER of the proposed system over AWGN and flat fading channels for different input back-offs

specific $P_{o,avg}$ requirement, the only way to save power is to reduce the input dc power consumption, that is, increase η. PAPR reduction allows power saving by decreasing the dc power consumption. The output back-off (OBO) of an amplifier is given in [136] as

$$OBO = \frac{P_{sat}}{P_{o,avg}}, \tag{4.13}$$

$$P_{o,avg} = \frac{P_{sat}}{OBO}, \tag{4.14}$$

where P_{sat} is the output saturation power. For a linear amplifier such as a Class A amplifier, IBO is equal to OBO [137]. Since IBO is equal to PAPR [50], we can conclude that OBO=PAPR. In addition, for a Class A HPA, $P_{dc} = 2P_{sat}$. Under these conditions, Eq. 4.14 becomes

$$P_{o,avg} = \frac{P_{sat}}{\zeta} = \frac{P_{dc}}{2\zeta}$$
$$P_{dc} = 2\zeta P_{o,avg}, \tag{4.15}$$

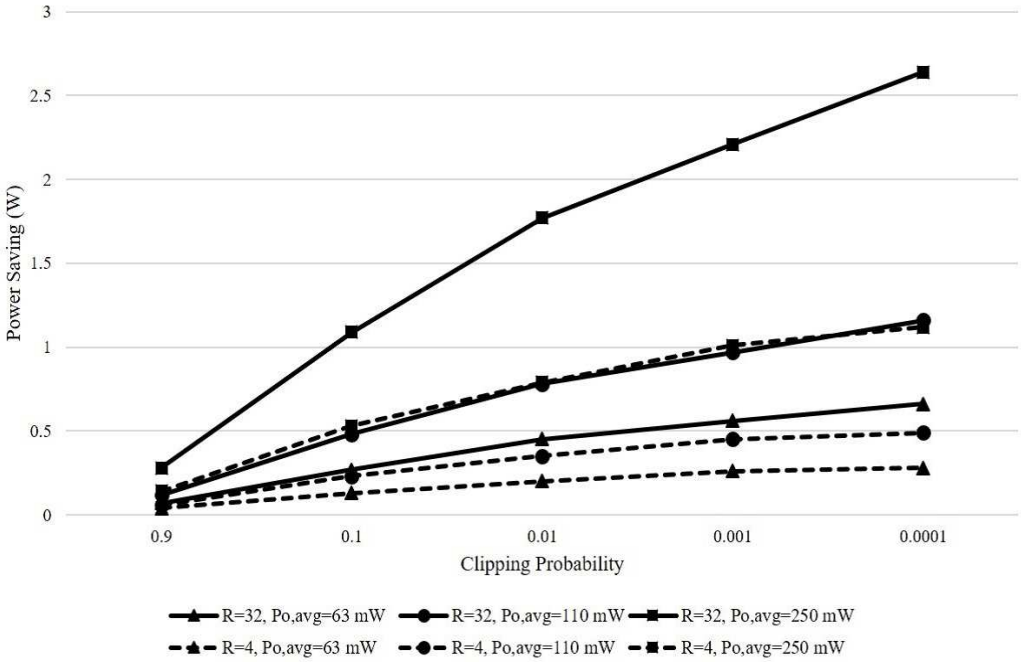

Figure 4.11: Power saving due to the PAPR reduction

where ζ represents PAPR. Suppose that the proposed PAPR reduction strategy decreases PAPR from ζ_1 to ζ_2, and that the input dc powers required to produce PAPRs of ζ_1 and ζ_2 are P_{dc_1} and P_{dc_2}, respectively. Since the average output power is considered constant, we obtain from Eq. 4.15

$$P_{dc_1} = 2\zeta_1 P_{o,avg}$$
$$P_{dc_2} = 2\zeta_2 P_{o,avg}.$$

The power saving resulting from the proposed PAPR reduction strategy is given by

$$P_{dc_1} - P_{dc_2} = 2P_{o,avg}(\zeta_1 - \zeta_2). \tag{4.16}$$

For a typical PAPR, $P_{o,avg}$ ranges from 63mW to 250mW for wireless communication [50].

The power saving achieved at different clipping probabilities due to the PAPR reduction is shown in Fig. 4.11. The higher the average output power $P_{o,avg}$, the higher the power saving. The power saving increases from a clipping probability of 0.9 and reaches its maximum value at a clipping probability of 10^{-4}. There is

a positive correlation between R and power saving. The highest power saving is obtained for $R = 32$ and $P_{o,avg} = 250$ mW for any clipping probability, in which case the power saving increases steadily from the lowest value of 0.28 W obtained at a clipping probability of 0.9 to its peak value of 2.64 W at a clipping probability of 10^{-4}, which is 136% higher than that obtained for $R = 4$ at the same clipping probability. The power-saving pattern obtained at $P_{o,avg} = 250$ mW for $R = 4$, with a maximum power saving of about 1.28 W for a clipping probability of 10^{-4}, is similar to that at $P_{o,avg} = 110$ mW for $R = 32$. At a clipping probability of 10^{-4}, the lowest power-saving trend for $R = 32$, which is obtained at $P_{o,avg} = 63$ mW, is higher than that for $R = 4$ with $P_{o,avg} = 110$ mW and $P_{o,avg} = 63$ mW. All these investigations reveal the importance of using a smaller number of pilots and a higher average output power for increased power saving.

4.5 Conclusion

In this chapter, a new approach based on shifting pilot symbols among data symbols to reduce the PAPR in OFDM was proposed. We changed pilot symbols' locations iteratively in a predefined manner. To avoid sending SI to inform the receiver of the pilot symbols' locations, a robust pilot subcarrier detection algorithm was proposed. Through simulations, the PAPR reduction capability and the BER of the resulting system were investigated. The PAPR of the proposed system is 2.2 dB smaller than that of conventional systems at a CCDF level of 10^{-2} and a significant improvement in BER was observed, especially over an AWGN channel. This approach facilitates considerable power saving as a result of the PAPR reduction.

Chapter 5

Low Complex Null Subcarrier-Assisted OFDM PAPR Reduction with Improved BER

In this chapter, we will present a null subcarriers assisted PAPR reduction scheme with improved BER and computational complexity. First of all, we will give a short description of the background of this scheme before explaing and evaluating the scheme.

5.1 Background

As we defined the null subcarriers in Chapter 4, they are used for confining the energy of a signal within its frequency band. Due to the sinc shape of the spectrum of each subcarrier of OFDM, the sidelobes of the subcarriers located in the higher and lower end of the frequency band encroach into the nearby OFDM symbols. Since first several sidelobes in both sides of a subcarrier spectrum carry significant energy, the encroaching causes energy leakage to the nearby symbols; this causes ACI, which in turn escalates BER. To alleviate the problem, a bandpass filtering can be carried out. Such filtering, however, requires enormous computational complexity for getting an acceptable performance. An alternative to using the bandpass filtering is to perform raised cosine (RC) windowing in both

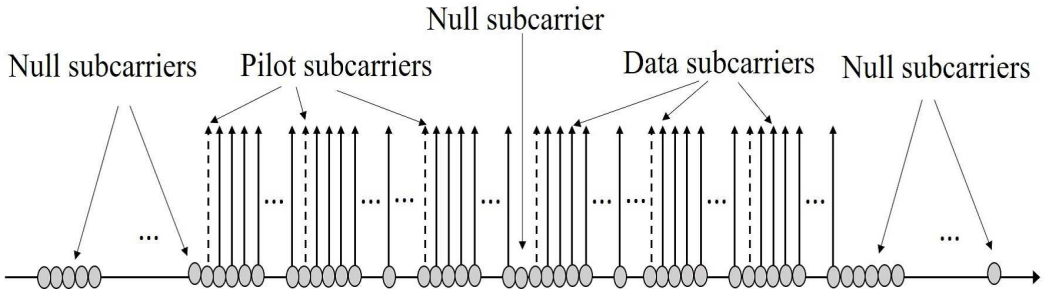

Figure 5.1: Conceptual representation of subcarriers arrangement in WLAN and WiMAX standards

the baseband and passband signal. This technique, however, requires to provide a long guard interval. The simplest technique is to keep some subcarriers unused in both sides of the used subcarriers. They are allocated no energy, so they have neither mainlobe nor sidelobes. For this reason, they do not cause interference to the nearby OFDM symbols. Such subcarriers are called null subcarriers or virtual subcarriers. The null subcarrier concept is adopted in a number of OFDM standards including WLAN and WiMAX. The subcarrier arrangement of these type of standards is illustrated in Fig. 5.1. Depending on the wireless standard, a certain number of subcarriers are used as null subcarriers. For example, 12 subcarriers in WLAN standards are used as the null subcarriers, out of which six and five subcarriers from the lower and upper end of the frequency bands are used as null subcarriers while the middle of the used subcarriers is null subcarrier which is also called as direct current (DC) subcarrier. The center radio frequency of the transmitting station is called the DC subcarrier. It corresponds to zero frequency if the IDFT signal is not modulated. It is used by mobile devices to locate the center of the OFDM frequency band. It also simplifies ADC and DAC operation if it is allocated zero energy [128]. In WiMAX, a total of 56 subcarriers are used as the null subcarriers. Of them, 28 and 27 subcarriers are used in the lower and upper ends of the the frequency band, respectively, and one in the middle.

Although the main purpose of the null subcarriers is to reduce energy leakage, it is sometimes tolerable to use a small fraction of the them for other purposes such as PAPR reduction [109]. One or more innermost null subcarriers from

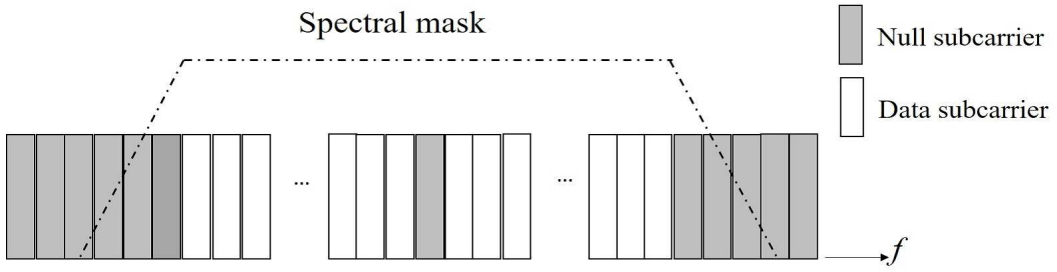

Figure 5.2: Spectral mask

both sides can be used in the purpose because they fall in the transition band of the spectral mask (see Fig. 5.2). Passing some energy using the selected inner-most null subcarrier does not degrade OOB radiation significantly. Inspired by the possibility, several PAPR reduction techniques are proposed. Among those, the recently proposed null subcarrier-assisted PAPR reduction scheme [110] has drawn a considerable attention. In such a scheme, some of the null subcarriers are used as a tool to reduce PAPR; the positions (which implies frequencies) of a certain number of null-subcarriers are switched with all data subcarriers iteratively and the combination that provides the lowest PAPR is transmitted. To show how this technique works, let us consider two sets: D of length N_d and G of length N_g, which consist of indices of the data and null subcarriers, respectively, and $N = N_d + N_g$; the indices are in an ascending order. If the inner-most P, which is an even integer, out of N_g null-subcarriers are selected for switching with P unknown data subcarriers, the set $G_s = \{g_{s1}, g_{s2}, ..., g_{sP}\}$ contains the indices of the P pre-selected null-subcarriers. The P out of N_d data subcarriers for interchanging positions with the P pre-selected null subcarriers can be selected in $\binom{N_d}{P} = \frac{N_d!}{P!(N_d-P)!}$ different ways. Suppose that the set $D_s = \{d_{s1}, d_{s2}, ..., d_{sp}\}$ contains the indices of the P data subcarriers selected to be switched in an ascending order. Switching between the data and pre-selected null subcarriers is carried out in $\binom{N_d}{P}$ times, and PAPR of each data and null subcarrier combination is computed; the combination which provides the lowest PAPR is selected for transmission. The switching between the data and null subcarriers is carried out in such a way that if $d_{sm} < d_{s(m+1)}$, then $g_{sm} < g_{s(m+1)}$; we will call this constraint as switching constraint in the rest of this chapter. Using the switching constraint and zero-energy property of the null subcarriers, the de-switching is

performed at the receiver without any kind of SI. As a result, it does not require to send any SI to receiver.

The null switching technique reduces PAPR significantly, requires no SI. However, it suffers from its extremely high computational complexity and poor BER due to a high error in switched null subcarrier (SNS) detection. To reduce its prohibitively high computational overhead, many work are carried out [111, 112, 113, 138, 139]. All these methods can shed a significant part of overall complexity. The resulting remaining complexity is, however, still very high compared to the other existing PAPR reduction techniques. To reduce the complexity, the authors of the original method [110] propose a technique in [114], where the main attractive feature of the null subcarrier-assited technique [110], no SI requirement, is sacrificed. In [138, 139], two optimization based approaches using Tabu and Cuckoo search algorithms, respectively, are proposed to reduce the computational complexity of the null subcarrier assisted PAPR reduction technique. Beside the PAPR reduction, the effect carrier frequency offset is also reduced. However, they compromise the striking feature of the original technique [110]: no-SI transmission. Such attempts make this technique unattractive because other existing SI-required techniques, such as SLM, PTS, and so on, can reduce more PAPR with much lower computational complexity. In addition to the high computational complexity, the poor SNS detection of the blind method escalates BER. To the best of our knowledge, no work has yet been done to address this problem.

5.2 Contribution

In this chapter, our objective is to find an efficient switching technique, which will reduce the system complexity in one hand and improve BER on the other hand. In this endeavour, we propose a new low-complex null subcarrier-assisted PAPR reduction scheme which improves BER dramatically. We propose to switch the positions of the data and null subcarriers in such a way that frequency separation between any two neighboring SNSs can be kept constant. This sheds more than 98% computational burden of the original method [110]. At the receiver, we use this property in addition to the conventional zero-energy property of null

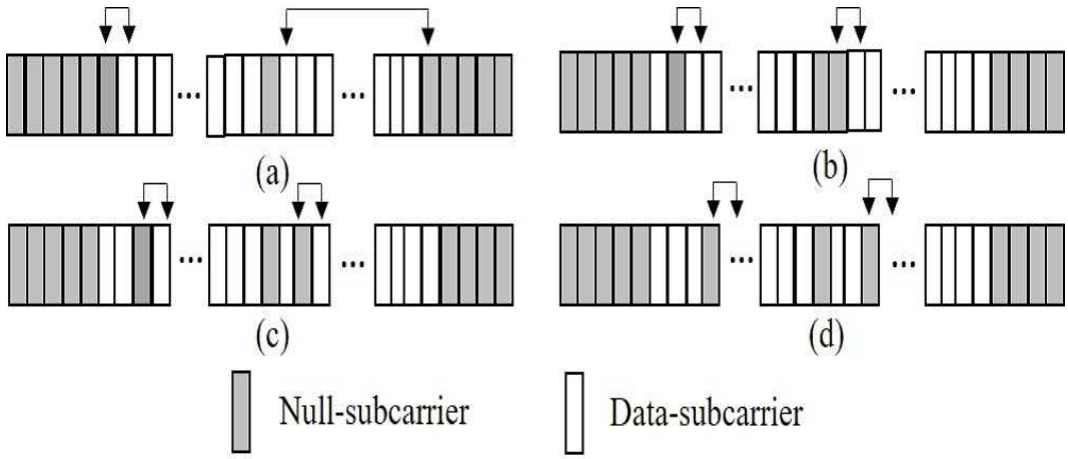

Figure 5.3: Switching between the data and null subcarriers

subcarriers for an efficient detection of SNSs. This increases detection accuracy rate, thereby improving the BER performance.

5.3 Proposed Scheme

We propose a new switching technique between data and null subcarriers. At the receiver, we exploit the features of the proposed switching technique to propose a novel SNS detection technique.

5.3.1 Transmitter Design

Here, we propose a null subcarrier based new blind PAPR reduction scheme to improve BER and computational complexity of the method proposed in [110]. Instead of swapping the positions of randomly-selected data subcarriers with the pre-selected set of null subcarriers, we plan to interchange the positions of these two kinds of subcarriers in a predetermined manner so that an equidistant property can be maintained, where the equidistant property is a characteristic of having a constant distance between any two consecutive switched-null subcarriers. This constant distance is defined by $R = \frac{N_d}{P}$. Usually, $\frac{N_g}{2}$ and $\frac{N_g}{2} - 1$ out of N_g null subcarriers are placed to the left and right of the data sequence, respectively, and the rest one is placed at the center of it. Fig. 5.3 shows the subcarrier arrangement and switching procedure between the data

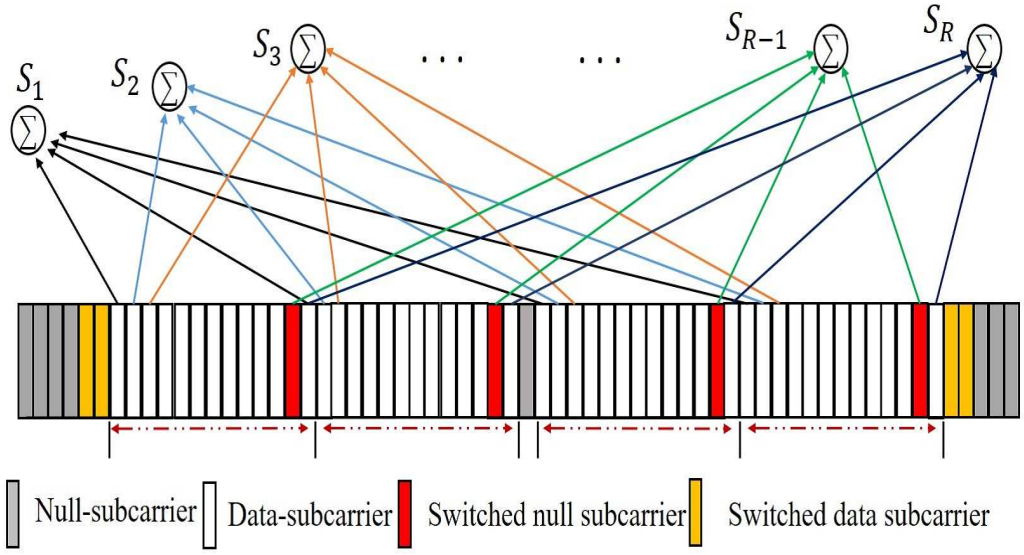

Figure 5.4: Schematic diagram of the proposed SNS detection scheme

and null subcarriers, where the double arrows indicate the data and null subcarriers between which switching will be done in this phase of switching. The conventional arrangement of subcarriers is shown in Fig. 5.3(a) for $P = 2$. The inner-most P (with $\frac{P}{2}$ from each side) null subcarriers are selected for switching. The first phase of switching is done using the following rule: for any positive integer $K \leq \frac{P}{2}$, the $\left(N - N_d - \frac{N_g}{2} - (\frac{P}{2} - K)\right)^{th}$ subcarsubrier is switched with the $\left(\frac{N_g}{2} + \frac{(K-1)N_d}{P} + 1\right)^{th}$ subcarrier, and when $K > \frac{P}{2}$, the switching is done between the $\left(N - (\frac{N_g}{2} - 1) + (K - \frac{P}{2})\right)^{th}$ and $\left(\frac{N_g}{2} + \frac{(K-1)N_d}{P} + 2\right)^{th}$ subcarriers. In the second phase of switching (see Fig. 5.3(b)), each switched-null subcarrier swaps its position with the data subcarrier located just to right. The resulting combination of the data and null subcarriers is shown in Fig. 5.3(c); in this phase, the switching is done following the rule used in the second phase, that is, the switched-null subcarrier with an index m interchanges its position with the data subcarrier having the index $m + 1$. This process of switching continues until the index of the last switched-null subcarrier is less than $N - \frac{N_g}{2} - 1$ or the allowable maximum iteration is met. PAPR of the TD version of each of these combinations is computed, and the combination which provides the lowest PAPR is selected for transmission.

5.3.2 Receiver Design

We change only the SNS detection technique of the null subcarrier based receiver. While the conventional receiver has only one clue, zero-energy property of the null subcarriers, to search the SNSs, we have two clues: usual zero-energy property and the equal frequency difference between two neighboring SNSs. Based on these two properties of the SNSs, we propose here a new SNS detection technique.

The schematic diagram of the proposed SNS detection technique is show in Fig. 5.4. The example is given considering WLAN standard. This technique assumes that P is known to both transmitter and receiver. The SNS detection technique is applied on the FD bandpass modulated symbols obtained from the received TD samples using FFT. First of all, the power of the subcarriers with frequencies allocated for used subcarriers (data and pilot subcarriers) are separated and divided into P different groups. Then the sum of powers of the first subcarrier, S_1, of each group is computed, which is followed by the computation of the sum of powers of the second subcarriers, S_2, of each group, and then the sum of powers of the third subcarriers of each group is computed. This process continues. Since there are R subcarriers in each group, we will have R sums of powers, and the sum having the lowest value among the R values provides information about the frequencies of the SNSs. Suppose that S_{R-1}^{th} has the lowest value among the S_i where i ranges from 1 to R. Then the S_{R-1}^{th} subcarrier of each group is a SNS. From implementation perspective, we can describe the SNS detection technique as follows: Firstly all possible sets of the SNSs' indices are generated. Let's consider a matrix Z of dimension $R \times P$, where each element of Z is defined in the following way:

$$Z_{i,j} = \begin{cases} u_i + nR & \text{for } 0 < n < \frac{P}{2} \\ u_i + nR + 1 & \text{for } P/2 \leq n \leq P \end{cases}$$

where $U = [u_1\ u_2\ u_3\ \ldots\ u_R]^T = [\frac{N_g}{2} + 1\ \frac{N_g}{2} + 2\ \frac{N_g}{2} + 3\ \ldots\ \frac{N_g}{2} + R]^T$, and n is an integer ranging from 0 to $P - 1$. Each row of Z represents a candidate set for indices of the SNSs. For each candidate set (i.e., each row of Z), the total power of the subcarriers whose indices are contained in that specific row of Z_i is computed, thereby getting S_i. The candidate set which provides the lowest total

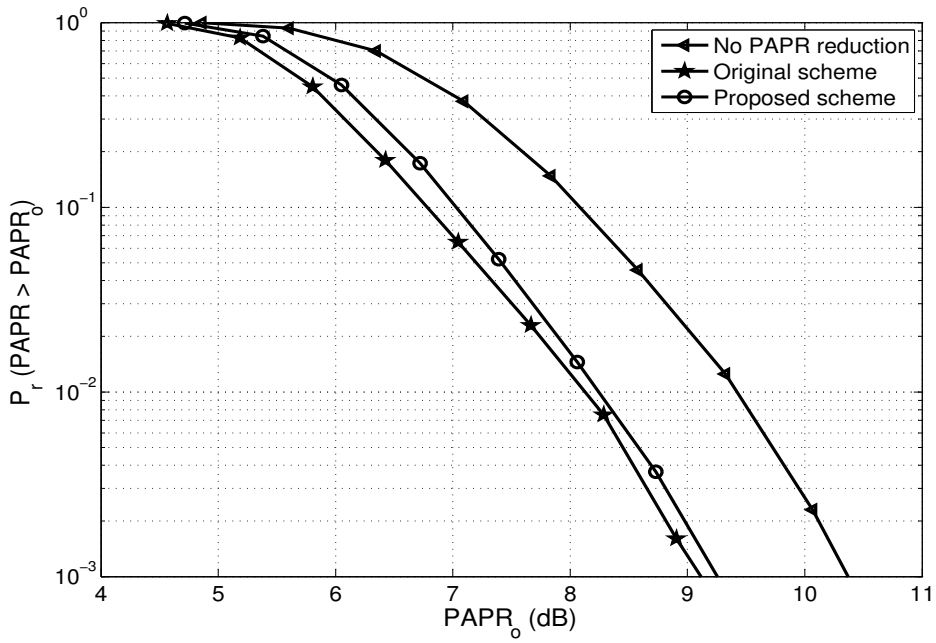

Figure 5.5: PAPR comparison between the conventional and proposed schemes

power among these R sets of candidates is selected as the set of indices of the true SNSs.

After the detection, de-switching between each SNS and its corresponding switched data subcarrier is performed. The de-switching is carried out utilizing the switching constraint: the SNS with the lowest frequency among all SNSs will be switched again with the switched data subcarrier having the lowest frequency among all switched data subcarriers. In our example, the 18^{th} subcarrier switches its frequency with the fifth subcarriers. Then the second switching is carried out between the SNS with the second lowest frequency with the switched data subcarrier having the second lowest frequency among the switched data subcarriers. In the example, the second switching occurs between the sixth and 31^{st} subcarriers. The same procedure is followed for the rest of the switchings.

Table 5.1: Switched-null subcarriers detection rate (%)

SNR (dB)		0	3	6	9	12
P=2	Conventional	0.7	4.1	27.9	82.8	99.8
	Proposed	20.5	49.2	88.3	99.8	100
P=4	Conventional	0	0.4	12.2	72.0	99.5
	Proposed	50.9	86.3	99.6	100	100

5.4 Performance Evaluation

Performance of the proposed system will be analyzed in terms of PAPR reduction capability, computational complexity, BER and spectrum efficiency. While the computational complexity and spectrum efficiency will be evaluated analytically, the rest two will be evaluated through simulations. The simulation parameters are as follows: 52 data subcarriers out of 64 total subcarriers similar to [113], 12 null-subcarriers, QPSK modulation, and four times oversampling. Every simulation result is taken sending 10^4 OFDM symbols.

A comparison of CCDF of PAPR of the proposed scheme to that of the conventional null subcarrier-based PAPR reduction scheme [110] and the original OFDM is shown in Fig. 5.5. It is clear that the PAPR reduction capability of the proposed scheme is very close to that of the conventional one; while PAPR of less than 0.1% of the transmitted symbols of the original OFDM exceeds 10.37 dB, the PAPR for the conventional and proposed systems are 9.11 dB and 9.23 dB, respectively, at the same CCDF level; that is, the proposed scheme degrades 9.5% of the PAPR reduction capability of the conventional null subcarrier-based PAPR reduction scheme. At CCDF level of 10^{-2}, this degradation goes down to 7.7%.

The BER of a null subcarrier-assisted blind PAPR reduction technique largely depends on the SNS detection accuracy at the receiver. Every wrong detection results in a wrong de-switching between the switched-data and null subcarriers, which ends up BER degradation. The SNS detection comparison between the conventional null subcarrier assisted PAPR reduction scheme and proposed one over AWGN channel in different SNR cases is given in Table 5.1. As is seen, the

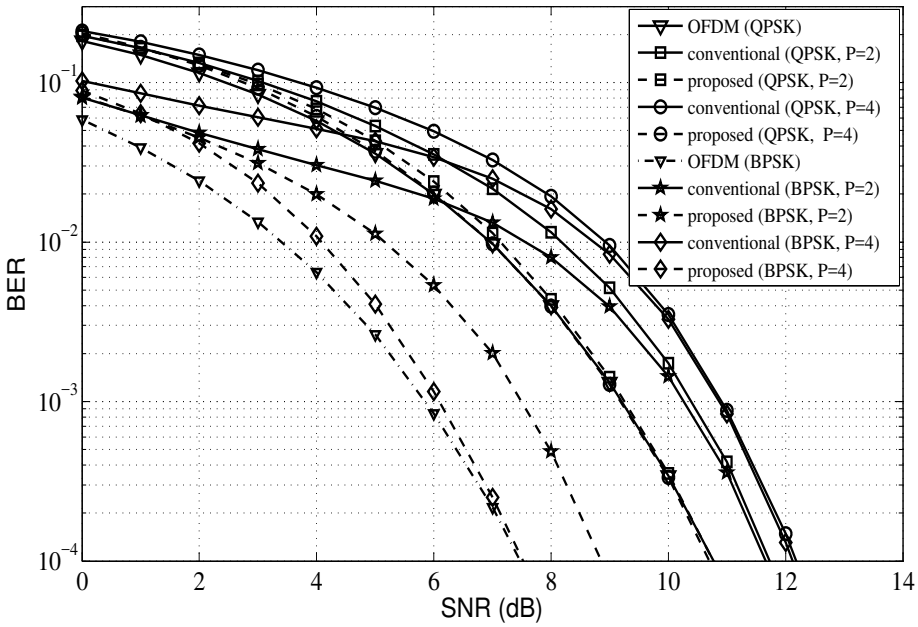

Figure 5.6: BER performance comparison

proposed scheme far outperforms the conventional one in detecting SNSs. For instance, the accuracies of the conventional systems are 0.7% and 0% for P =2 and 4, respectively, at 0 dB SNR. In contrast, the corresponding detection rates of the proposed system are about 20% and 51%. While the detection accuracy of the conventional scheme degrades with the increase of the SNSs, a reverse relation is observed for the proposed scheme; an outstanding improvement is found with larger number of SNSs.

The effect of the pilot detection accuracy on the BER is presented in Fig. 5.6. To reveal how much BER degradation the blind PAPR reduction scheme itself is responsible for, no HPA is included in the transmitter. Fig. 5.6 reveals that the improvement in SNS detection causes better BER. For $P = 4$ and BPSK modulation, while a target BER of 10^{-3} can be achieved by the conventional schemes at 10.85 dB SNR (which is about 6 dB higher than that of the original OFDM), the proposed one can reach the target with 6.1 dB (only 0.2 dB higher than that of the original OFDM). For QPSK modulation, the proposed scheme does not cause SNR loss to achieve the target BER for any value of P. The

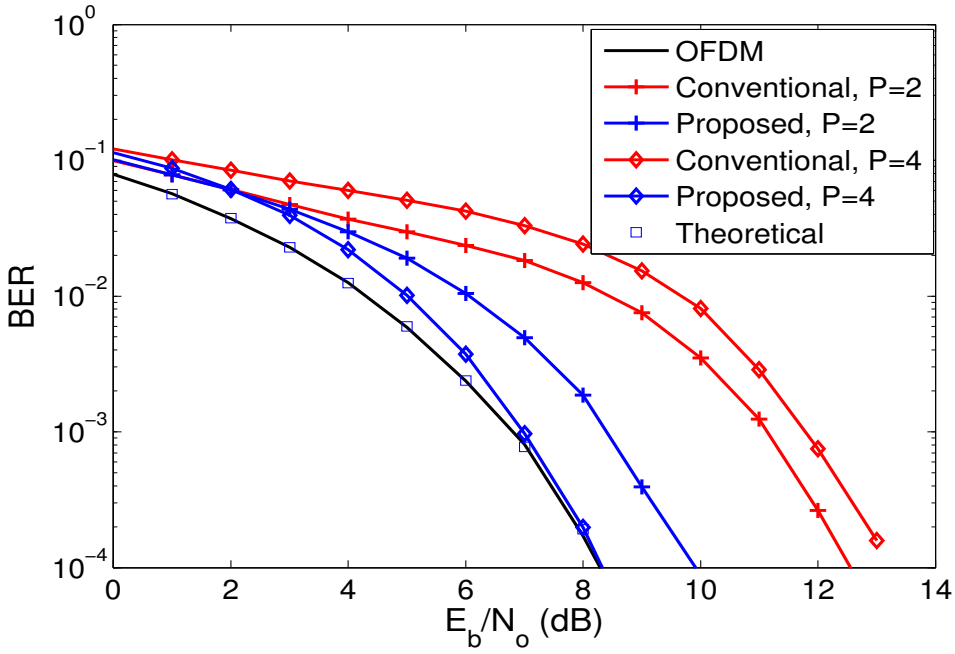

Figure 5.7: BER performance comparison for BPSK modulation with respect to E_b/N_o

conventional schemes, however, require 1.3 and 1.7 dB more SNR for $P = 2$ and 4, respectively, for the same target BER. Fig. 5.6 also shows that higher P lets the proposed scheme achieve better BER, although an opposite result is observed for the conventional scheme. Similar to the performance improvement in PSK, the proposed scheme outperforms the conventional one in non-constant envelope modulation as well. The BER in Fig. 5.6 is about 1 dB lower than the theoretical SNR of BPSK. This is due to the use of some subcarriers as null subcarriers; this issue is explained in detail in Section 2.5.5. As the Fig. 5.7 shows, the system BER increases by almost 1 dB and matches with the theoretical BER when we use E_b/N_o. The BER performance for higher-order QAM is investigated in Fig. 5.8 for $P = 4$. While the conventional scheme requires 1.2 and 0.55 dB more SNR to achieve the target BER of 10^{-3} for 16-QAM and 64-QAM, respectively, the proposed scheme does not cause any SNR penalty to attain the same BER for both modulations. It is observed that the SNR gain reduces with the increase of modulation order; this is due to the fact that the effect of closer constellation points of the higher modulation becomes more dominant than the SNS detection

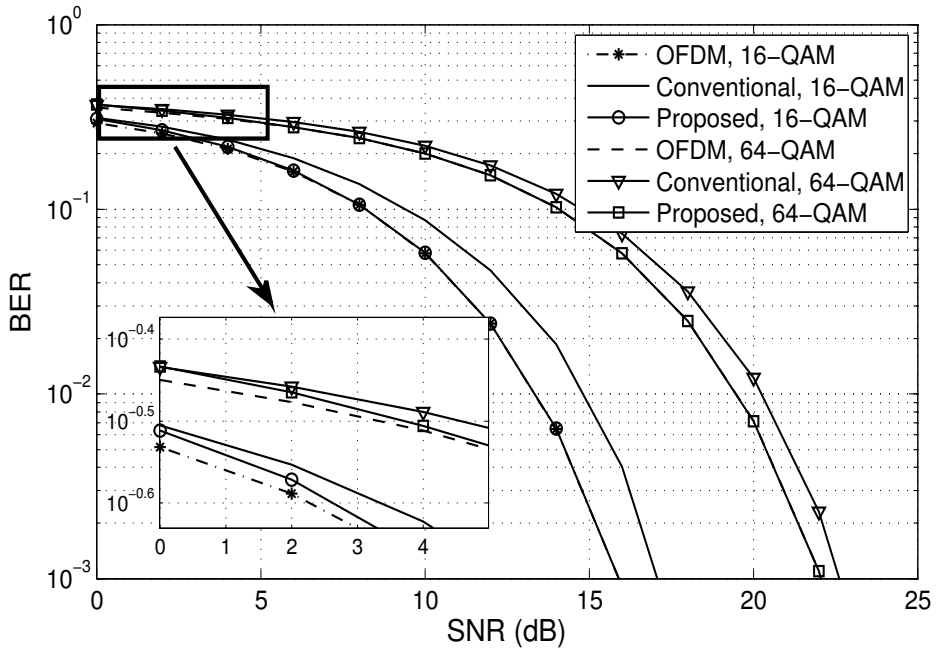

Figure 5.8: BER performance comparison in non-constant envelope modulation

rate in determining BER. Since the SNR gain solely depends on the effect of SNS detection rate, this decreasing effect of the detection rate reduces the SNR gain.

We will now evaluate the computational complexity of the proposed system in comparison to the conventional ones. The number of IFFT operations, PAPR calculations at the transmitter and null subcarrier detection at the receiver contribute a staple part of the total complexity of the system. For this reason, the complexities contributed by these three tasks are considered here and the tasks whose complexities are common for all the methods are not considered. We compare the complexity of our proposed scheme with that of the data-null subcarrier switching based methods which do not require SI (e.g., techniques proposed in [110, 112]). The number of IFFT operations required by the original method [110] and our proposed one are $\binom{N_d}{P}$ and R, respectively. The generalized formula for the maximum number of required IFFT operations, M_s, in [112] is

Table 5.2: Computational Complexity Comparison

Scheme	No. of additions	No. of multiplications
[110]	$\binom{N_d}{P}(Q+4N-1)$	$\binom{N_d}{P}\frac{Q+8N+2}{2}$
[112]	$M_s(Q+4N-1)$	$\frac{M_s(Q+8N+2)}{2}$
Proposed	$R(Q+4N-1)+\frac{(4R-2P^{-1}+1)}{2P}$	$\frac{R(Q+8N+2)}{2}+N_d$

derived as follows:

$$\begin{aligned} M_s &= R+(2R-1)+(3R-2)+(4R-3)+\ \ldots \\ &\quad +[PR-(P-1)] \\ &= \left(\frac{P^2}{2}+\frac{P}{2}\right)R-\left(\frac{P^2}{2}-\frac{P}{2}\right) \\ &= \frac{P}{2}[(P+1)R-P+1] \end{aligned}$$

Each N-points IFFT operation requires $\frac{N}{2}log_2(N)$ multiplications and $Nlog_2(N)$ additions. Suppose that $Q = Nlog_2(N)$. The number of additions and multiplications required in the computation of PAPR of OFDM data block of length N are $4N-1$ and $4N+1$, respectively. The null detection operation of the proposed scheme is slightly more complex than the other methods. The required number of additions and multiplications in the detection process of the proposed system are $\frac{(4R-2P^{-1}+1)}{2P}$ and N_d, respectively. A comparative complexity of the original method [110], Ahmed et. al. [112], and proposed method is given in Table 5.2. For $P = 2$, while the maximum number of additions and multiplications needed in the original method are 847314 and 595374, respectively, the corresponding numbers are 16640 and 11726 for our proposed scheme, with 98.04% and 98.03% reduction of the total additions and multiplications, respectively. It is worth noting that the complexity of our proposed system is 66.10% lower than that of the scheme presented in [112].

The spectrum efficiency of the proposed scheme will be analyzed now. We see that the propose scheme attains the same BER with 5 dB less SNR compared to the original scheme [110]. The 5 dB SNR gain allows the transmitter to lower 5 dB transmit power. However, the SNR gain can be utilized in improving spectrum efficiency. If the two techniques are operating at the same SNR, the proposed

one can operate with spectral efficiency that is about 2 b/s/Hz higher than that in [110] because SNR increase by 3 dB in any system allows to improve the spectrum efficiency by 1 b/s/Hz [140]. We will look into the spectrum efficiency of the proposed scheme with respect to the other schemes [114, 138, 139] which require SI transmission. Since the proposed scheme does not require to send any SI, all subcarriers can be used for data transmission and its spectrum efficiency is equal to that of the unmodified OFDM. The techniques [114, 138, 139] requires to send $P \times log_2(N)$ bits as SI. If BPSK moduation with $\frac{1}{2}$-rate coding is used to send the SI, it requires to reserve $2P \times log_2(N)$ subcarriers for the SI transmission. The resulting spectrum efficiency becomes

$$S_{eff,SI} = \frac{log_2(M)\,(N - 2P \times log_2(N))}{N + L_{cp}} \tag{5.1}$$

Referring to Eq. 2.16, we can formulate the spectrum efficiency loss due to the SI transmission as

$$\begin{aligned} S_{eff} - S_{eff,SI} &= \frac{log_2(M)N}{N + L_{cp}} - \frac{log_2(M)\,(N - 2P \times log_2(N))}{N + L_{cp}} \\ &= \frac{2P \times log_2(M) log_2(N)}{N + L_{cp}} \end{aligned} \tag{5.2}$$

In the system such as [114], the no-SI advantage is compromised to reduce the system complexity and improve BER. If we consider our proposed scheme in 'non-blind' scenario, it remains more spectrally efficient compared to [114]. If P data-null subcarriers switchings are done, the indices of the P SNSs are needed to send as SI in [114]. For a system of N total subcarriers, the number of bits needed to send as SI becomes $P \times log_2(N)$. In contrast, the non-blind scenario of the proposed scheme requires to send only $log_2(\lceil \frac{N}{P} \rceil)$ bits irrespective of the number of data-null switchings, where $\lceil . \rceil$ represents ceil function; this is due to the fact that since the equal frequency difference property is maintained, only the index of the first SNS is required to send to the receiver and all indices of the subsequent SNSs can be derived from this received index at the receiver using the equal frequency difference property.

5.5 Conclusion

Due to the high complexity and poor BER of the conventional data-null subcarrier switching based PAPR reduction scheme, we propose an improved PAPR reduction scheme, with low computational overhead, which can decrease such effects dramatically. Compromising only 9.5% of the PAPR reduction capability at 10^{-3} CCDF level, our scheme reduces the system complexity by more than 98% and achieves up to 5 dB SNR gain.

Chapter 6

PAPR reduction for OFDM systems using pilot derived phase factors

In this chapter, we will present a PAPR reduction scheme utilizing pilot subcarriers to improve PAPR reduction capability, computational complexity and preserve spectrum efficiency. We will first discuss the background of the proposed scheme before presenting it.

6.1 Background

The conditions for efficient pilot subcarriers are as follows: any two neighboring pilots must be equidistant and all pilots must be equipowered. There is no restriction on the phases of the pilot subcarriers. The pilots can have any phases. However, the phases must be known to the receiver to estimate the phase rotation effect of a channel. Inspired by the flexibility of the pilot phases, a PAPR reduction technique is proposed [106]. The main idea is to iteratively change the pilot phases to find a set of optimal phases that provides the desired PAPR or the lowest PAPR within the allowable maximum iteration. Since the same set of phases of the pilots does not provide the desired PAPR for all data sequence, it is required to find the optimal pilot phases for every data sequence. For this reason, the pilot phases need to be sent to the receiver as SI in all transmissions. The amount of the SI is markedly large because it needs to send the phase of

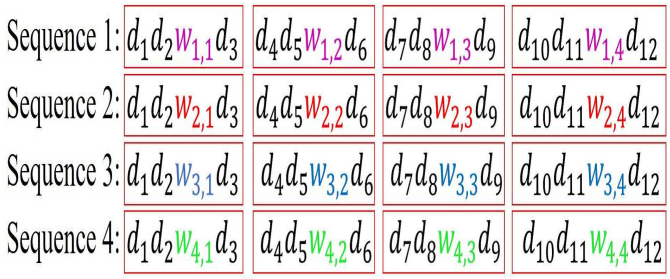

Figure 6.1: An example of the OPS scheme

each pilot. Furthermore, the searching of the optimal phase set for every data sequence is computationally expensive.

To eliminate the SI requirement, the authors in [106] propose a new technique using orthogonal pilot sequence (OPS) [107], which we will refer to as OPS scheme in the rest of the chapter. Unlike [106] where the phases are changed randomly, the phases in the OPS scheme is changed according to a set of orthogonal sequences. In [107], W-H sequence is used. To get a greater look, let's consider an example of an OFDM system with 12 data subcarriers and 4 pilot subcarriers. First of all, a 4×4 W-H matrix, W, is generated; each row of the matrix is an orthogonal sequence.

$$W = \begin{vmatrix} w_{1,1} & w_{1,2} & w_{1,3} & w_{1,4} \\ w_{2,1} & w_{2,2} & w_{2,3} & w_{2,4} \\ w_{3,1} & w_{3,2} & w_{3,3} & w_{3,4} \\ w_{4,1} & w_{4,2} & w_{4,3} & w_{4,4} \end{vmatrix}.$$

The amplitude and phases of the four pilot subcarriers are changed according to a particular row of the W matrix at a time; and this gives us 16 FD symbols. One row of W acts as a pilot sequence. Since there are four rows, there will be four FD symbol sequences, where the data symbols remain same in all the sequences. Fig. 6.1 shows the example. The four FD sequences provide four TD sample sequences with four different PAPRs. The sequence having the lowest PAPR is transmitted. However, the information about which orthogonal sequence (e.g., row of W) gives the transmitted sequence is not transmitted to the receiver. Instead, a blind pilot subcarriers' phase detection technique is proposed in [107] exploiting the orthogonality property of the pilot sequence.

The OPS scheme does not compromise spectrum efficiency because of the no-SI transmission. However, one limitation of the technique is that its PAPR reduction capability is very limited. The extent of the PAPR reduction depends on the number of pilot sequences used, with larger number of pilot sequences causes more reduction of the PAPR. To increase the number of orthogonal sequences, we need to increase the dimension of the W-H matrix. Since it is a square matrix, any increase in the number of rows will need to increase the number of columns which in turn will require to increase the number of pilot subcarriers. However, any increase in the pilot subcarriers results in a reduction of the number of subcarriers available for data transmission; this reduces spectrum efficiency. To maintain the spectrum efficiency, it is imperative to improve the PAPR reduction capability without increasing the number of pilot subcarriers.

An OPS based PAPR reduction technique proposed in [108] which attains more reduction of PAPR without increasing the number of pilot subcarriers. Since it is not possible to increase the number of pilot sequences without increasing the number of pilot subcarriers in case of the W-H sequence, the reference [108] proposes to use sub-sampled Zadoff-Chu sequence (SZCS); we will call this technique SZCS technique throughout the chapter. In this technique, a Zadoff-Chu sequence of length $N_{zcs} = I \times N_p^2$ is produced, which is then partitioned into I groups with each group consists of N_p^2 elements. Then, the elements of each group is divided into N_p subgroups. Afterwards, i^{th} orthogonal sequence of length N_p is formed by taking i^{th} element from each subgroup. This procedure gives N_p sequences in each subgroup. Finally, there will be I groups of sequences, with each group consists of N_p orthogonal sequences of length N_p elements. By increasing I, it is possible to generate as many orthogonal sequences as required. All sequences in each group are used as the pilot sequences to check which sequence provides the lowest PAPR. Due to the increased number of pilot sequences, this technique can significantly improve the PAPR reduction. However, it requires to send SI. If a sequence of the k^{th} group, for $1 \leq k \leq I$, provides the lowest PAPR, the value of k must be sent to the receiver as SI. For this reason, it requires to send $log_2(I)$ bits as SI. In addition, the computational complexity is more than I-times higher compared to the OPS scheme [107]. This scheme attains more PAPR reduction compromising the striking feature of the OPS scheme: no-SI transmission.

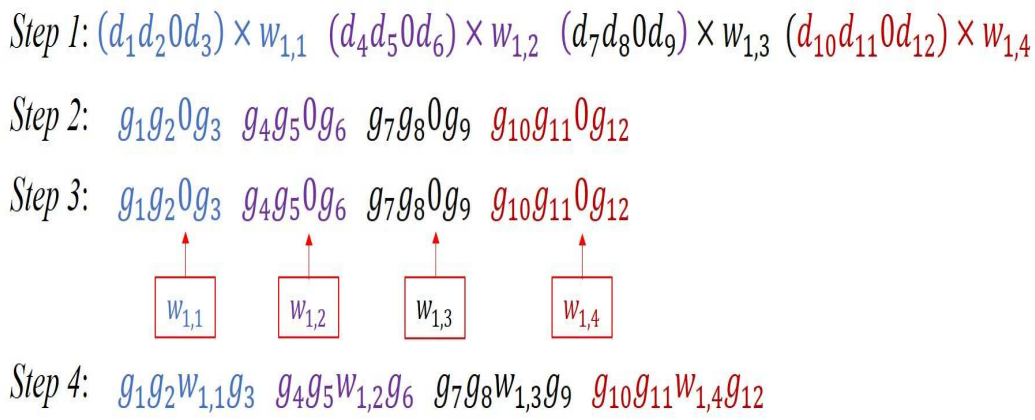

Figure 6.2: An example of the proposed PDPF scheme

Therefore, *a rigorous investigation is required to find a scheme which will improve the PAPR reduction capability of the OPS scheme without sacrificing the no-SI transmission feature, and which will not increase the computational complexity significantly.*

6.2 Contribution

We propose a new PAPR reduction scheme, called pilot derived phase factor (PDPF) scheme, by modifying the OPS scheme to achieve more PAPR reduction. It has two forms: modified OPS (MOPS) scheme which is based on the original OPS scheme [107] and modified SZCS (MSZCS) which uses SZCS sequence as the orthogonal sequence. Similar to [107], MOPS use the W-H sequence as the pilot sequence. The change of only the phases of the pilot symbols, as is done in [107, 108], does not affect other frequency-domain symbols. To bring more diversity among the frequency-domain symbols, we introduce the notion of phase factors which are derived from the pilot subcarriers. The MOPS scheme achieves more PAPR reduction compared to the OPS scheme. In addition, it outperforms the SZCS scheme in terms of PAPR reduction capability as well as computational complexity. Furthermore, the BER of the proposed system is found almost similar to that of the OPS scheme. Thus, the MOPS scheme is a less complex, SI-free PAPR reduction scheme which achieves less PAPR than the conventional schemes does. For applications where least PAPR is the only desired criterion

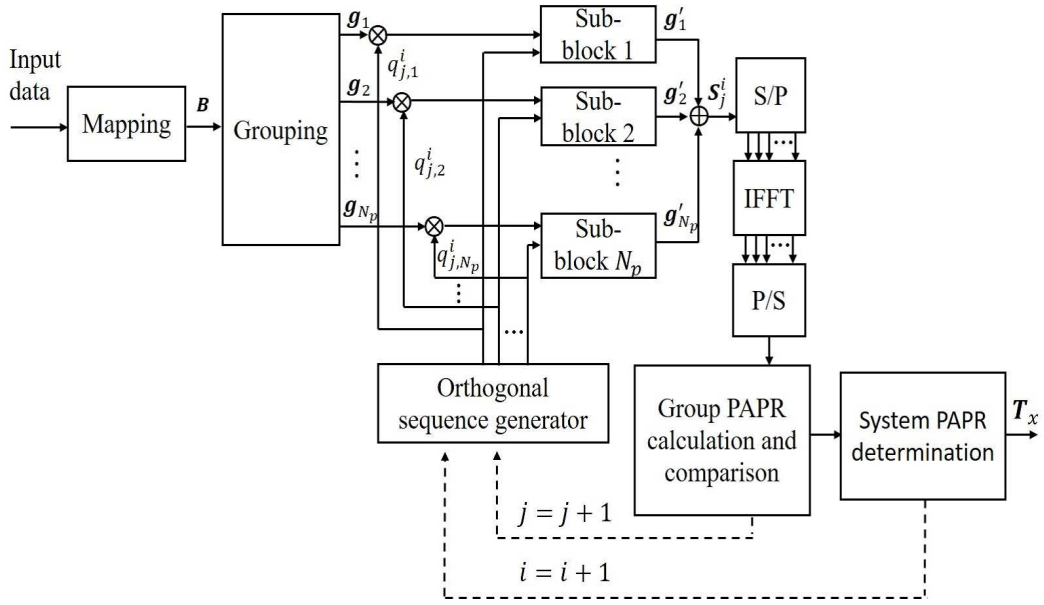

Figure 6.3: Block diagram of the PDPF transmitter

and spectrum efficiency can be compromised to achieve the goal, we propose, MSZCS scheme, to integrate the phase factor based scheme with the SZCS to achieve further PAPR reduction compromising no-SI transmission feature.

6.3 Proposed Scheme

To reduce PAPR, it is necessary to reduce correlation among the subcarrier phases. Our idea is based on increasing randomness among the subcarriers. In this endeavor, we firstly partition the data symbols into a number of groups and then multiply each of these groups by different phase factors with the phases derived from the pilot symbols as is shown in Fig. 6.2. This causes changes in the phases of all symbols in a group. However, the change occurs in different ways in different groups depending on the pilot symbol associated with a particular group. Then one pilot symbol is inserted to a specific location in each group maintaining all the requirements of efficient pilot symbols (e.g, equidistance between any two neighboring pilots and equipower of the pilots). The pilot symbols' phases are changed iteratively following the W-H sequence, which results in changes of the phase factors. The phase combination which provides the lowest PAPR is kept as

Table 6.1: Simulation Parameters

Parameter	Value
No. of Subcarriers	64
Modulation	QPSK
Oversampling	4 times
No. of OFDM symbols	3×10^5
No. of subcarrier groups for [108]	16
Channel	AWGN

the phases of the pilot symbols. Instead of sending the lowest-PAPR providing W-H sequence, unlike [108], we detect this transmitted phase factor vector from the received phases of the pilot symbols using the phase factor detection technique proposed in [107]. This enable us to avoid allocating a portion of bandwidth for sending SI. Since the proposed scheme exploits the inherent feature of IEEE 802.11 and IEEE 802.16 standards, it can be integrated to any WiFi and WiMAX devices for better energy-efficiency due to the low PAPR and quality of service because of more spectrum.

The block diagram of the PDPF scheme is shown in Fig. 6.3. In the PDPF scheme, the available subcarriers are divided into two groups: data subcarriers and pilot subcarriers. Suppose that N_d and N_p denote the number of data and pilot subcarriers, respectively. Hence, the total number of subcarriers is $N = N_d + N_p$. The input binary data sequence is firstly converted to a vector of complex numbers, $B = [b_1\ b_2\ b_3\ \ldots\ b_{N_d}]^T$, where T denotes matrix transpose operation, according to a mapping technique. The mapped data symbols are partitioned into N_p disjoint groups. Suppose that the set $G = \{g_1,\ g_2,\ g_3,\ \ldots, g_{N_p}\}$ consists of all data groups, where $g_k = [g_k[1]\ g_k[2]\ \ldots\ g_k[N]]^T$ denotes the k^{th} group. The content of the k^{th} group is given by

$$g_k[l] = \begin{cases} b_\rho & \text{for } (k-1)R + k \leq l < (k-1)R + \gamma + k - 1 \\ & \text{and } (k-1)R + \gamma + k - 1 < l \leq kR + k \\ 0 & \text{otherwise,} \end{cases} \tag{6.1}$$

where $R = \frac{N_d}{N_p}$, l and k are integers for $0 < l \leq N$ and $1 \leq k \leq N_p$, respectively, and γ is the index of the first zero element of g_1. Actually, γ is equal to the lowest

value of l for which $g_1[l] = 0$, indicating the location of the first pilot symbol. The parameter ρ is an integer defining the index of a particular element of B, b_ρ, copied to g_k. The relationship between ρ, l and k is defined as

$$\rho = \begin{cases} l-k+1 & \text{for } (k-1)R+k \leq l < (k-1)R+\gamma+k-1 \\ l-k & \text{and } (k-1)R+\gamma+k-1 < l \leq kR+k. \end{cases} \tag{6.2}$$

In MOPS scheme, each group, g_k, is then multiplied by the phase factor, $q^i_{j,k}$, where $q^i_{j,k}$ is the k^{th} element of the j^{th} W-H sequence of the i^{th} group of sequences. In the first turn, the k^{th} group is multiplied by the k^{th} element of the first W-H sequence. After the multiplication, the $[(k-1)R+\gamma+k-1]^{th}$ symbol of the k^{th} group is replaced by the k^{th} pilot symbol of the first W-H sequence to form the k^{th} sub-block. The resulting N_p sub-blocks are added together to form a block, S^i_j, where i is an integer ranging from 1 to I and I equals to 1 and N_p for MOPS and MSZCS, respectively, and $j = 1$ for the first W-H sequence. The newly formed block S^i_j is then converted to a time-domain (TD) signal by inverse fast Fourier transform (IFFT). Then PAPR of this TD signal is computed and stored along with the signal. Afterwards, a new W-H sequence is generated (the increment of j in Fig. 6.3 indicates the new sequence generation). Each of the previously formed groups is multiplied by the respective element of this newly generated W-H sequence, and all the subsequent operations are carried out as before. This loop continues until the target PAPR is achieved or the allowable maximum number of sequence N_p is reached. Out of the N_p TD signals, the signal having the lowest PAPR is selected and transmitted. Pertinently, the system PAPR determination block of Fig. 6.3 has no function for the MOPS scheme. It is only used by the MSZCS scheme. The W-H sequence which provides the transmitted signal is detected at the receiver using the algorithm proposed in [107].

The MOPS is designed to improve PAPR without sending any SI. However, we can further improve the PAPR using MSZCS in which the no-SI requirement is compromised. We generate a number of groups of orthogonal sequences using Zadoff-Chu sequence, and each group consists of N_p sequences with each sequence consisting of N_p elements. For I groups, a Zadoff-chu sequence of IN_p^2 elements are generated, which is followed by a sub-sampling which in turn is followed by an interleaving. The process of the whole sequence generation is given by

$$Z[v] = e^{\frac{\sqrt{-1}\pi v^2}{IN_p^2}}, \tag{6.3}$$

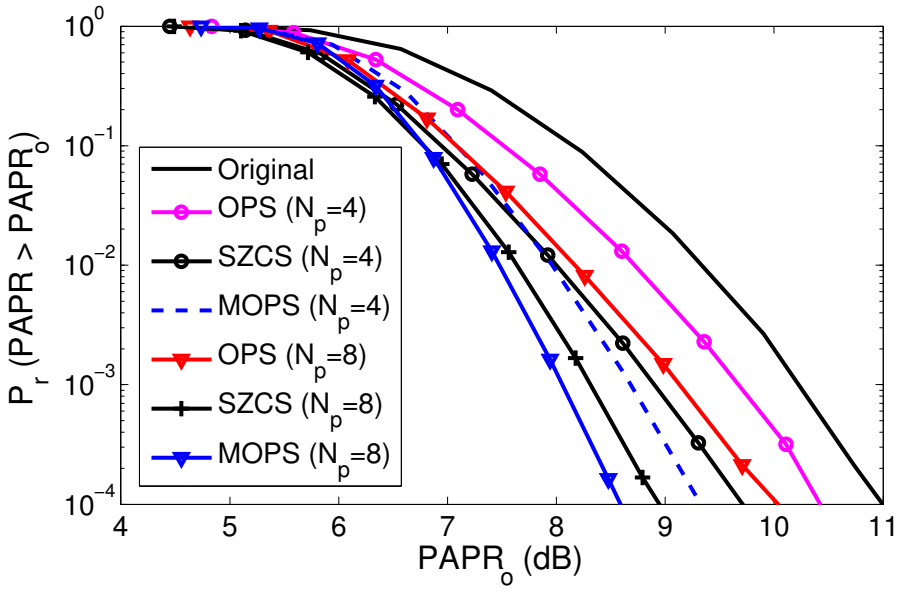

Figure 6.4: Comparative PAPR of MOPS scheme

where v is an integer ranging from 0 to IN_p^2. Then, the sub-sampling is carried out. The u^{th} element of the j^{th} sequence in the i^{th} group is produced using the following interleaving rule [108]:

$$Y_{j,u}^{i} = Z[(i-1)N_p + j + uIN_p]. \tag{6.4}$$

All sequences in a particular group, generated following Eq. (6.4), are orthogonal to each other [108].

For a particular group i, the MSZCS scheme works similarly to the MOPS scheme: for each sequence of the group, it produces a TD signal along with its PAPR; thereby, each group provides N_p TD signals with N_p PAPRs. Of them, the signal having the lowest PAPR is stored, and the next group of SZCS sequences is tried, which is shown in Fig. 6.3 by the increment of i. Thus, this procedure gives I TD signals with PAPR, one from each group. Of them, the lowest-PAPR providing signal is transmitted, and the index of the group which contributes the transmitted signal is transmitted as SI. It requires to send $log_2(I)$ bits as SI. Since the SI is usually not included in the OFDM block and is transmitted separately, its transmission does not affect the PAPR of an OFDM signal. Knowing the lowest-PAPR providing group index, i, the receiver uses the OPS

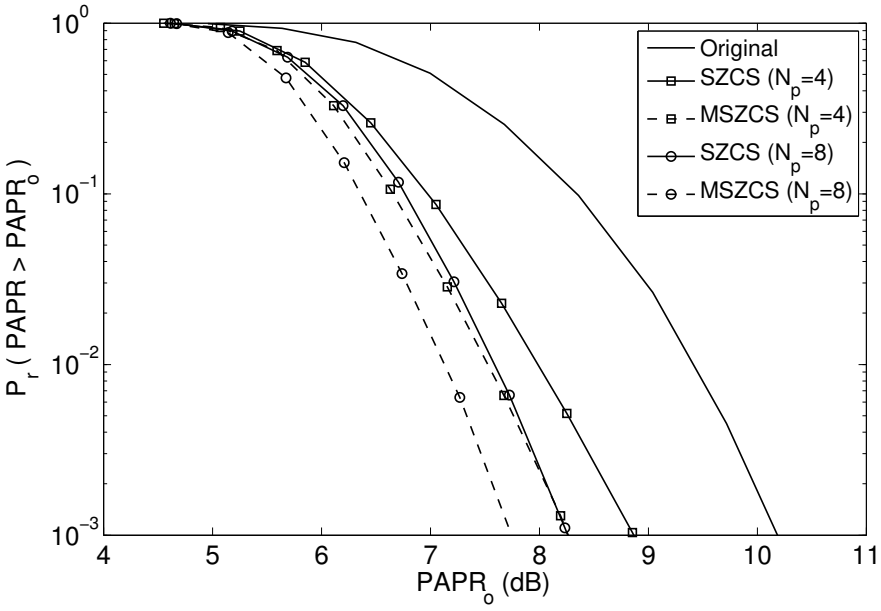

Figure 6.5: Comparative PAPR of MSZCS scheme

detection algorithm [107] to find the i^{th} group's j^{th} sequence which provided the lowest PAPR signal.

6.4 Performance evaluation

We evaluate the proposed system's performance in terms of PAPR, BER, and computational complexity. The simulation parameters are enlisted in Table 6.1

Fig. 6.4 shows the comparative PAPRs of MOPS scheme using complementary cumulative distribution function (CCDF). It is evident that MOPS can achieve more PAPR reduction compared to both OPS and SZCS. At a CCDF level of 10^{-4} with $N_p = 4$, it achieves three times and 40% more PAPR reduction compared to the OPS and SZCS, respectively, from the original OFDM. It also reveals that the use of more pilot subcarriers results in more PAPR reduction. PAPR of the MOPS scheme with $N_p = 4$ is less than that of the OPS and SZCS with $N_p = 8$. Since using more subcarriers as pilot reduces data subcarriers, MOPS achieves better spectrum efficiency compared to both schemes. Pertinently, the SZCS achieves PAPR reduction compromising the no-SI transmission while MOPS does not compromise it. The PAPR reduction performance of the MSZCS scheme is

Table 6.2: Computational complexity comparison

Scheme	Additions	Multiplications	Complex exponential
OPS	N_pP	N_pQ	$\times$
SZCS	N_pIP	$N_pI(Q+3N_p)$	N_p^2I
MOPS	N_pP	$N_p(Q+2N_d)$	$\times$
MSZCS	N_pIP	$N_pI(Q+3N_p+2N_d)$	N_p^2I

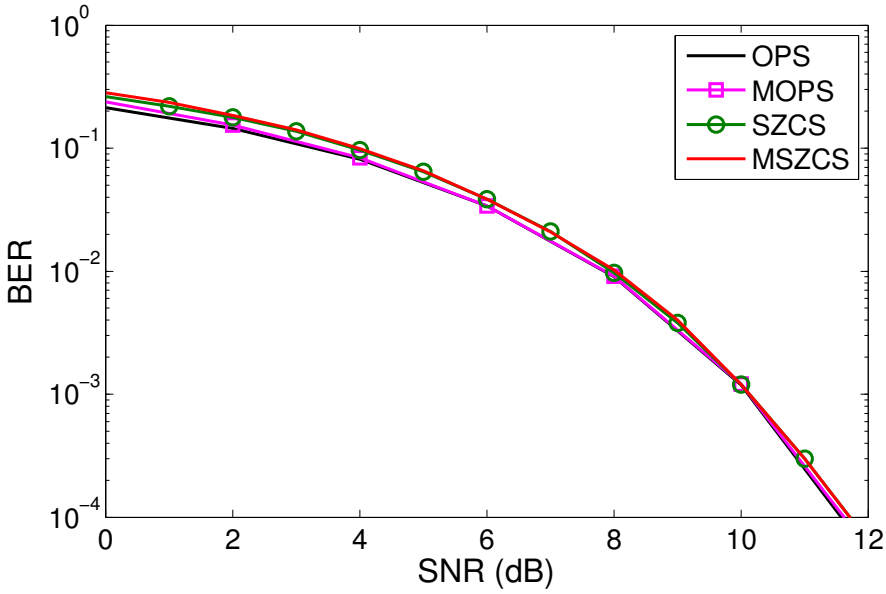

Figure 6.6: BER performance of MOPS and MSZCS

investigated in Fig. 6.5 for $I = 32$. The MSZCS outperforms the SZCS. For $N_p = 4$, it improves PAPR by 45% compared to the SZCS. When the number of pilot subcarriers increases, it still outperforms the SZCS by 0.51 dB. One interesting point is that the PAPR achieved by the SZCS for $N_p = 8$ can be obtained by the MSZCS using only four pilot subcarriers. Thus, for a given PAPR performance, the MSZCS is more spectrum efficient. In terms of BER, the PDPF has almost the same performance as the OPS and SZCS schemes as is revealed from Fig. 6.6. Thus, we can say that the PDPF improves PAPR significantly without markedly affecting other performance factors. In computational complexity comparison, the computations that are common in all schemes are not considered. Table 6.2 gives the computational complexity comparison, where $P = Nlog_2(N) + 4N - 1$ and $Q = \frac{N}{2}log_2(N) + 4N + 1$. MOPS scheme is found slightly more complex than

the OPS scheme in case of multiplications. For $N = 64$, $N_p = 4$, and $I = 16$ in case of the SZCS scheme, the MOPS scheme requires 94% and 97% less addition and multiplication operations, respectively, compared to the SZCS scheme. The MSZCS scheme has slightly more computational complexity compared to the SZCS scheme.

6.5 Conclusion

We proposed a new distortionless PAPR reduction scheme for OFDM systems. We partitioned the data symbols into a number of groups, and each group was multiplied by the phase factor derived from the pilot symbols' phases; the pilot symbols' phases were changed iteratively following a W-H matrix. Through simulations, the proposed scheme was found to be able to reduce more PAPR than the traditional schemes. In addition, it did not increase computational complexity significantly. To attain more PAPR, it did not compromise BER performance. In a short, by overcoming the problem of low PAPR reduction feature of OPS without sacrificing no-SI transmission, the proposed scheme made the OPS-based scheme a limitation-less scheme.

Chapter 7

Spectrum Efficient DSI-Based OFDM PAPR Reduction by Subcarrier Group Modulation

The PAPR reduction techniques belonging to the subcarrier reservation category suffer from spectrum efficiency loss. In this chapter, a new scheme will be proposed to overcome the shortcoming. Before going to the proposed scheme, the necessary background techniques will be described in short.

7.1 Background

There are two most popular techniques which require to reserve a certain number of subcarriers for reducing PAPR: TR and DSI. The performance of both techniques are excellent. However, they reduces throughput due to the reduction of the spectrum efficiency caused by the subcarrier reservation. A short explanation of the principle of the TR technique has been provided in Chapter 3. We will describe the DSI scheme next.

The block diagram of the DSI scheme is shown in Fig. 7.1. The input data stream is first bandpass modulated before performing a S/P conversion. For a total of N subcarriers, N_A subcarriers are used for sending $\alpha_A = N_A \times log_2(M)$ data bits, where M is the modulation order; the rest of the $N_B = N - N_A$ subcarriers are used for PAPR reduction purpose. To these N_B subcarriers, either

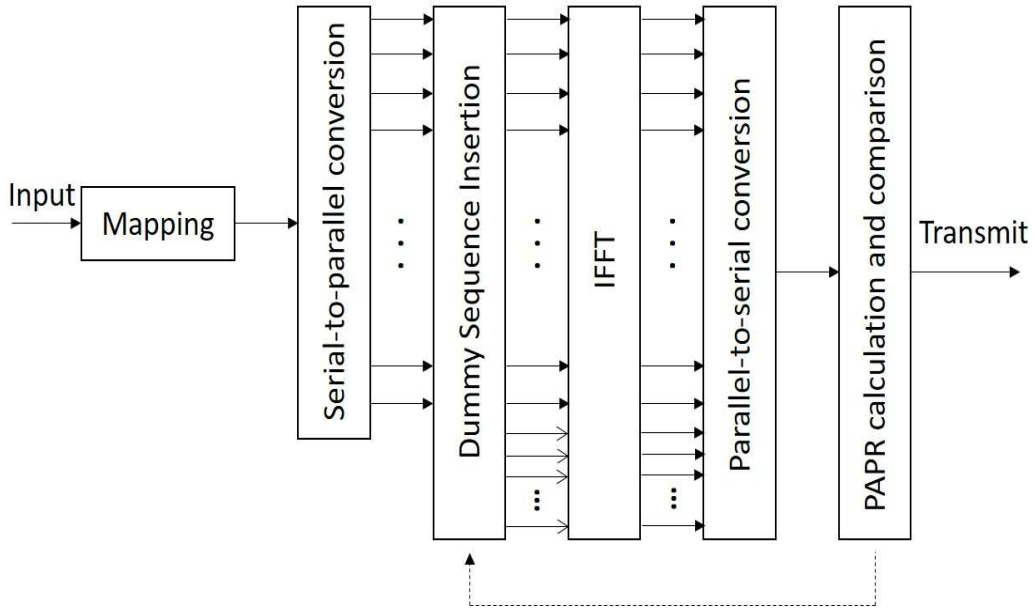

Figure 7.1: Block diagram of the DSI scheme

a complementary sequence or a correlation sequence is assigned. The resulting N symbols are fed to the IFFT block for the frequency-to-time domain conversion, which is followed by a P/S conversion. The PAPR of the resulting sequence is calculated, and the sequence along with its PAPR is stored. Then a new sequence for PAPR reduction is assigned to the N_B subcarriers, while the data to the first N_A subcarriers remain unchanged. The resulting sequence is converted to a TD sample sequence which then undergoes a P/S conversion. This sequence along with its PAPR is stored as before. Then, another sequence is tried, and this process continues until the allowable maximum number of sequences are tried. For R sequences, it produces R TD signals. Then the PAPRs of all signals are compared, and the TD signal having the lowest PAPR is selected for transmission.

In this technique, N_B subcarriers are used for PAPR reduction rather than data transmission. For this reason, it transmits $\alpha_B = N_A \times log_2(M)$ bits less than the conventional OFDM system. This reduction of bit transmission causes spectral efficiency degradation. Recalling the spectral efficiency of an OFDM system in

fading channel from 2.16

$$\eta_1 = \frac{\alpha}{N + L_{cp}}, \tag{7.1}$$

where $\alpha = \alpha_A + \alpha_B$. In AWGN channel, there is no intersymbol interference issue, hence requires no CP. In this case, (7.1) becomes

$$\eta_2 = \frac{\alpha}{N}. \tag{7.2}$$

Equation (7.1) can be rewritten as:

$$\eta_1 = \frac{(N_A + N_B) log_2 M}{N + L_{cp}}. \tag{7.3}$$

The spectral efficiency of the DSI scheme is

$$\eta_{1,d} = \frac{N_A log_2 M}{N + L_{cp}}. \tag{7.4}$$

Equation (7.4) can also be written in the following form:

$$\begin{aligned} \eta_{1,d} &= \frac{\alpha - \alpha_B}{N + L_{cp}} \\ &= \eta_1 - \frac{\alpha_B}{N + L_{cp}}. \end{aligned} \tag{7.5}$$

From (7.3) and (7.4), we get

$$\eta_{1,d} = \frac{N_A}{N_A + N_B} \eta_1. \tag{7.6}$$

In the DSI scheme, $N_B > 0$; as a result $\eta_{1,d} < \eta_1$; in other words, the spectral efficiency of the DSI scheme is always less than that of the conventional OFDM system. It is $\frac{N_A}{N_A+N_B}$ times lower than that of OFDM system. It degrades more with the increase of N_B.

Similar to the DSI scheme, the TR scheme equally suffers from the spectrum efficiency loss. After the proposal of TR [55] in 2000, many works [92, 93, 94] have been carried out on TR. All these works, however, have either dealt with attaining more PAPR reduction or complexity reduction of the technique. Similarly, several works have been carried out on DSI scheme; most of which either propose the applicability of it in different scenarios or to improve the PAPR reduction capability of it. To the best of our knowledge, *no work has yet been done to address the bandwidth inefficiency issue of these two schemes.*

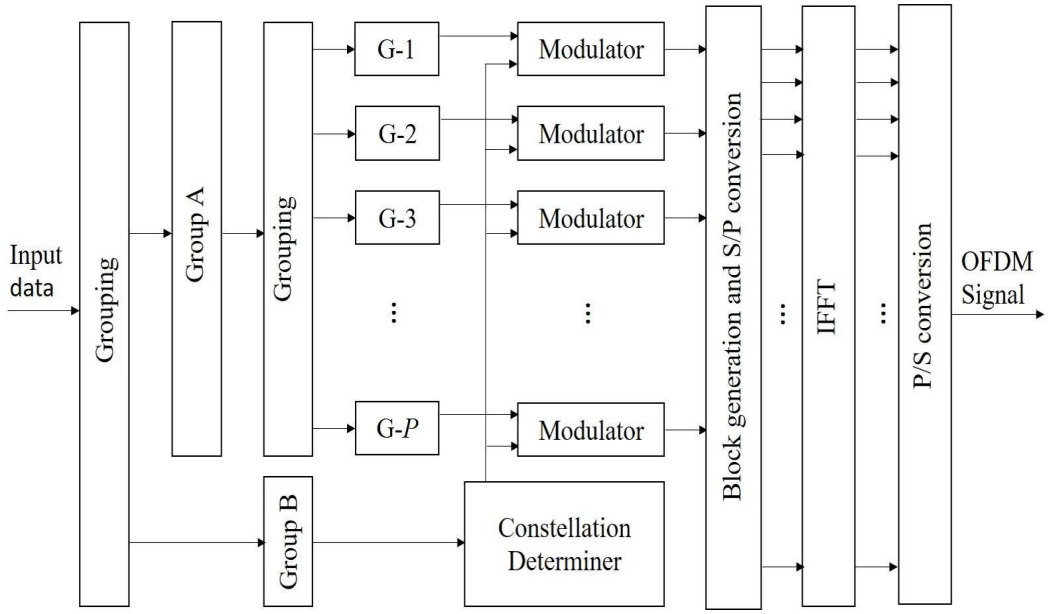

Figure 7.2: Block diagram of SGM

7.2 Contribution

In this chapter, we address the bandwidth inefficiency issue to make the schemes such as DSI and TR bandwidth efficient. We propose a concept of subcarrier group modulation (SGM), where the available subcarriers are divided into a number of groups, and each group is modulated by one of the candidate constellations of the 4-QAM; each group of the subcarriers is associated with an extra bit depending on the constellation used in the group. At the receiver, a maximum likelihood (ML) detection is used to identify the constellation used in a particular group. The extra bit sent with each group can compensate for the reduction of the number of transmitted bits due to the reservation of a certain number of subcarriers for PAPR reduction, hence both DSI and TR schemes do not need to compromise the throughput in attaining the low PAPR. Thus, the SGM makes both schemes bandwidth efficient. Here, we integrate the SGM with the DSI scheme to show its performance. Through simulations, we show that the SGM-based DSI scheme attains the same PAPR as the DSI scheme does. In addition, the blind detection of modulation at the receiver does not degrade BER significantly.

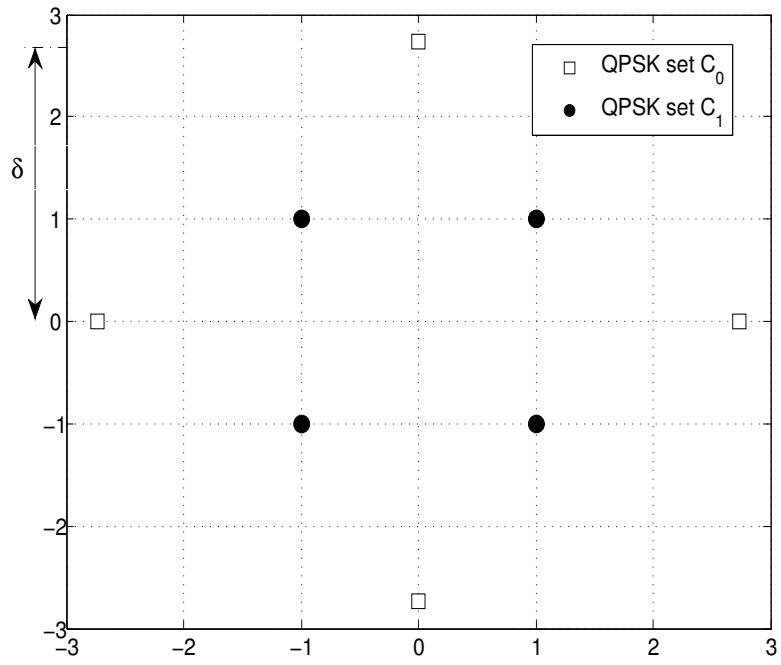

Figure 7.3: A constellation design example for SGM

7.3 Proposed Scheme

The notion of the SGM scheme is explained first before it is integrated to the DSI scheme for PAPR reduction.

7.3.1 Subcarrier Group Modulation

SGM is a technique of sending more bits than the conventional OFDM system. The conventional OFDM system of N subcarriers can transmit $\alpha = Nlog_2M$ bits. However, the proposed OFDM with SGM can transmit more than α bits. Figure 7.2 shows a block diagram of the proposed SGM. The incoming bits of length α are first divided into two groups: group A and group B, where the length of the group A, α_A, should be greater than that of the group B, α_B. Out of the N subcarriers, N_A subcarriers are allocated for group A bits, and the rest $N_B = N - N_A$ subcarriers for the group B bits. The number of bits in the groups

A and B are as follows:

$$\alpha_A = N_A log_2 M, \tag{7.7}$$

$$\alpha_B = N_B log_2 M. \tag{7.8}$$

Then, the α_A bits are divided into P subgroups, where $P = \alpha_B$, with each group which consists of $K = \frac{\alpha_A}{P}$ bits. Each of these groups is modulated by the 4-QAM modulation. However, not all groups are modulated according to the same constellation; rather, two different constellations are used. An example of such constellations is given in Fig. 7.3, which has recently been independently proposed to use in OFDM with index modulation [141], and δ is a design parameter whose value depends on a specific scenario. Either set C_0 or set C_1 as constellation will be used in a particular group depending on the respective bit in the set B. Since $P = \alpha_B$, there is a one-to-one correspondence between a group and a bit in the group B. The constellation set used to modulate the i^{th} group depends on the i^{th} bit in the group B. Suppose that the constellation set C_0 corresponds to bit 0 and the set C_1 to bit 1. Thus, if the i^{th} bit in the group B is 0, the constellation set C_0 will be used to modulate the i^{th} group of data; otherwise, the set C_1 will be used. In this way, one bit is associated to a data group, and each group carries one bit more than K bits. The bits of the group B are never transmitted directly, rather, these are indirectly transmitted by associating these bits with the data groups. Now, the subcarriers allocated for α_B bits become free. These N_B subcarriers can be used for transmitting α_B more bits. In this way, the OFDM with SGM scheme of N subcarriers can transmit $\alpha + \alpha_B$ bits, which is α_B bits more than that of the conventional OFDM system. The conventional OFDM cannot transmit these α_B bits. If it wants to transmit the α_B bits, it requires N_B more subcarriers. However, the OFDM with SGM transmits α_B more bits compared to the conventional OFDM without using any additional subcarriers. After the modulation, the outputs of the P modulators are rearranged to form a block of N symbols, which is followed by a S/P conversion. The parallel data block is then converted from the FD to the TD using the IFFT before it is again converted to a serial data block. Then a CP is appended at the beginning of the TD serial OFDM block to reduce the effects of intersymbol interference.

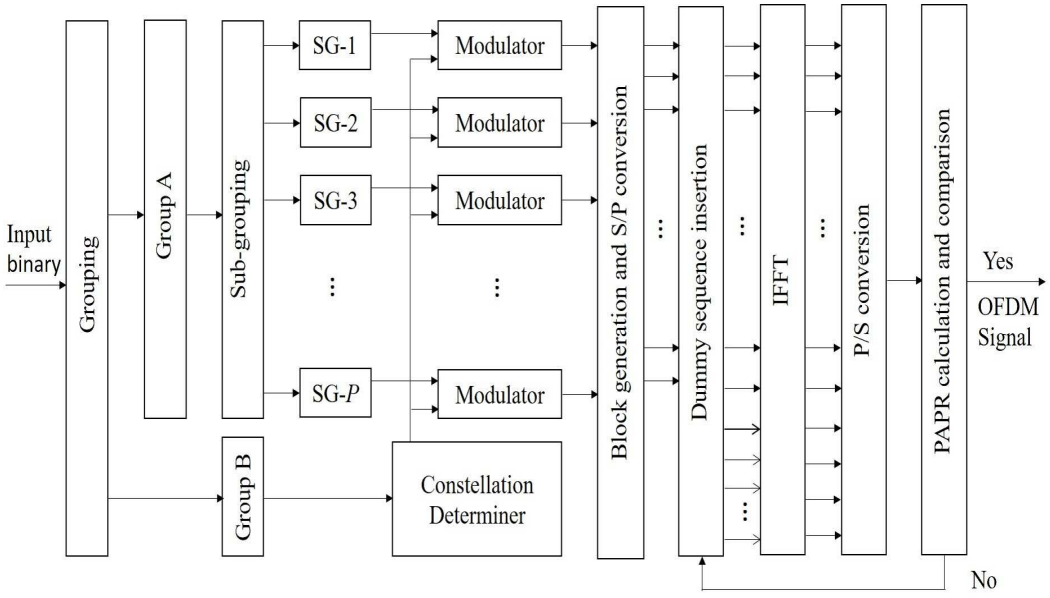

Figure 7.4: Block diagram of the DSI scheme with SGM

In the conventional OFDM, the same mapping scheme is used throughout an OFDM block, and the receiver knows the constellation of the mapping scheme. However, OFDM with SGM does not use the same constellation throughout the block; rather it changes the constellation from group to group. Thus, the receiver does not know the constellation with which a particular data group has been modulated. For this reason, the receiver needs to detect the constellation used in each group. Since no SI is sent to the receiver, it needs to detect the constellation set blindly. We propose to use an optimal ML detection algorithm to detect the constellation set used in a particular group of the received OFDM block. At the receiver, the CP is first removed, and the resulting signal of length N is converted to FD by the FFT. If Y is the received FD OFDM symbol, then its k^{th} element, Y_k, can be modelled in the following way:

$$Y_k = X_k H_k + W_k \tag{7.9}$$

where H_k and W_k are the frequency response of the fading channel and frequency domain additive noise with zero mean and variance of σ^2, respectively, and X_k denotes the k^{th} transmitted symbol. Then the data block is partitioned into P groups with each group consisting of $\beta = K/log_2 M$ symbols, thereby creating a new matrix Z such that $Z_{l,k}$ indicates the k^{th} element of the l^{th} group. To

determine which set of constellation is used in each of the data groups, ML detection is carried out in each group. Given that S_l is the l^{th} group of the received OFDM symbol Y, the probability that S_l is modulated by the C_i constellation set is given by [142]

$$P(S_l|C_i) = \prod_{k=1}^{\beta} \left(\frac{1}{M\sqrt{2\pi\sigma^2}} \sum_{j=1}^{M} e^{\frac{|Z_{l,k}H_{l,k}^{-1} - c_j^i|^2}{2\sigma^2}} \right) \tag{7.10}$$

where C_i and M are the i^{th} constellation set and constellation size, respectively, and c_j^i is the j^{th} constellation point of the i^{th} constellation set. Since both constellations are of equiprobable, the data group S_l will be considered as modulated by the q^{th} constellation if $P(S_l|C_i)$ is maximized at $i = q$. Upon the constellation detection, each group is de-mapped according to the detected constellation, and converted to a binary sequence.

7.3.2 DSI with SGM PAPR reduction scheme

The DSI with SGM scheme combines the DSI scheme with the SGM scheme to eliminate the spectral efficiency degradation of the DSI scheme. A block diagram of the proposed scheme is shown in Fig. 7.4. Similar to the SGM scheme discussed in Section III, the incoming data of length α is first divided into two groups: A and B. Depending on the length of B, the group A is divided into a number of subgroups. Each subgroup is either modulated by the constellation C_0 or C_1 depending on the content of B. After the modulation, the content of B becomes embedded in N_A subcarriers. In this way, all α bits are transmitted. Even after this, there are still N_B unused subcarriers which we use for PAPR reduction. The remaining subcarriers can be used in any PAPR reduction scheme such as DSI or TR. If we use DSI, the sequence for PAPR reduction is assigned to the rest N_B subcarriers, thereby making a FD data block of N symbols which are assigned to N subcarriers. Then this block is converted to a TD signal before converting back to the serial sequence. The PAPR of this TD signal is calculated, and the signal with its PAPR is stored similarly to the DSI scheme. Then a new PAPR reduction sequence is inserted in the last N_B sequence in the dummy sequence insertion block before IFFT and P/S conversion are performed on the resulting signal. As before, PAPR computation is carried out, and the signal along with

Table 7.1: Simulation Parameters

Parameter	**Value**
N	128
L	4
Modulation	QPSK
L_{cp}	1/4
No. of OFDM symbols	5×10^4

the PAPR is stored. This process continues as long as the allowable maximum number of sequences for PAPR reduction are tried. Then the TD signal having the lowest PAPR signal is transmitted. The spectral efficiency of an OFDM with SGM system is given by

$$\begin{aligned}
\eta_{os} &= \frac{P\left(\frac{N_A log_2 M}{P} + 1\right) + N_B log_2 M}{N + L_{cp}} \\
&= \frac{(N_A log_2 M + P) + N_B log_2 M}{N + L_{cp}} \\
&= \frac{(N_A log_2 M + N_B log_2 M) + N_B log_2 M}{N + L_{cp}} \\
&= \frac{\alpha + \alpha_B}{N + L_{cp}} \\
&= \eta_1 + \frac{\alpha_B}{N + L_{cp}}.
\end{aligned} \tag{7.11}$$

Since the second term in the right side of the above equation is a positive number, the OFDM with SGM scheme attains more spectral efficiency compared to that of the conventional OFDM scheme. The spectral efficiency of the DSI with SGM

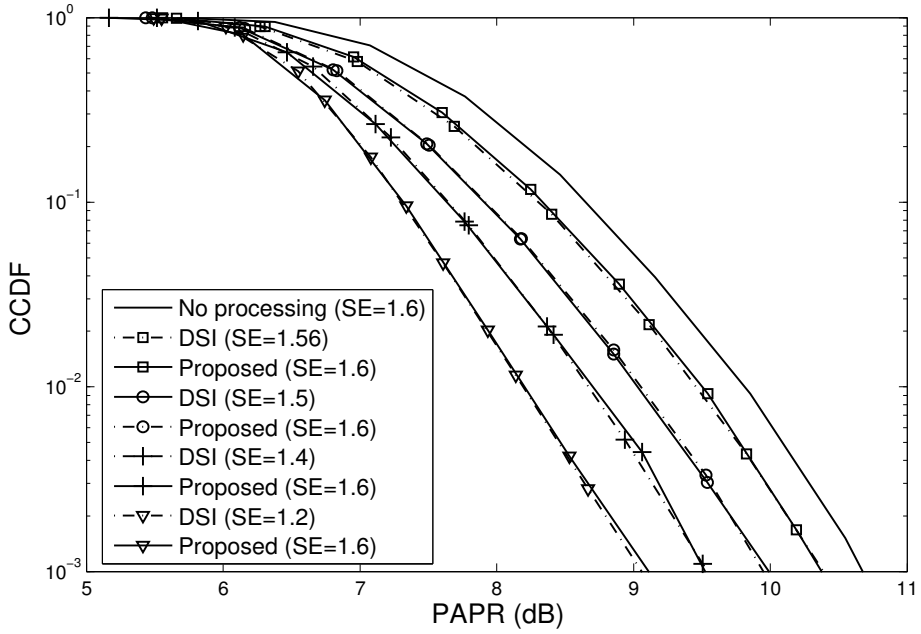

Figure 7.5: Comparative PAPR for $\delta = 1.5$

scheme is given by

$$\begin{aligned}
\eta_{dp} &= \frac{P\left(\frac{N_A log_2 M}{P} + 1\right)}{N + L_{cp}} \\
&= \frac{N_A log_2 M + P}{N + L_{cp}} \\
&= \frac{N_A log_2 M + N_B log_2 M}{N + L_{cp}} \\
&= \frac{\alpha_A + \alpha_B}{N + L_{cp}} \\
&= \frac{\alpha}{N + L_{cp}} \\
&= \eta_1.
\end{aligned} \tag{7.12}$$

Thus, unlike the DSI scheme, the DSI with SGM attains PAPR reduction maintaining the same spectral efficiency of the conventional OFDM system.

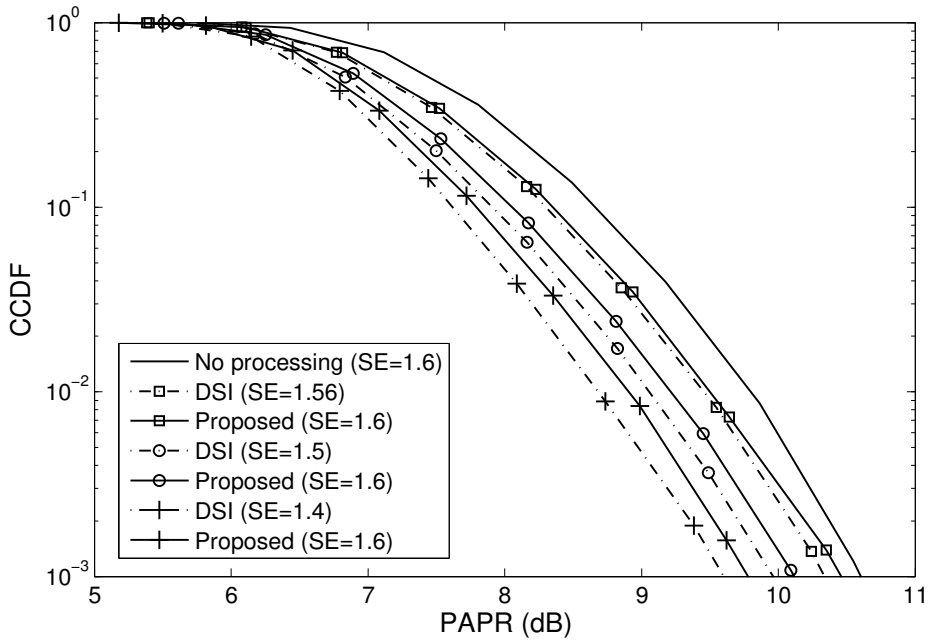

Figure 7.6: Comparative PAPR for $\delta = 2.5$

7.4 Performance Evaluation

The spectral efficiency improvement of the proposed DSI with SGM scheme has been explained in detail analytically in Section IV (B). It is found that the proposed PAPR reduction scheme can attain the same spectral efficiency of the original OFDM system. To attain the spectral efficiency, the frequency domain signal is changed in the transmitter. Through simulations, the impact of such changes on some other performance factors, such as PAPR reduction capability and BER, will be investigated. The simulation parameters used throughout the paper are listed in Table 7.1, unless otherwise stated.

A comparison of the PAPR reduction performance between the proposed SGM integrated DSI and conventional DSI schemes is shown in Fig. 7.5 for $\delta = 1.5$ with the help of CCDF, where SE stands for spectrum efficiency. It reveals that without degrading spectrum efficiency compared to the unmodified OFDM, the proposed scheme attains as much PAPR reduction as the DSI scheme does. The OFDM with no PAPR reduction technique, indicated as no processing in

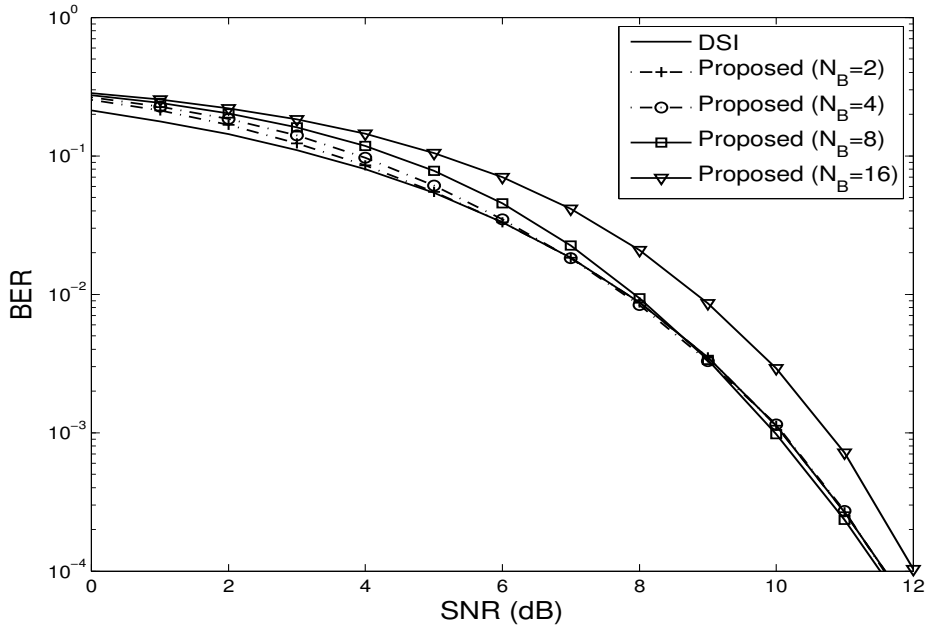

Figure 7.7: BER comparison between the proposed and DSI scheme over AWGN channel

Fig. 7.5, has 1.6 bit/sec/Hz spectrum efficiency. The DSI scheme degrades the spectrum efficiency in improving PAPR. For example, the DSI scheme sacrifices 0.1 bit/sec/Hz spectrum efficiency to reduce 0.73 dB PAPR. However, the SGM integrated DSI scheme attains the PAPR similar to the SGM scheme maintaining the spectrum efficiency of 1.6 bit/sec/Hz. More PAPR reduction in the DSI scheme causes further degradation of the spectrum efficiency. For example, it degrades 25% spectrum efficiency compared to the unmodified OFDM in reducing about 1.6 (dB) PAPR. The SGM integrated DSI scheme, on the other hand, achieves the same PAPR reduction without causing any degradation of the spectrum efficiency. The impact of using the constellation C_0 with higher power is investigated in Fig. 7.6 for $\delta = 2.5$. It reveals that the proposed scheme results in a slight degradation of PAPR compared with the DSI scheme. This degradation is found to have a direct relationship with the number of subcarriers employed for PAPR reduction: a system having more PAPR reducing subcarriers experiences slightly more degradation. At CCDF level of 10^{-2}, 10% to 20% degradation of PAPR reduction capability occurs depending on the number of subcarriers used

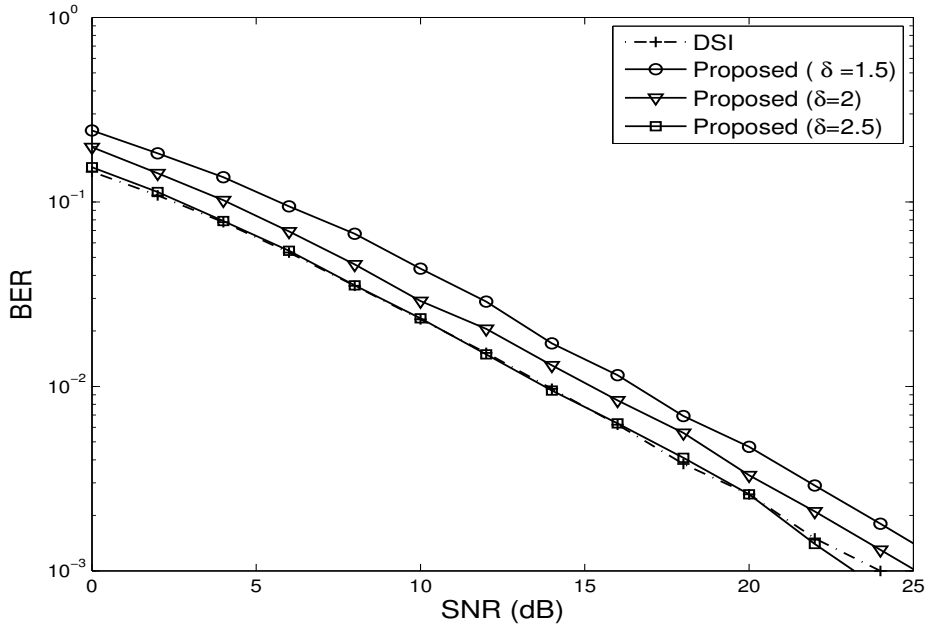

Figure 7.8: BER comparison between the proposed and DSI scheme over Rayleigh fading channel

for PAPR reduction. The reason behind the degradation might be the fact that the comparatively larger power in constellation C_0 increases both the peak power and average power, but the peak power increase is slightly higher than the average power increase. For this reason, the corresponding ratio is increasing. However, it is pertinent to mention here that the proposed scheme results in the slight loss of PAPR reduction capability while preserving the spectrum efficiency of original OFDM system. On the other hand, the DSI scheme decreases the spectrum efficiency significantly.

The BER performance of the proposed scheme is evaluated over both AWGN and fading channels. A comparison of the BER performance of the proposed scheme with the DSI scheme over AWGN channel for $\delta = 1.5$ is shown in Fig. 7.7. A direct relation is observed between N_B and BER. For low N_B, the BER degradation compared to the DSI due to the proposed scheme is insignificant. In addition, the degradation increases to a maximum value for $N_B = 16$. With the larger N_B, the number of subgroups under group A increases; thus, for a specific

N, the number of symbols in a specific group decreases. The reduced number of symbols make the ML detector difficult at the receiver to detect the constellation set properly, hence the error rate increases. This might be a reason behind the degradation of the BER performance in higher N_B. It is seen in Fig. 7.7 that the BER degrades with higher N_B. The worst case scenario is $N_B = 16$. Under this value, the effect of δ on the BER in fading channel is investigated. The BER performance over fading channel is investigated in Fig. 7.8. A slowly-varying frequency selective Rayleigh fading channel with four taps is used in the simulation in Fig. 7.8. It reveals that higher δ provides better BER compared to the lower ones, and $\delta = 2.5$ attains the same BER such as the DSI scheme. The increased δ helps symbols to combat the effect of fading channel, which results in better detection by the ML detector. However, the use of high power can be avoided in application such as wireless optical OFDM where fading is not an issue. In such an application, the PAPR reduction similar to the conventional DSI scheme can be achieved alongside 100% spectral efficiency without increasing constellation power markedly. Considering Figs. 7.5, 7.6, and 7.8, the impact of δ on the system performance can be assessed. On the one hand, the large δ degrades PAPR performance. It improves BER performance, on the other hand. Thus, the choice of δ is application dependent. If PAPR reduction is the most desired criterion, a lower δ such as $\delta = 1.5$ is more suitable. However, if any degradation of BER performance is not permitted, a higher δ such as $\delta = 2.5$ is more suitable.

7.5 Conclusion

In this chapter, a concept of SGM has been proposed to eliminate the spectral inefficiency issue of most of the existing PAPR reduction schemes. It can be integrated to a number of different PAPR reduction schemes like DSI, TR, PTS, SLM and so on. In this paper, we investigated the performance of the SGM integration to the DSI scheme. We showed analytically that the proposed scheme attains 100% spectral efficiency. Through simulations, it was shown that it achieves PAPR similar to the DSI scheme in certain scenarios. In fading channel, a constellation with higher power is required to use to ensure perfect BER. The use of the constellation causes a degradation of 10% to 20% PAPR reduction capability. However, the advantage of the 100% spectral efficiency attainment

outweighs the slight loss of the PAPR reduction capability. We do not need to sacrifice any PAPR reduction capability in applications like wireless optical OFDM.

Chapter 8

Conclusions and Future work

8.1 Conclusions

The contemporary wireless systems are based on OFDM because of its excellent spectrum efficiency and resilience to multipath fading. To date, most of the candidate waveforms for 5G wireless systems are also variations to the OFDM; thus, it is being anticipated that OFDM will play a vital role in the future wireless systems as well. In this thesis, we dealt with the most serious drawback of the OFDM system: high PAPR. The contributions of the thesis can be summarized as follows:

- We provided a thorough explanation on the fundamentals of OFDM. The characteristics of wireless channels were shortly described. Then the evolution of OFDM from telegraph system was discussed. In addition, the principle of orthogonality and its inclusion in the OFDM system were explained in detail. Afterwards, we described different merits and demerits of the OFDM system. Chapter 2 can be considered as a tutorial on OFDM.

- A short survey on PAPR reduction techniques were provided. The reason behind the high PAPR was thoroughly explained. Furthermore, the performance criteria of a PAPR reduction technique were described. Then, different existing PAPR reduction techniques were critically analyzed. Most of the distortionless techniques were found spectrum inefficient, while the signal distortion techniques were found less complex but nonlinear. To

avail the full advantages of a PAPR reduction technique, the distortionless techniques were found most effective.

- We proposed a distortionless PAPR reduction technique utilizing pilot subcarriers. It was based on iteratively changing positions of the pilot subcarriers among the data subcarriers to find a set of optimum pilot positions for producing the reduced PAPR. We designed a receiver that can effectively detect pilot subcarriers. The performance of the scheme was investigated with respect to its PAPR reduction capability, BER and power saving. It was found outperformed existing techniques in terms of PAPR reduction capability while preserving spectrum efficiency. However, it put an increased computational overhead on the receiver. Furthermore, signal average power was found to be increased slightly.

- An improved null subcarrier assisted PAPR technique was proposed to eliminate the two major shortcomings of the existing techniques: prohibitively high computational complexity and BER. We proposed a new transmitter design that can shade 98% computational complexity. Moreover, the proposed receiver improved BER dramatically. The improved performance made the null-data switching technique practically feasible. The proposed scheme, however, sacrifices about 10% PAPR.

- Considering the limited PAPR reduction capability of the conventional OPS based PAPR reduction techniques, we proposed a new transmitter design that can attain significantly improved PAPR. While the existing improved OPS scheme needed to compromise the no-SI transmission feature of the OPS scheme to attain twice the PAPR reduction capability, the MOPS scheme was found to achieve three-times more PAPR reduction without sacrificing the no-SI transmission. Furthermore, the proposed OPS scheme required 90% less computations compared to the existing SZCS scheme.

- Our final contribution was to transform all subcarrier reservation based PAPR reduction techniques into spectrum efficient ones. Proposing the concept of the subcarrier group modulation, we showed that the proposed spectrum efficient DSI and TR techniques can attain as much PAPR as their conventional designs can. It was also found that BER performance is

not required to be compromised. However, the computational complexity of the proposed receiver was found significantly high.

Among the proposed schemes, not all schemes perform equally with respect to a particular performance criterion. In terms of PAPR, while the MOPS scheme attains the highest PAPR reduction, the null-switching based scheme achieves the lowest reduction of PAPR. The MOPS scheme is also found to have the lowest computational overhead compared to the other ones, whereas the SGM-integrated OFDM has the highest computational complexity due to the optimal ML-detection at the receiver. In the SGM-integrated OFDM, the transmitter has the same complexity as the traditional OFDM systems and is the least complex compared to the rest of the proposed transmitters; however, the receiver is considerably complex in terms of computational overhead. For this reason, it is well suited to the uplink because the base station has more computation power compared to user equipment. The pilot repositioning scheme and null-switching scheme require almost similar computational complexity. In reducing PAPR, the null-switching scheme may give rise of OOB interference because of the reduced number of null subcarriers reserved for spectral leakage containment. If the similarities among the proposed schemes are considered, it is found that all schemes are spectrum efficient compared to the traditional schemes. In addition, all of them escalate BER by some negligible amounts.

8.2 Future Work

The thesis poses few new challenges to solve as well as opportunity to avail in future. We will outline the future research questions next.

- The BER of the pilot repositioning scheme largely depends on the pilot detection technique. To get better BER performance, it requires to assign more energy to the pilot subcarriers. Although the overall increase of the signal average power is negligible, it is better to use as less pilot power as possible. Further research can be carried out in this direction. In the proposed pilot detection technique, we have used the equidistant and high power properties of the pilot subcarriers. Since the phases of the pilot

symbols has not been used in the proposed pilot detection technique, they may also be incorporated in the pilot detection in addition to the equidistant and large-power properties. The pilot subcarriers can be assigned phases intelligently so that they can be used in the pilot detection. The combined effects of utilizing these three properties may significantly improve the pilot detection accuracy, and hence BER.

- In the null subcarrier assisted PAPR reduction schemes, the SNSs are no longer working to reduce OOB. The possibility of assigning a little energy to the SNSs and including their phases in the SNSs detection algorithm can be explored in future. Although it will further increase the receiver complexity, there is a possibility of getting improved BER performance.

- A hybrid PAPR reduction technique can be designed by combining the pilot repositioning scheme and the proposed OPS scheme. It will have two-stage PAPR reductions: (a) performing the repositioning to find the low PAPR providing frequencies of the pilot subcarriers, then (b) setting pilot phases according to either W-H sequence or SZCS sequence to further reduce the PAPR. The receiver also needs to carry out two-stage detection: pilot subcarreirs and pilot phases.

- The subcarrier group modulation is a new concept in communication systems. It requires to do a lot of further research to make it versatile. Some possible research scope include:

  - The proposed receiver of the SGM scheme uses optimal ML detection, whose complexity is markedly high. Hence, the foremost future research will be to design a low-complex receiver. Log-likelihood detection based receiver may significantly reduce the complexity.
  - The SGM scheme can be employed to any multicarreir communication in addition to the OFDM. For example, it can be a good research topic to explore the possibility of using it to MC-CDMA and estimate the corresponding merits.
  - It can be integrated to all PAPR reduction techniques which suffer from a loss of spectrum efficiency. For example, the coding techniques

can attain very much PAPR reduction but suffer from low spectrum efficiency. The possibility of the integration of the SGM with the coding techniques can be explored to assess the performance in terms of BER.

References

[1] ITU, "The world in 2014: ICT facts and figures (Release 2014)," *International Telecommunication Union*, 2014. x, 2

[2] A. S. Alam, *Scalable base station switching framework for green cellular networks*. PhD thesis, Open University, United Kingdom, 08 2014. x, 4

[3] Cisco, "White paper: Cisco visual networking index: global mobile data traffic forecast update, 2016 2021," tech. rep., Cisco, 2 2017. x, 5

[4] S. Cha, M. Park, S. Lee, K. J. Bang, and D. Hong, "A new PAPR reduction technique for OFDM systems using advanced peak windowing method," *IEEE Transactions on Consumer Electronics*, vol. 54, no. 2, pp. 405–410, 2008. xi, 48, 49, 50

[5] ITU, "The world in 2016: ICT facts and figures (Release 2016)," *International Telecommunication Union*, 2016. 1

[6] R. J. Baxley and G. T. Zhou, "Power savings analysis of peak-to-average power ratio reduction in OFDM," *IEEE Trans. on Consumer Electronics*, vol. 50, no. 3, pp. 792–798, 2004. 3

[7] P. Frenger and P. Moberg, "Reducing energy consumption in lte with cell dtx," in *Proc. IEEE Vehicular Technology Conference (VTC Spring)*, pp. 1–5, 2011. 4

[8] V. Mancuso and S. Alouf, "Reducing costs and pollution in cellular networks," *IEEE Communications Magazine*, vol. 49, no. 8, pp. 63–71, 2011. 4

[9] T. Jiang and Y. Wu, "An overview: peak-to-average power ratio reduction techniques for OFDM signals," *IEEE Trans. on Broadcasting*, vol. 54, no. 2, pp. 257–268, 2008. 4

[10] D.-W. Lim, S.-J. Heo, and J.-S. No, "An overview of peak-to-average power ratio reduction schemes for OFDM signals," *Journal of Communications and Networks*, vol. 11, no. 3, pp. 229–239, 2009. 4, 61, 62

[11] Y. Rahmatallah and S. Mahan, "Peak-to-average power ratio reduction in OFDM systems: a survey and taxonomy," *IEEE Communications Surveys and Tutorials*, vol. 15, no. 4, pp. 1567–1592, 2013. 4, 44, 51, 56, 67

[12] T. S. Rappaport, *Wireless Communication: Principles and Practice*. Prentice Hall PTR, 2002. 10, 11

[13] A. Goldsmith, *Wireless Communications*. Cambridge University Press, 2005. 10, 13

[14] M. Shawartz, *Mobile Wireless Commmunications*. Cambridge University Press, 2005. 10

[15] M. Engels, *Wireless OFDM Systems: How to Make Them Work?* Springer Science and Business Media, 2002. 11, 19, 20

[16] L. Yang, *Multicarrier Communications*. John Wiley and Sons Ltd, 2009. 11

[17] E. P. L. Be, *Adaptive Techniques for Multiuser OFDM*. PhD thesis, James Cook University, Australia, 12 2001. 13, 20

[18] K. G. Beauchamp, *History of Telegraphy*. IEE, 2001. 14

[19] A. G. Bell, "Improvement in telegraphy," 03 1876. 14

[20] M. Schwartz and C. Batchelor, "The origins of carrier multiplexing: major George Owen Squier and AT&T," *IEEE Communication Magazine*, vol. 46, no. 5, pp. 20–24, 2008. 14

[21] R. W. Chang, "Synthesis of band-limited orthogonal signals for multichannel data transmission," *The Bell System Technical Journal*, vol. 45, no. 10, pp. 1775–1796, 1966. 14

[22] Y. Xiao, "Orthogonal frequency division multiplexing modulation and inter-carrier interference cancellation," Master's thesis, Graduate Faculty, Louisiana State University, 2003. 14

[23] B. R. Saltzberg, "Performance of an efficient parallel data transmission system," *IEEE Trans. on Communication Technology*, vol. 15, no. 6, pp. 805–811, 1967. 14

[24] R. W. Chang and R. A. Gibby, "A Theoretical Study of Performance of an Orthogonal Multiplexing Data Transmission Scheme," *IEEE Trans. on Communication Technology*, vol. 16, no. 4, pp. 529–540, 1968. 14

[25] S. Weinstein and P. Ebert, "Data Transmission by Frequency-Division Multiplexing Using the Discrete Fourier Transform," *IEEE Trans. on Communication Technology*, vol. 19, no. 5, pp. 628–634, 1971. 14

[26] R. Peled and A. Ruiz, "Frequency domain data transmission using reduced computational complexity algorithms," in *Proc. IEEE Intl. Conf. Acoustics, Speech, and Signal Processing*, pp. 964–967, 1980. 14

[27] B. Hirosaki, "An Orthogonally Multiplexed QAM System Using the Discrete Fourier Transform," *IEEE Trans. on Communications*, vol. 29, no. 7, pp. 982–989, 1981. 15

[28] L. Cimini, "Analysis and Simulation of a Digital Mobile Channel Using Orthogonal Frequency Division Multiplexing," *IEEE Trans. on Communications*, vol. 33, no. 7, pp. 665–675, 1985. 15

[29] I. Kalet, "The multitone channel," *IEEE Trans. on Communications*, vol. 37, no. 2, pp. 119–124, 1989. 15

[30] S. B. Weinstein, "The history of orthogonal frequency-division multiplexing [History of Communications]," *IEEE Communications Magazine*, vol. 47, no. 11, pp. 26–35, 2009. 15

[31] M. Aldinger, "Multicarrier cofdm scheme in high bitrate radio local area networks," in *Proc. IEEE Int'l Symposium on Personal, Indoor and Mobile Radio Communications (PIMRC)*, pp. 969–973, 1994. 20

[32] H. Rohling, "Introduction," in *OFDM: Concepts for Future Communication Systems* (H. Rohling, ed.), ch. 1, Heidelberg, Germany: Springer-Verlag, 2011. 20

[33] H. Schulze and C. Luders, *Theory and Applications of OFDM and CDMA*. John Wiley and Sons Ltd, UK, 2005. 21

[34] Y. S. Cho, J. Kim, W. Yang, and C. G. Kang, *MIMO-OFDM Wireless Communications with MATLAB*. John Wiley and Sons (Asia) Pte Ltd, Singapore, 2010. 27, 65

[35] C. Johnson, *Long Term Evolution in Bullets*. CreateSpace Independent Publishing Platform, Chris Johnson, Northampton, England, 2012. 29

[36] E. Basar, U. Aygolu, E. Panayrc, and H. V. Poor, "Orthogonal frequency division multiplexing with index modulation," *IEEE Trans. on Signal Processing*, vol. 61, no. 22, pp. 5536–5549, 2013. 30, 33

[37] G. Hill, *Peak power reduction in orthogonal frequency division multiplexing transmitters*. PhD thesis, Victoria University of Technology, Australia, 03 2011. 30

[38] J. G. Proakis and M. Salehi, *Digital communications*. The McGraw-Hill Companies Inc. New York, USA, 2008. 33, 34

[39] R. G. Gallagar, *Principle of digital communications*. Cambridge University Press, 2008. 33, 34

[40] B. Sklar, *Digital communications: Fundamentals and applications*. Prentice-Hall Inc., New Jersey, USA, 2001. 33, 34

[41] P. K. Frenger and N. A. B. Svensson, "Parallel combinatory OFDM signalling," *IEEE Trans. on Communications*, vol. 47, no. 04, pp. 558–567, 1999. 34

[42] Y. Cho, J. Kim, W. Y. Yang, and C. G. Kang, *MIMO-OFDM wireless communications with Matlab*. John Wiley and Sons (Asia) Pte Ltd. Singapore, 2010. 34

[43] T. Pollet and M. Moeneclaey, "Synchornizability of ofdm signals," in *Proc. IEEE Global Telecommunication Conference (Globecom)*, pp. 2054–2058, 1995. 35, 36

[44] L. Wei and C. Schlegel, "Synchronization requirements for multi-user OFDM on satellite mobile and two-path Rayleigh fading channels," *IEEE Trans. on Communications*, vol. 43, no. 2/3/4, pp. 887–895, 1995. 35, 36

[45] L. Hanzo, W. Webb, and T. Keller, *Single- and Multi-carrier Quadrature Amplitude Modulation*. John Wiley and Sons, 2002. 36

[46] O. Edfors, M. Sandell, J. J. van de Beek, D. Landstorm, and F. Sjoberg, "Technical report: An introduction to orthogonal frequency division multiplexing," tech. rep., Division of Signal Processing, Lulea University of Technology, Lulea, Sweden, September 1996. 36

[47] M. S. Madani, A. Abdipour, and A. Mohammadi, "Analyticl performance evaluation of the OFDM systems passing through nonlinear circuit," *IEICE Electronics Express*, vol. 7, no. 3, pp. 138–145, 2009. 37

[48] X. Li and L. J. Cimini., "Effects of clipping and filtering on the performance of OFDM," *IEEE Communications Letters*, vol. 2, no. 5, pp. 131–133, 1998. 41

[49] S. C. Cripps, *RF Power Amplifiers for Wireless Communications*. Artech House, Norwood, MA, USA, 1999. 42

[50] R. J. Baxely and G. T. Zhou, "Powe saving analysis of peak-to-average power ratio reduction in OFDM," *IEEE Trans. on Consumer Electronics*, vol. 50, no. 3, pp. 792–797, 2004. 42, 85, 86

[51] R. V. Nee and R. Prasad, *OFDM for Wireless Multimedia Communications*. Artech House, Inc., 2000. 42

[52] M. Sharif, M. G. Alkhansari, and B. H. Khalaj, "On the peak-to-average power of OFDM signals based on oversampling," *IEEE Trans. on Communications*, vol. 51, no. 1, pp. 72–78, 2003. 42, 43

[53] C. Tellambura, "Computation of the continuous-time PAR of an OFDM signal with BPSK subcarriers," *IEEE communications Letters*, vol. 5, no. 5, pp. 185–187, 2001. 42, 44

[54] D. Wulich, "Comments on the peak factor of sampled and continuous signals," *IEEE Communication Letters*, vol. 4, no. 7, pp. 2013–2014, 2000. 43

[55] J. Tellado, *Multicarrier modulation with low PAR*. Kluwer Academic Publishers, USA, 2000. 43, 55, 116

[56] R. V. Nee and A. D. Wild, "Reducing the peak-to-average power ratio of ofdm," in *Proc. IEEE Vehicular Technology Conference*, pp. 2072–2076, 1998. 44, 48

[57] T. Jiang, M. Guizani, H. Chen, W. Xiang, and Y. Wu, "Derivation of PAPR distribution for OFDM wireless systems based on extreme value theory," *IEEE Trans. on Wireless Communications*, vol. 7, no. 4, pp. 1298–1305, 2008. 44

[58] R. O'Neill and L. B. Lopes, "Envelope variations and spectral splatter in clipped multicarrier signals," in *Proc. IEEE Int'l Symposium on Personal, Indoor and Mobile Radio Communications (PIMRC)*, pp. 71–75, 1995. 48

[59] H. Ochiai and H. Imai, "On the clipping for peak power reduction of ofdm signals," in *Proc. IEEE Global Communications Conference (GLOBECOM)*, p. 731735, 2000. 48

[60] H. Ochiai and H. Imai, "Performance analysis of deliberately clipped OFDM signals," *IEEE Trans. on Communications*, vol. 50, no. 1, pp. 89–101, 2002. 48

[61] J. Heiskala and J. Terry, *OFDM Wireless LANs: A Theoretical and Practical Guide*. Sams Publishing, 2002. 48

[62] J. Amstrong, "Peak to average power reduction for OFDM by repeated clipping and fequency domain filtering," *IET Electronics Letters*, vol. 38, no. 5, pp. 246–247, 2002. 48

[63] H. Chen and A. M. Haimovich, "Iterative estimation and cancellation of clipping noise for OFDM signals," *IEEE Communication Letters*, vol. 7, no. 7, pp. 305–307, 2003. 48

[64] M. Pauli and H. P. Kuchenbecker, "Minimization of the intermodulation distortion of a nonlinearly amplified OFDM signal," *Wireless Personal Communications*, vol. 4, no. 1, pp. 93–101, 1997. 48

[65] O. Vaananen, J. Vankka, and K. Halonen, "Reducing the peak to average ratio of multicarrier gsm and edge signals," in *IEEE Int'l Symposium on Personal, Indoor and Mobile Radio Communications (PIMRC)*, pp. 115–119, 2002. 48

[66] H. Xiao, L. Jianhua, C. Justin, and Z. Junli, "Companding transform for the reduction of peak-to-average power ratio of ofdm signals," in *Proc. IEEE Vehicular Technology Conference (VTC)*, pp. 835–839, 2001. 50

[67] H. Xiao, L. Jianhua, Z. Junli, J. Chuang, and G. Jun, "Reduction of peak-to-average power ratio of OFDM signals with companding transform," *IET Electronic Letters*, vol. 37, no. 8, pp. 506–507, 2001. 50

[68] X. Wang, T. T. Tjhung, , and C. S. Ng, "Reduction of peak-to-average power ratio of OFDM system using a companding technique," *IEEE Trans. on Broadcasting*, vol. 45, no. 3, pp. 303–307, 1999. 50

[69] X. Wang, T. T. Tjhung, and Y. Wu, "On the SER and spectral analyses of A-law companding multicarrier modulation," in *Proc. IEEE Vehicular Technology Conference (VTC)*, pp. 1408–1412, 2003. 50

[70] T. G. Pratt, N. Jones, L. Smee, and M. Torrey, "OFDM link performance with companding for PAPR reduction in the presence of nonlinear amplification," *IEEE Trans. on Broadcasting*, vol. 52, no. 2, pp. 261–267, 2006. 51

[71] T. Jiang and G. Zhu, "Nonlinear companding transform for reducing peak-to-average power ratio of OFDM signals," *IEEE Trans. on Broadcasting*, vol. 50, no. 3, pp. 342–346, 2004. 51

[72] T. Jiang, W. Xiang, P. C. Richardson, D. Qu, and G. Zhu, "On the nonlinear companding transform for reduction in PAPR of MCM signals," *IEEE Trans. on Wireless Communications*, vol. 6, no. 6, pp. 2017–2021, 2007. 51

[73] S. S. Jeng and J. M. Chen, "Efficient PAPR reduction in OFDM systems based on a companding technique with trapezium distribution," *IEEE Trans. on Broadcasting*, vol. 57, no. 2, pp. 291–298, 2011. 51

[74] R. W. Bauml, R. F. H. Fisher, and J. B. Huber, "Reducing the peak-to-average power ratio of multicarrier modulation by selected mapping," *IET Electronics Letters*, vol. 32, no. 22, pp. 2056–2057, 1996. 52, 76

[75] D. W. Lim, S. J. Heo, J. S. No, and H. Chung, "On the phase sequence set of SLM OFDM scheme for a crest factor reduction," *IEEE Trans. on Signal Processing*, vol. 54, no. 5, pp. 1931–1935, 2006. 52

[76] N. V. Irukulapati, V. K. Chakka, and A. Jain, "SLM based PAPR reduction of OFDM signal using new phase sequence," *IET Electronics Letters*, vol. 45, no. 24, pp. 1231–1232, 2009. 53

[77] H. Jeon, K. H. Kim, J. S. No, and D. J. Shin, "Bit-based SLM schemes for PAPR reduction in QAM modulated OFDM signals," *IEEE Trans. on Broadcasting*, vol. 55, no. 3, pp. 679–685, 2009. 53

[78] D. Lim, J. S. N. C.-W. Lim, and H. Chung, "A new SLM OFDM scheme with low complexity for PAPR reduction," *IEEE Signal Processing Letters*, vol. 12, no. 2, pp. 93–96, 2005. 53

[79] S. A. Adegbite, S. G. Mcmeekin, and B. G. Stewart, "Low-complexity data decoding using binary phase detection in SLM-OFDM systems," *IET Electronics Letters*, vol. 50, no. 7, pp. 560–562, 2014. 53

[80] J. Ji and G. Ren, "A new modified SLM scheme for wireless OFDM systems without side information," *IEEE Signal Processing Letters*, vol. 20, no. 11, pp. 1090–1093, 2013. 53

[81] A. D. S. Jayalath and C. Tellambura, "SLM and PTS peak-power reduction of OFDM signals without side information," *IEEE Trans. on Wireless Communications*, vol. 4, no. 5, pp. 2006–2013, 2005. 53

[82] S. H. Muller and J. B. Huber, "OFDM with reduced peak-to average power ratio by optimum combination of partial transmit sequences," *IET Electronics Letters*, vol. 33, no. 5, pp. 368–369, 1997. 53

[83] L. J. Cimini and N. R. Sollenberger, "Peak-to-average power ratio reduction of an OFDM signal using partial transmit sequences," *IEEE Communication Letters*, vol. 4, no. 3, pp. 86–88, 2000. 53

[84] S. H. Han and J. H. Lee, "An overview of peak-to-average power ratio reduction techniques for multicarrier transmission," *IEEE Trans. on Wireless Communications*, vol. 12, no. 2, pp. 56–65, 2005. 54, 57

[85] A. D. S. Jayalath and C. Tellambura, "An adaptive PTS approach for the reduction of peak-to-average power ratio of an OFDM signal," *IET Electroncis Letters*, vol. 36, no. 14, pp. 1226–1228, 2000. 55

[86] C. Ye, Z. Li, T. Jiang, C. Ni, and Q. Qi, "PAPR Reduction of OQAM-OFDM Signals Using Segmental PTS Scheme With Low Complexity," *IEEE Trans. on Broadcasting*, vol. 60, no. 1, pp. 141–147, 2014. 55

[87] K. S. Lee, Y. J. Cho, J. Y. Woo, J. S. No, and D. J. Shin, "Low-complexity PTS schemes using OFDM signal rotation and pre-exclusion of phase rotating vectors," *IET Communications*, vol. 10, no. 5, pp. 540–547, 2016. 55

[88] H. Kim, E. Hong, C. Ahn, and D. Har, "A Pilot Symbol Pattern Enabling Data Recovery Without Side Information in PTS-Based OFDM Systems," *IEEE Transactions on Broadcasting*, vol. 57, no. 2, pp. 307–312, 2011. 55

[89] L. Yang, K. K. Soo, S. Q. Li, and Y. M. Siu, "PAPR reduction using low complexity PTS to construct of OFDM signals without side information," *IEEE Transactions on Broadcasting*, vol. 57, no. 2, pp. 284–290, 2011. 55

[90] J. Tellado, *Peak to average power reduction for multicarrier modulation*. PhD thesis, Stanford University, USA, 2000. 56, 57

[91] M. Hu, Y. Li, X. Lu, and H. Zhang, "Tone reservation to rinimize ronlinearity impact on OFDM signals," *IEEE Transactions on Vehicular Technology*, vol. 64, no. 9, pp. 4310–4314, 2015. 56

[92] J. Hou, J. Ge, and F. Gong, "Tone reservation technique based on peak-windowing residual noise for PAPR reduction in OFDM systems," *IEEE Trans. on Vehicular Technology*, vol. 64, no. 11, pp. 5373–5378, 2015. 56, 116

[93] P. Yu and S. Jin, "A low complexity tone reservation scheme based on time-domain kernel matrix for PAPR reduction in OFDM systems," *IEEE Transactions on Broadcasting*, vol. 61, no. 4, pp. 710–716, 2015. 56, 116

[94] T. Jiang, C. Ni, C. Xu, and Q. Qi, "Curve fitting based tone reservation method with low complexity for PAPR reduction in OFDM systems," *IEEE Communication Letters*, vol. 18, no. 5, pp. 805–802, 2014. 56, 116

[95] H. G. Ryu, J. E. Lee, and J. S. Park, "Dummy sequence insertion (DSI) for PAPR reduction in the OFDM communication system," *IEEE Trans. on Consumer Electronics*, vol. 50, no. 1, pp. 89–94, 2004. 56, 63, 76

[96] J. K. Lee, J. S. Park, and J. U. Kim, "Modified dummy sequence insertion method for papr reduction of ofdm signal," in *IEEE Vehicular Technology Conference (Fall)*, pp. 1265–1268, 2007. 56

[97] W. Wang, M. Hu, Y. Li, and H. Zhang, "A low-complexity tone injection scheme based on distortion signals for PAPR reduction in OFDM systems," *IEEE Trans. on Broadcasting*, vol. 62, no. 4, pp. 948–956, 2016. 57

[98] J. Hou, X. Zhao, F. Gong, F. Hui, and J. Ge, "PAPR and PICR Reduction of OFDM Signals With Clipping Noise-Based Tone Injection Scheme," *IEEE Trans. on Vehicular Technology*, vol. 66, no. 1, pp. 222–232, 2017. 57

[99] S. H. Han, J. M. Cioffi, and J. H. Lee, "Tone injection with hexagonal constellation for peak-to-average power ratio reduction in OFDM," *IEEE Communication Letters*, vol. 10, no. 9, pp. 646–648, 2006. 57

[100] A. D. S. Jayalath and C. Tellambura, "Reducing the peak to-average power ratio of orthogonal frequency division multiplexing signal through bit or symbol interleaving," *IET Electronic Letters*, vol. 36, no. 13, p. 13, 1161-1163. 58

[101] A. D. S. Jayalath and C. Tellambura, "The use of interleaving to reduce the peak to-average power ratio of an ofdm signal," in *Proc. IEEE Global Communications Conference (GLOBECOM)*, pp. 82–86, 2000. 58

[102] L. Wang, D. Yoon, and S. K. Park, "Side information inserted pilot tone transmission for PAPR reduction in OFDM," *IEICE Trans. on Communications*, vol. E92-B, no. 2, pp. 687–690, 2009. 59

[103] E. Hong, H. Kim, K. Yang, and D. Har, "Pilot-aided side information detection in SLM-based OFDM systems," *IEEE Trans. on Wireless Communications*, vol. 12, no. 7, pp. 3140–3147, 2013. 59

[104] S. Hosokawa, K. A. D. Teo, and T. H. S. Ohno, "Pilot tone design with low peak-to-average power ratio in OFDM," *IEICE Trans. on Fundamentals of Electronics, Communications and Computer Sciences*, vol. E88-A, no. 8, pp. 2117–2123, 2005. 59, 66, 76

[105] I. M. Mahafeno, Y. Louet, J. F. Helard, Y. Nasser, and A. T. Ho, "PAPR reduction technique using pilot symbols for OFDM systems," *European Trans. on telecommunications*, vol. 21, no. 5, p. 435442, 2010. 59

[106] M. J. F. G. Garcia, O. Edfors, and J. M. P. Borrallo, "Joint channel estimation and peak-to-average power reduction in coherent ofdm: a novel approach," in *IEEE Vehicular Technology Conference-Spring*, pp. 815–819. 59, 103, 104

[107] M. J. F. G. Garcia, O. Edfors, and J. M. P. Borrallo, "Peak power reduction for OFDM systems with orthogonal pilot sequences," *IEEE Trans. on Wireless Communications*, vol. 5, no. 1, pp. 47–51, 2006. 59, 63, 80, 104, 105, 106, 108, 109, 111

[108] W. W. Hu, C. P. Li, and J. C. Chen, "Peak power reduction for pilot- Aided OFDM systems with semi-blind detection," *IEEE Communication Letters*, vol. 16, no. 7, pp. 1056–1059, 2012. 59, 105, 106, 108, 110

[109] X. Li, F. Y. Li, B. W. Ji, D. C. Yao, and Z. D. Zhong, "A low complex virtual sub-carrier reservation algorithm for papr reduction," in *Proc. IEEE Int'l Conf. on Wireless Communications, Networking and Mobile Computing*, pp. 1366–1369, 2009. 60, 89

[110] K. T. Wong, B. Wang, and J. C. Chen, "OFDM PAPR reduction by switching null subcarriers and data-subcarriers," *IET Electronics Letters*, vol. 47, no. 1, pp. 62–63, 2011. 60, 63, 80, 90, 91, 92, 96, 99, 100, 101

[111] S. Ahmed and M. Kawai, "A reduced complexity subcarrier switching scheme for papr reduction in ofdm system," in *Proc. Int'l Conf. on Future Generation Communication and Networking, Springer CCIS Part I*, pp. 67–76, 2011. 60, 91

[112] S. Ahmed and M. Kawai, "Dynamic null-data subcarrier switching for OFDM PAPR reduction with low computational overhead," *IET Electronics Letters*, vol. 48, no. 9, pp. 498–499, 2011. 60, 80, 91, 99, 100

[113] S. Ahmed and M. Kawai, "Grouped-subcarrier based null-data switching for papr reduction of ofdm with low computational complexity," in *Proc. Int'l Conf. on Wireless Networks*, pp. 464–469, 2012. 60, 91, 96

[114] B. Wong, P. H. Ho, and C. H. Lin, "OFDM PAPR reduction by shifting null subcarriers among data subcarriers," *IEEE Communication Letters*, vol. 16, no. 9, pp. 1377–1379, 2012. 60, 91, 101

[115] D. L. Jones, "Peak power reduction in ofdm and dmt via active channel modification," in *Proc. IEEE Asilomar Conference on Signals, Systems, and Computers*, pp. 1076–1079, 1999. 60

[116] B. S. Krongold and D. L. Jones, "PAR reduction in OFDM via active constellation extension," *IEEE Trans. on Broadcasting*, vol. 49, no. 3, pp. 258–268, 2002. 60

[117] A. Saul, "Generalized active constellation extension for peak reduction in ofdm systems," in *Proc. IEEE Int'l Conference on Communication (ICC)*, pp. 1974–1979, 2005. 61

[118] S. H. Wang, W. L. Lin, B. R. Huang, and C. P. Li, "PAPR reduction in OFDM systems using active constellation extension and subcarrier grouping techniques," *IEEE Communications Letters*, vol. 20, no. 12, pp. 2378–2381, 2016. 61

[119] A. E. Jones, T. A. Wilkinson, and S. K. Barton, "Block coding scheme for reduction of peak to mean envelope power ratio of multicarrier transmission schemes," *IET Electronics Letters*, vol. 30, no. 25, pp. 2098–2099, 1994. 61

[120] D. Wulich, "Reduction of peak to mean ratio of multicarrier modulation using cyclic coding," *IET Electronics Letters*, vol. 32, no. 29, pp. 432–433, 1996. 62

[121] Y. Zhang, A. Yongacoglu, J. Chouinard, and L. Zhang, "Ofdm peak power reduction by sub-block-coding and its extended versions," in *Proc. IEEE Vehicular Technology Conference (VTC)*, pp. 695–699, 1999. 62

[122] S. B. Slimane, "Reducing the peak-to-average power ratio of OFDM signals through precoding," *IEEE Trans. on Vehicular Technology*, vol. 56, no. 2, pp. 686–695, 2007. 62

[123] M. J. Hao and C. H. Lai, "Precoding for PAPR reduction of OFDM signals with minimum error probability," *IEEE Trans. on Broadcasting*, vol. 56, no. 1, pp. 120–128, 2010. 62

[124] K. Patterson, "Generalized reed-muller codes and power control in OFDM modulation," *IEEE Trans. on Information Theory*, vol. 46, no. 1, pp. 104–120, 2000. 62

[125] J. A. Davis and J. Jedwab, "Peak-to-mean power control in OFDM, golay complementary sequences, and reed-muller codes," *IEEE Trans. on Information Theory*, vol. 45, no. 7, pp. 2397–2417, 1999. 62

[126] Y. Tsai, S. Deng, K. Chen, , and M. Lin, "Turbo coded OFDM for reducing PAPR and error rates," *IEEE Trans. on Wireless Communications*, vol. 7, no. 1, pp. 84–89, 2008. 62

[127] S. Ohno and G. B. Giannakis, "Optimal training and redundant precoding for block transmission with application to wireless OFDM," *IEEE Trans. on Communications*, vol. 50, no. 12, pp. 2113–2123, 2002. 64, 66

[128] L. Nuaymi, *WiMAX Technology for Broadband Wireless Access*. John Wiley and Sons Ltd, England, 2007. 66, 89

[129] A. Z. C. Devlin and T. J. Brazil, "Papr reduction techniques for ofdm signals using unused tones with phase information," in *Proc. IEEE Conf. Circuits and Systems for Communications*, pp. 6–10, 2008. 66

[130] P. Venkatasubramanian and J. Illow, "Opportunistic configuration of pilot tones for papr reduction in ofdm systems," in *Proc. IEEE Conf. Personal, Indoor and Mobile Radio Communication (PIMRC)*, pp. 1–5, 2007. 66, 67, 78

[131] J. J. Tattersall, *Elementary Number Theory in Nine Chapters*. Cambridge University Press, 1999. 71

[132] T. Jiang, W. D. Xiang, P. C. Richardson, J. H. Guo, and G. X. Zhu, "PAPR reduction of OFDM signals using partial transmit sequences with low computational complexity," *IEEE Trans. on Broadcasting*, vol. 53, no. 3, pp. 718–724, 2007. 80

[133] C. Rapp, "Effects of hpa-nonlinearity on a 4-dpsk/ofdm signal for a digital sound broadcasting system," in *Proc. European Conf. Satellite Communications*, pp. 179–184, 1991. 83

[134] R. Prasad, *OFDM for Wireless Communication*. Artech House Publishers, 2004. 83

[135] L. Liu, K. Hamaguchi, and H. Wakana, "Analysis of the combined effects of nonlinear distortion and phase noise on OFDM systems," *IEICE Trans. on Communications*, vol. E88-B, no. 1, pp. 304–311, 2005. 83

[136] T. Itoh, G. Haddad, and J. Harvey, *RF Technologies for Low-Power Wireless Communications*. Wiley-IEEE Press, 2001. 85

[137] A. K. Gurung, F. S. Al-Qahtani, A. Z. Sadik, and Z. M. Hussain, "Power saving analysis of clipping and filtering method in ofdm systems," in *Proc. IEEE Conf. Australian Telecommunication Networks and Applications*, pp. 204–208, 2008. 85

[138] A. S. Namitha and S. M. Sameer, "A novel joint method for frequency offset estimation and peak-to-average power ratio reduction in ofdm systems using null subcarriers," *Wireless Personal Communications*, vol. 83, no. 1, pp. 343–359, 2015. 91, 101

[139] A. S. Namitha and S. M. Sameer, "A combined technique for carrier frequency offset estimation and peak-to-average power ratio reduction in ofdm systems using null subcarriers and cuckoo search algorithm," *Telecommunication Systems*, vol. 63, no. 2, pp. 275–285, 2016. 91, 101

[140] E. A. Lee and D. G. Messerschmitt, *Digital communication*. Springer Science & Business Media, 2012. 101

[141] T. Mao, Z. Wang, Q. Wang, S. Chen, and L. Hanzo, "Dual-mode index modulation aided ofdm," *IEEE Access*, vol. 5, pp. 50–60, 2017. 119

[142] K. Honma and T. Shimamura, "Constellation folding for sub-optimum maximum-likelihood method in blind modulation detection," in *IEEE Int'l Symposium on Intelligent Signal Processing and Communications Systems (ISPACS)*, pp. 103–107, IEEE, 2013. 121